UNIVERSITY OF SOUTHAMPTON

PERTURBATIONS TO SPINNING SPACECRAFT IN ELLIPTIC ORBITS

ADRIAN JOHN MARKWELL B.Eng

M.Phil

DEPT OF AERONAUTICS AND ASTRONAUTICS

APRIL 1992

ABSTRACT

The work presented in this thesis is the conclusion of three years' research into the attitude control of small spinning satellites in geostationary transfer orbits. The work is primarily based upon the Space Technology Research Vehicle (STRV) but can be adapted so as to enable the analysis to be used for other spacecraft. This thesis includes a brief description of the STRV satellite and the hazards it will encounter. The design of the satellite's magnetorquer coil is examined and it is proposed to use an aluminium coil rather than one constructed from copper, giving either a mass saving or an increased torquing capability.

The main perturbation to the spacecraft's attitude comes from the aerotorques as the satellite passes through perigee. The magnitude of these torques is predicted but is found to be dependent on the type of interaction which occurs between the spacecraft surfaces and the atmospheric molecules. The spin rate decay of the spacecraft is also examined, but here the dominant effect is that caused by induced eddy currents rather than the aerotorques.

Finally, an experiment is proposed to use observations of the magnitude of the spin axis perturbations for a real spacecraft, and implement a least squares differential correction (LSDC) method to improve knowledge of the gas-surface interaction. Further work is necessary to perform this experiment and this is also discussed. The LSDC software has to be written and a spacecraft identified for the analysis. This identification process will be influenced by the sensor accuracy required for the experiment to give useful results and also the positioning of the centre of mass of the satellite.

CONTENTS

LIST OF FIGURES

LIST OF TABLES

ACKNOWLEDGEMENTS

I would like to thank Dr Graham Swinerd for the weekly consultations throughout the period of this work and the detailed comments he made on the first draft of this thesis. I would also like to thank the Defence Research Agency (Aerospace Division) Farnborough for funding this project for its duration of three years (MOD Agreement Number 2040/478/SP3(F)).

Finally, I would like to thank Ian Harris and Dr Richard Crowther for their useful comments and encouragement in the last three years.

NOMENCLATURE

a	Semi-major axis
A	Area enclosed by coil
A_{KxN}	Partial derivative matrix
$A_i, i=0\text{-}2$	Satellite side surface areas
$b_i, i=0\text{-}3$	Shape coefficients defined in Appendix B
B_m	Mean geomagnetic field strength
C	Circumference of coil
C_D	Drag coefficient
$d_i, i=1\text{-}4$	Functions of accommodation coefficients
e	Eccentricity
E	Eccentric anomaly
E_{Kx1}	Error matrix
$f(E)$	Function defined in text
$f(z_2)$	Change in spin axis orientation as a function of z_2
$f'(z_2)$	Differential of $f(z_2)$
F_i	Force on face i
$F(E)$	Function defined in text
i	Inclination
I	Moment of inertia of satellite
$\underline{i},\underline{j},\underline{k}$	Unit vectors for torque analysis
H	Angular momentum of spacecraft
H_p	Density scale height
K	Constant
Kn	Knudsen number
L	Characteristic length
m_c	Mass of coil
M	Magnetic moment of coil
M_e	Magnetic dipole strength of Earth
$\underline{\hat{n}}_{1,2}$	Unit vectors normal to faces 1 and 2
N	Number of turns in coil

P	Momentum flux normal to surface
P_c	Power consumed by coil
r	Radius of satellite structure
r_p	Distance from focus to perigee
R	Distance from focus to satellite
$R_{0,x,y,z}$	Satellite dimensions
s	$(1-e^2)^{1/2}$
S	Surface area
t	Time
T	Torque acting on spacecraft
T_w	Wall surface temperature
v	Velocity
v_m	Thermal velocity of molecules
v_w	Velocity of molecules emitted from surface at temperature T_w
W^{-1}	Weighting matrix
$\hat{\underline{z}}$	Spin axis unit vector prior to perigee
$\underline{z}^+$	Spin axis direction after perigee pass
$\Delta\underline{z}$	Change in spin axis orientation
$z_{1,2,3}$	Components of spin axis
β	ae/H_p
ϵ	Rotation of spin axis
η	Matrix of changes for LSDC procedure
γ_{10}	Function defined in text
Γ	Function for aerodynamic spin decay
μ	Earth's Gravitational Constant
μ_p	Clock angle
λ_∞	Mean free path of atmospheric molecules
λ_p	Cone angle
Υ	Initial estimate in LSDC procedure
τ	Momentum flux tangential to surface
σ	Conductivity

σ_K^2	Variance matrix of η
$\sigma_{n,t}$	Accommodation coefficients, Normal and Tangential to surface
θ	True anomaly
θ_i	Angle of incidence of flow on face i
Θ	Angle through which spin axis moves
ω	Argument of perigee
ω_s	Satellite spin rate
ω_0	Initial spin rate
ω_{max}	Max spin rate
ω_{min}	Min spin rate
ϕ	Precession angle
Ω	Right ascension of ascending node
ρ	Density
ρ_p	Atmospheric density at perigee
ξ_p, η_p, ζ_p	Perigee reference frame
ψ	Tangent direction on ellipse
χ	Resistivity of coil material

SUPERSCRIPTS

o	Initial
ob	Observed
p	Predicted

SUBSCRIPTS

i	Incident flow
r	Reflected flow
w	Wall
p	Perigee
N,K,1	Matrix dimensions

ABBREVIATIONS

AMF	Apogee Motor Firing
AO	Atomic Oxygen
ASAP	Ariane Structure for Auxiliary Payloads
DC	Direct Current
DEC	Declination of spin axis
DRA	Defence Research Agency - Aerospace Division, Farnborough Hants, UK.
GSI	Gas-Surface Interaction
GTO	Geostationary Transfer Orbit
IAP	Initial Acquisition Phase
IGRF	International Geomagnetic Reference Frame
LSDC	Least Squares Differential Correction
MAC	Momentum Accommodation Coefficient
MARECS	Maritime European Communications Satellite
OBC	On Board Computer
PC	Personal Computer
PRF	Perigee Reference Frame
RA	Right Ascension of spin axis
SAA	Solar Aspect Angle
SCD	Data Collecting Satellite
SSS-A	Small Scientific Satellite
STRV	Space Technology Research Vehicle

1 INTRODUCTION

1.1 General

Spacecraft operational requirements mean that satellites are often injected into elliptical orbits. Some are used as a means to an end, for example geostationary transfer orbit (GTO), and others are utilised for the duration of the spacecraft mission, for example the Molniya communications orbit. The work presented in this report is primarily concerned with the GTO, but it could be applied to other types of eccentric orbit with little effort. The funding is provided by the Defence Research Agency (DRA) (Aerospace Division), Farnborough, UK, who have developed the Space Technology Research Vehicle (STRV). The proposed vehicle is a small satellite (mass $\sim$50kg) which will be launched as a minor partner on the European Ariane 4 booster in July 1993. It will be spin stabilised and remain in GTO for the planned mission duration of one year. Because of this involvement in the STRV programme the majority of the results are directly applicable to this satellite configuration.

1.2 Thesis Plan

The work contained in this report aims at developing knowledge of the perturbations that are expected to be induced in the attitude of spinning spacecraft in elliptic orbits. In the perigee region of the orbit the satellite passes through the Earth's upper atmosphere and is therefore affected by atmospheric drag. This drag force is dependent on how the surface and atmospheric molecules interact and the model used to describe this interaction, the gas-surface interaction (GSI), is discussed later in this chapter (Section 1.3).

In Chapter 2 there is a description of STRV-1, its orbit and the hazards that it is likely to encounter. This will enable readers to acquaint themselves with the terminology used in the remaining parts of the text. Environmental disturbances to the spin axis direction and the spin rate are introduced and basic

control philosophies are discussed with a view to maintaining the attitude control requirements using a single magnetic coil (magnetorquer) aligned with the spacecraft spin (+z) axis. Other attitude control system (ACS) hardware questions are raised and the need for a magnetometer is examined. Results from software are also included showing how the operational ACS requirements can be met by operating the magnetorquer.

Chapter 3 contains a detailed examination of the perturbations to the spin axis direction caused by aerodynamic effects as the spacecraft passes through the upper reaches of the Earth's atmosphere during the GTO perigee passage. This employs work carried out by Van der Ha [Ref 1] and predicts the magnitude of the attitude perturbations expected in the perigee region. The work in this section highlights the effect of density variations in the atmosphere (due to solar activity and local time) and also indicates possible attitude control problems if the satellite is launched at a time when luni-solar perturbations cause the perigee height to decrease significantly, hence increasing the aerodynamic attitude perturbations.

Chapter 4 then addresses the issue of verification of the predictions made by the aerotorque software using various approaches. In the first of these, the software predictions are compared with spacecraft flight data obtained from several sources. MARECS-A attitude data is given in Ref 1 and was used along with Explorer 45 data. Also SKYNET 4C data was obtained from the DRA and compared with the results from the software. The second approach comprises a check of the results by comparison with an independently derived theoretical result.

Chapter 5 investigates spin rate decay mechanisms. If these effects are significant then this will place large demands on the STRV cold gas thrusters. These operate using xenon gas as propellant. However the primary role of the xenon gas thrusters is to perform the initial spacecraft spin-up manoeuvre. The gas also supports the neutraliser experiment, the objective of which is to reduce any build-up of electrical charge on the satellite structure, therefore lowering the

risk of arcing occuring. A significant decay in the spacecraft spin rate during the mission would deplete the xenon supply and jeopardise the neutraliser experiment.

Two causes of likely spin decay for the STRV-1 satellite have been identified, aerodynamic torques and induced eddy current torques. The 'aerotorques' have been examined using two methods, the first using a drag coefficient method, and the other using momentum accommodation coefficients (see Section 1.3). The eddy current spin decay analysis has been extended from an approach used by Shrivastava & Rajasingh [Ref 2] which looked at this spin decay mechanism in a circular orbit. The eddy current torques appear to be the more dominant cause of spin decay in GTO, possibly causing the spin rate to fall from 10rpm to below 6.5rpm in the year long mission.

The work described in Chapters 3 and 5 leads to the aerotorque perturbations, causing both attitude changes and spin rate decay, being derived in terms of the momentum accommodation coefficients. We can therefore, in theory, propose an experiment to improve our estimates of these coefficients. This experiment will be based on a least squares differential correction (LSDC) method which compares theoretical predictions with experimental observations iteratively to refine the values of the coefficients.

To carry out this procedure we must first measure the change in either attitude or spin rate and ascertain the errors involved. These data are likely to be available from the general house-keeping information from the satellite, but it is unlikely that the change in spin rate due to aerodynamic effects will be of use here because of the dominance of the eddy current effect. The change in attitude can then be predicted using the software written for the analysis and an initial estimate for the momentum accommodation coefficients. The difference between the predicted and observed changes in attitude can then be used in the LSDC procedure to update the values of the accommodation coefficients. This idea leads to an experiment for STRV which is developed in Chapter 6 and can be

carried out without any further hardware design changes as it uses standard house-keeping data.

The final chapter summarises the experiment and the work as a whole, including a general overview of the attitude control system of the STRV-1 satellite.

1.3 Gas-Surface Interaction Model

The resultant drag force acting on a spacecraft in the upper reaches of the Earth's atmosphere is dependent on the flow regime in which the spacecraft is travelling. This is defined by the Knudsen Number, Kn, where

$$Kn = \frac{\lambda_\infty}{L} . \qquad (1)$$

Here λ_∞ is the mean free path of the atmospheric molecules and L is a characteristic length of the satellite. There are three types of flow defined by

$Kn \ll 1 \quad \Rightarrow$ Continuum Flow

$Kn \approx 1 \quad \Rightarrow$ Slip Flow (Transitional)

$Kn \gg 1 \quad \Rightarrow$ Free Molecular Flow.

With L=0.452m and $\lambda_\infty > 250$m at 200km this puts STRV-1 in the free molecular flow regime. In this regime intermolecular collisions happen so infrequently that they can be ignored and so molecules approaching a spacecraft surface are not affected by any reflected flux. The forces, and hence torques, induced on the satellite are therefore dependent on the nature of re-emission from the surface, but the problem is that this re-emission is little understood.

The model used in this work was first suggested by Schaaf and Chambre [Ref 3] and resolves the momentum of the incoming molecules normal and

tangential to the spacecraft surface. The coefficients are known as 'Momentum Accommodation Coefficients' (MAC's) and are given by

$$\sigma_n = \frac{P_i - P_r}{P_i - P_w}, \qquad \sigma_t = \frac{\tau_i - \tau_r}{\tau_i}, \tag{2}$$

where σ_n and σ_t are the MAC's normal and tangential to the surface respectively. P_i and P_r are the normal components of the incident and reflected molecular momentum flux, and P_w is the normal momentum component for molecules re-emitted from the surface at the Maxwellian thermal speed corresponding to T_w, where T_w is the wall temperature. τ_i and τ_r are the tangential components of incident and reflected molecular momentum flux.

The values of the MAC's lie within the range $0 \leq \sigma_{n,t} \leq 1$. When $\sigma_n = \sigma_t = 0$ we have specular re-emission, and when $\sigma_n = \sigma_t = 1$ we have diffuse re-emission. Specular re-emission occurs when there is no reduction in the tangential momentum component of the atmospheric molecules and a reversal in the normal component (See Figure 1.1a). That is the reflection is analogous to an elastic collision and the molecules are said not to be accommodated to the surface. In the diffuse re-emission scenario the molecules are fully accommodated to the surface and are re-emitted with a cosine velocity distribution (Figure 1.1b) dependent upon the temperature of the spacecraft wall.

1.4 The Importance Of This Work

There are several models available to describe the GSI, but one of the major problems is that ground-based experimentation is difficult because of the complexities of simulating the orbit/satellite environment. This environment consists of a low vacuum, 5eV atomic oxygen flux and varying surface properties (temperature and cleanliness). An in-orbit experiment is described here which will hopefully improve our knowledge of the MAC's and this will allow more accurate attitude perturbation predictions to be made. It will also facilitate better

estimates of fuel budgets to overcome the effect of drag in low Earth orbit (LEO), and it will allow more precise predictions of satellite lifetimes to be made.

For these reasons the experiment proposal in Chapter 6 will be of importance in improving our present knowlegde of the spacecraft-atmosphere interaction. It is unfortunate that this work will not be extended to cover the period of the launch of STRV-1, but it is hoped that the ideas formulated here will be of use either to the STRV team or to other investigators to examine the GSI parameters. The other area covered in this work is necessary so that spin decay rates for similar spacecraft can be predicted prior to the mission and strategies can be devised to cope with the reduced rate. These may involve the implementation of a re-useable spin-up mechanism or the redefinition of any electronics for scanning sensors to cope with a variable spin rate.

1.5 Summary

This Chapter indicates the progression of the work for the remainder of the Thesis and introduces the important concept of the gas-surface interaction described in terms of the momentum accommodation coefficients, $\sigma_{n,t}$. These will be used in Chapter 3 to formulate expressions for the magnitude of the spin axis perturbations to a satellite in an elliptic orbit, and also in Chapter 5 to evaluate the magnitude of the aerodynamic spin rate decay. The MAC's are also the subject of a proposed experiment developed in Chapter 6 which aims to improve our knowledge of the gas-surface interaction process.

2 STRV-1

2.1 Introduction

This work was carried out under an Agreement between the Defence Research Agency (Aerospace Division)(DRA - formerly Royal Aerospace Establishment, Farnborough, UK) and Southampton University, with the aim to undertake attitude control system work related to the Space Technology Research Vehicle (STRV-1). This chapter begins by introducing the spacecraft, its mission and objectives and then progresses to discuss the attitude control system (ACS) in more detail. The sensors and ACS constraints were defined by the design team at DRA but the work here includes design analysis of the magnetic coil (magnetorquer) and a study into the need for an on-board magnetometer. Finally, examples of attitude control manoeuvres are given and software is used to predict spin axis direction changes.

2.2 Mission Objectives And Definition

STRV-1 is a small spin stabilised satellite planned for launch on the European Ariane 4 booster from French Guiana in July 1993. It will weigh approximately 50kg and will measure 0.452m x 0.452m x 0.3935m high (see Figure 2.1). It is planned to be launched on the Ariane structure for auxiliary payloads (ASAP) ring, in a similar manner to the UoSAT spacecrafts. STRV is a small satellite programme being led by the DRA, the aim of which is to test new space technology in a low financial risk environment. The satellite structure is made of a Carbon/PEEK material which has not been flown in space before as the primary structure of a satellite. There will also be various types of solar cells and electronic equipment mounted on the structure to evaluate the degree of degradation experienced in the severe GTO radiation environment.

One of the major experiments on the satellite is called the Neutraliser Experiment which consists of a neutraliser head from the UK-10 ion thruster

programme. This will be used to try and alleviate spacecraft charging that occurs at the high altitudes near the apogee region. A langmuir probe will be used to judge the success (or otherwise) of this experiment. It is for this experiment that the spacecraft has its only non-renewable resource, xenon gas. This gas will also be used to spin the spacecraft up to its nominal spin rate of 10rpm at the start of the mission, and also to perform any further 'top-up' manoeuvres which may be required due to spin decay mechanisms.

The on-board computer (OBC) will be a MIL STD 1750 processor which will be programmed in ADA, and the antennae will be omni-directional so as to minimise any pointing requirements placed on the attitude control system (see Section 2.3.1). As the satellite will be monitored from a single ground station at Lasham, UK, it will be out of ground station control for long periods of time. Therefore it must have the capability of autonomous control for periods of up to 3 days. The whole strategy of the project is to make the system as simple as possible to reduce any possible single point failures to a minimal level.

The orbit of STRV-1 for the duration of the mission is known as a Geostationary Transfer Orbit (GTO). For an Ariane launch from Kourou (French Guiana), the nominal orbit parameters are as follows:-

Perigee	200 $\pm$ 1 km
Apogee	35975 $\pm$ 52 km
Eccentricity	0.731132 $\pm$ 0.00029
Period	635 minutes
Inclination	7 $\pm$ 0.018 degrees
Argument of perigee	178 $\pm$ 0.14 degrees.

This orbit exposes the spacecraft to a particularly hostile environment, principally because it passes through the Van Allen Radiation belts twice each orbit (4 times each day). This means that in the year long mission it will receive the same equivalent dose of radiation as a communications satellite in

geosynchronous orbit in a ten year life. GTO can therefore be used to carry out accelerated testing on radiation tolerant (rad-hard) electronic components, and there is also a radiation monitor as one of the payload experiments. Spacecraft charging becomes a particular problem at the high altitudes because the build-up of electrical charge can cause arcing between surfaces. This can cause failures in sensitive electronics and surface degradation. At the lower altitudes in the perigee region, there are the problems associated with atmospheric atomic oxygen (AO). The interactions between this species and satellite surfaces can cause material erosion and spacecraft induced luminescence [Refs 4 & 5]. An AO monitor is being developed at the University of Southampton and will be flown on the satellite. This instrument consists of 12 silver film sensors, some of which will be covered with test materials. The action of AO will convert the silver into non-conducting oxides. Measuring the resistance of the films will reveal the oxygen flux that the spacecraft encounters.

The vehicle is essentially a technology demonstrator and the main areas of research interest are

1) New structure
2) New solar cells
3) Rad-hard components
4) Charge alleviation
5) ADA software
6) AO Monitor

The principal hazards to the spacecraft in GTO can be summarised as

a) High radiation dose
b) Electrostatic charging
c) Atomic oxygen erosion.

For further detailed information on the STRV-1 satellite and the research programme see Refs 6, 7 and 8.

2.3 STRV-1 Attitude Control System

2.3.1 ACS Sensors and requirements

The ACS constraints for the STRV satellite have been determined by the team at DRA and are designed to reduce manoeuvres to a minimum, thus decreasing the complexity of the software used and increasing its reliability. The two main constraints for the attitude are power raising and thermal limitations, and it has been decided to restrict the attitude of the spin axis to lie in the plane perpendicular to the sun vector (see Figure 2.2) to within 20 degrees. That is the solar aspect angle (SAA) must be $90^{\circ} \pm 20^{\circ}$. If this constraint is met then this will ensure that there is 94% of power raising capability at all times when not in eclipse, and also a good thermal balance maintained. As the attitude is not referenced to the Earth then the antenna coverage must be broad, and this implies that the data rates must be kept low at 1 kb/s.

The primary attitude sensors on board are V-slit Sun and Earth sensors mounted on the +x and -x faces. These will allow a sensing accuracy of at least $\pm 1^{\circ}$ and control of the spin axis should be to $\pm 2^{\circ}$ (data values taken from Ref 8). Therefore it should be possible to maintain the spacecraft's attitude well within the specified ACS limits. The remainder of this chapter discusses the hardware design and the development of software to simulate attitude manoeuvres.

2.3.2 Magnetorquer Coil Design

The relaxed attitude constraints for STRV-1 mean that the spin axis direction will have to be precessed by approximately 1 degree per day for the year long mission so to retain the SAA of 90°. To correct the spacecraft spin axis it was decided, by the design team at the DRA, to use a magnetic coil known

as a magnetorquer [Ref 7]. The coil's axis will be parallel to the spin axis (hereafter known as a 'spin axis coil') and so when a current is passed through the coil a magnetic dipole is created with its axis along the spin vector. The interaction of this dipole with the Earth's field causes a torque at right angles to both the Earth's and the magnetorquer's magnetic field, therefore causing pure precession of the spin axis about the local Earth field lines (Figure 2.3).

Careful analysis of both the coil and mission parameters should be made when designing the magnetorquer as this will have a large effect on its final performance. The design of the STRV coil was based upon a worst case scenario when, for operational reasons, it may be required to precess the spin axis through 90° in one perigee pass. The magnitude of the Earth's magnetic field relative to a spacecraft in GTO varies as shown in Figure 2.4. The intensity of the field is such that there is a precession capability throughout the complete orbit, but to avoid inefficient use it is recommended that only the period between $|E| < 75°$ is used for this purpose, where E is the eccentric anomaly (see Figure 2.5). This corresponds to a 1 hr period either side of perigee where it is possible to operate the magnetorquers usefully.

Early work investigating magnetorquers for STRV [Ref 9] assumed an average field strength of B_m = 10000nT for the complete torquing period and evaluated the required magnetic moment (M) from the coil using

$$M = \frac{|\dot{\phi}| L_z}{B_m} , \qquad (3)$$

where $\dot{\phi}$ is the mean rate of precession given by $\Delta\phi/\Delta t$, and L_z is the angular momentum of the satellite about the z axis. This equation arises from the equation for a net torque ($\underline{T}$) on a spinning body, given by

$$\underline{T} = \underline{M} \times \underline{B} \tag{4}$$

and

$$\underline{T} \equiv \frac{d\underline{L}}{dt} \ . \tag{5}$$

$\underline{M}$, $\underline{B}$ and $\underline{T}$ are orthogonal (from Equation 4) and the angular momentum vector $\underline{L}$ is either parallel or anti-parallel to $\underline{M}$, therefore the torque is also normal to the $\underline{L}$ vector. Hence only the direction of the spin vector will be changed, and the magnitude of the angular momentum (spin rate) will not be affected by the operation of this coil. Because of this, Equation 5 can be re-written as

$$\underline{T} = L \frac{d\hat{\underline{s}}}{dt} \tag{6}$$

where $\hat{\underline{s}}$ is the unit vector directed along the spin axis of the spacecraft. Equations 3-6 can be combined to give

$$\frac{d\hat{\underline{s}}}{dt} = \left(\frac{M}{L}\right)\hat{\underline{s}} \times \underline{B} = \dot{\phi} \times \hat{\underline{s}} \tag{7}$$

where

$$\dot{\phi} \equiv - \left(\frac{M}{L}\right)\underline{B} \ , \tag{8}$$

which can be re-arranged to give Equation 3. Equation 7 is the usual equation describing the precession of the spin axis, $\hat{\underline{s}}$, about the magnetic field vector $\underline{B}$ [Ref 10].

Now using Equation 3 and the values for STRV-1 gives a required magnetic moment of at least $22.6 Am^2$ to ensure the attitude can be precessed 90°

on a single perigee pass. The magnetic moment of a coil is given by Flatley [Ref 11] as

$$M = NIA \tag{9}$$

where I is the current flowing in the coil consisting of N turns of wire and A is the area enclosed by the coil. The resistance of each turn can be written as $R = C(\chi/a)$ ohms where the circumference of the coil is C, the cross sectional area of the wire is a and χ is the resistivity of the wire. The power, $P_c = NI^2R$, is then given by

$$P_c = \frac{NI^2C\chi}{a} \tag{10}$$

If we combine Equations 9 and 10 and write the mass of the coil m_c as

$$m_c = NCa\rho \tag{11}$$

we get

$$M = \frac{A}{C}\sqrt{\frac{P_c m_c}{\chi\rho}} \quad Am^2 \tag{12}$$

where ρ is the density of the coil material. The initial work at DRA used a copper coil and so to achieve the required $22.6Am^2$ with a power allocation of 8 Watts for the magnetorquer required a coil mass of 1.25kg. However, it was noted from the above equation that for a given coil size, mass and power, it is possible to increase the magnetic moment M by reducing the product $\chi\rho$. That is, the choice of material used has a large impact on the efficiency of the coil.

Table 1 shows the product $\chi\rho$ for several materials and the value for aluminium is a factor of 2 lower than that for copper. The effect of this is that using the STRV design parameters of m_c = 1.25kg and P_c= 8W, as above, but

an aluminium coil, gives a magnetic moment of $42.2Am^2$. That is a much larger torquing capability is produced than with the copper coil. To obtain this moment from the coil requires 393 turns of aluminium wire (from Equation 9) and the radius of the wire is given indirectly by Equation 10 as 0.46mm.

Table 1

Material Properties

Material	Resistivity, χ	Density, ρ	$\chi\rho$
Copper	1.72×10^{-8}	8.9×10^{3}	1.53×10^{-4}
Aluminium	2.63×10^{-8}	2.7×10^{3}	7.1×10^{-5}
Silver	1.47×10^{-8}	1.1×10^{4}	1.54×10^{-4}
Iron	1.00×10^{-8}	7.8×10^{3}	7.8×10^{-4}

The coil parameters evaluated above result in a larger magnetic moment than is required for a 90° precession per pass. This allows for more rapid movement of the spin axis during a perigee pass (167° per pass) or a better precession capability in a part of the orbit previously considered to be inefficient. This is useful as it will allow magnetorquer commands to be sent direct to the spacecraft during a ground station pass and some precessional capability will be available to move the spin axis if the orientation is considered detrimental to the spacecraft's well-being.

Software was used to implement the 1975 International Geomagnetic Reference Field (IGRF) model and to evaluate an average value for the Earth's field strength during the apogee section of the orbit which turned out to be 230nT (cf an estimated 10000nT in the designated torquing region), and if the coils are activated for the complete period (8.5hrs) then this will result in 19.2° of possible precession capability. This could well be used to manoeuvre the spacecraft out of a threatening orientation in an emergency. Alternatively, the mass of the coil could be reduced but still maintaining the 90° precession capability at perigee.

2.3.3 The need for a magnetometer

The torque produced through the interaction of the dipole from the spin axis coil on STRV and the Earth's magnetic field will be perpendicular to the spin axis (Equation 4) and therefore will not alter the magnitude of the spin rate. The only way to achieve spin rate changes using magnetorquers is to employ a coil with its axis normal to the spin vector (a 'spin plane coil') and switch the current direction twice per revolution. This is called commutation and is required to obtain a net torque after the rotation of the satellite through 360°. This net torque will have a component parallel to the spin axis and will therefore change the magnitude of the spin vector as well as its direction.

The successful commutation of the current requires detailed knowledge of the spin phase of the satellite with respect to the direction of the Earth's field, which can be accomplished in two ways. The first is to analyse spin rate and attitude data and then to calculate the relative field vector using the OBC. However, this is time consuming and would require a significant amount of computer storage space. The second approach is to use a magnetometer to measure the field vector and to switch the coil current accordingly. This second method is much simpler but imposes a small mass penalty on the spacecraft design. Even so, this is the more commonly used method, for example the Small Scientific Satellite (SSS-A), the Data Collecting Satellite (SCD-2) and the ISIS ionospheric research satellites (ISIS-I and ISIS-B) all had magnetometers. [Refs 11, 12, 13, 14].

As there is not a spin plane coil in the hardware definition for STRV-1 the need for inclusion of a magnetometer is not so well defined. Knowledge of the field vector is needed for the operation of the spin axis coil, but can this be accomplished without the magnetometer? A series of questions was generated relating to the inclusion of this hardware to aid the decision-making process. The answers to any of these could of course automatically include/exclude the magnetometer from the satellite.

Question 1 Can we sense STRV-1's attitude without a magnetometer ?
Answer Yes, the sun and Earth sensors on the satellite will enable the attitude to be evaluated fully.

Question 2 Are the orbit and magnetic field models accurate enough for the reconstruction ?
Answer Yes, they will enable the attitude manoeuvres to be predicted and the spacecraft attitude to be reconstructed on the ground at a later date.

Question 3 Is there room in the OBC for the models ?
Answer No, but the predictions can be made on the ground and uploaded at a suitable opportunity.

Question 4 What magnetic noise is present and can this be filtered out ?
Answer There will be much high frequency noise from the electronic circuits, but this can be filtered out as the magnetometer electronics are measuring a slowly varying DC field.

Question 5 Is it necessary to have the magnetometer on a boom ?
Answer No, see above answer. If the answer to this was yes, then this would immediately exclude it from the design as there are to be no deployable structures on STRV-1.

Question 6 What mass has been allocated for the magnetometer ?
Answer 250 grams have been allocated and it should be possible to build one to this specification.

The above questions and answers did not unambiguously determine the need, or otherwise, for a magnetometer and so a compromise had to be made. Rather than using a magnetometer and the associated electronics it was decided to employ a strategy which could evaluate the magnetorquer ON/OFF times on the ground and upload them as time tagged commands. The calculations required to

predict switching times for the spin axis coil are much simpler than those needed to determine the complex commutation times for the spin plane coil and as there is no spin plane coil it was therefore felt that a magnetometer should not be included.

It should be noted here that as there is no spin plane coil on the satellite then the only means to achieve spin-up manoeuvres is to use the xenon gas supply and thrusters.

2.4 STRV-1 Attitude Manoeuvres

2.4.1 Introduction

During the STRV mission it will be routinely necessary for the spin axis direction to be re-aligned either so that the SAA remains within the attitude constraints (90° $\pm$20°) or due to the effect of any perturbations to the vector, for example aerotorque perturbations (see Chapter 3). These manoeuvres will be carried out primarily using the magnetorquer as described in the previous sections. The secondary (and back-up) method of performing manoeuvres is using the cold gas thrusters; this secondary method is not preferred and will not be considered here.

The largest manoeuvres are likely during the initial acquisition phase (IAP) of the mission, and this will be briefly described here. Immediately after release the satellite is likely to be in a tumbling state, the angular momentum vector being in an arbitrary direction. The gas jets will be used to apply the spin-up torque about the z axis and then the residual nutation will be damped out using the fluid-loop nutation damper. This will result in the satellite spinning about the z-axis of the spacecraft which is the axis of greatest moment of inertia. After the nutation has been damped the spin axis will lie in an arbitrary direction and the attitude constraints should be met as quickly as possible to avoid endangering the

spacecraft systems. This could involve the precession of the spin axis through a maximum of 90°.

Activating the spin axis coil of the satellite when in the Earth's magnetic field produces pure precession of the spin axis as described above. The only control of that precession of STRV is achieved by altering the direction of the current in the coil, and hence reversing the polarity of the magnetic dipole. Software was written so that the operation of the magnetorquer could be investigated, and a simple control algorithm was devised.

2.4.2 Hill-climbing algorithm

The control strategy used in the software will be described as a 'hill-climbing' method [Ref 9] and requires some simple on board processing of sensor data. For this method to be effective, it requires that the SAA is calculated prior to a perigee pass and if the attitude violates the limits then the magnetorquer is activated with the current in an arbitrary direction when the geomagnetic field strength is adequate. This will cause the spin axis to precess and hence the SAA will change. The new SAA must then be calculated and compared with the previous value and if the attitude has moved away from the required angle then the direction of the current is reversed. The effect of the torquing is monitored and by this means the attitude is brought to within the required limits.

It is desirable to have the satellite under ground station control for the IAP of the mission as this will allow each subsystem to be checked out before allowing autonomous control. For this reason the hill-climbing algorithm will not be used in the early stages but time tagged commands will be predicted on the ground and uploaded to the spacecraft at a suitable opportunity. Another reason for not using the hill-climbing algorithm immediately after launch is that the spacecraft will be launched into a midnight perigee and there will be a short eclipse lasting approximately 15 mins [Ref 15]. The hill-climbing algorithm

relies on sun sensor data for its operation and as there will be none available during this period the performance of the ACS will be inhibited.

During later stages of the mission when the spacecraft systems have been checked and the eclipse period does not coincide with perigee, it will be possible to use this proposed method of control.

2.4.3 Software models

Throughout this work software is used to test the ideas and models proposed in the various areas of attitude manoeuvres, aerotorque predictions and spin rate decay. This software is written in FORTRAN 77 for implementation on an IBM compatible Personal Computer (PC) using a ProFortran compiler. As the commands used are all standard FORTRAN it is possible to transfer the programmes so that they can be used with other machines and compilers with little effort. This should be unnecessary because the computing hardware in the ground station will consist of IBM 386 PC's.

The most frequently used programme is called POSIGEN (POSition GENerator) which is an orbit generator converted from software which was previously written at Southampton. The original programme operated by incrementing the time by a fixed amount and then calculating the position of the spacecraft at the new time. This is adequate for analysis of orbits over a long period of time, but for this application it is necessary for there to be high resolution around perigee. Equal time steps give low resolution at perigee and high resolution at apogee (see Figure 2.6) and are therefore unsuitable. This problem can be overcome by using increments in eccentric anomaly (E) instead of time. A step size of $E = 15°$ was chosen for the analysis with this being reduced to $E = 5°$ in the perigee region to increase the resolution at perigee passage (see Figure 2.7). The perigee region here corresponds to $-75° < E < +75°$ so to allow the magnetorquer operation to be carried out in the higher resolution part of

the orbit (see Section 2.3.2). The magnitude of these steps is however, arbitrary and can be easily altered.

Once the spacecraft's position is evaluated it is necessary to calculate the components of the geomagnetic field. This is done using a programme called MAGMOD (MAGnetic field MODel) which evaluates the components of the field at each position of the spacecraft from the International Geomagnetic Reference Field (IGRF). This software was written entirely for this work and uses the first three coefficients from the IGRF model. This could be altered to use more values if the required accuracy is felt necessary.

The control algorithm from the previous section was then tested using a programme called MOVESA (MOVE Spin Axis) and like MAGMOD was written specifically for this work. This programme calculates the attitude of the spin axis at each point in the orbit by evaluating the effect of the torques induced by the magnetorquer coil and aerotorques (Chapter 3). The output from this programme gives the spacecraft attitude in terms of right ascension and declination of the spin axis and also the solar aspect angle.

A further piece of software was developed called NUMINT. This was written to carry out the NUMerical INTegration of complex functions for the spin decay chapter (Chapter 5). This programme outputs the spin rate of the satellite as a function of the time after the spin up manoeuvre was carried out.

Programme descriptions and User Guides for this software will be produced as documents independent of this thesis.

2.4.4 Software simulation

Figure 2.8 shows the predicted variation in SAA for STRV, starting at an arbitrary orientation with SAA = 70°. This is on the limit of the $\pm 20°$ band required for mission purposes, but will be used here to indicate spin axis motion

under the influence of the control coil. The time is measured from the first apogee, the SAA is calculated and the magnetorquer is switched on as the spacecraft leaves perigee for the first time (P1), with the effect of increasing the SAA towards 90° as required.

At this stage the magnetic field strength is a maximum and so, therefore, is the precession rate (Equation 3). Because of the step size between SAA calculations there is a small overshoot before the current in the coil can be reversed. When the SAA goes back below 90° the current is reversed again and this oscillation decays as the satellite departs the torquing region because the field strength is continuously decreasing. For the next 9 hrs the coil is left inactive unless there is an emergency situation, in which case there is a small, inefficient (Section 2.3.2) precessional capability. The SAA varies slightly here due to the Earth's motion about the Sun, and at the next perigee, P2, the attitude determined is found to be below the 90° requirement and so the coil is activated again. This causes a relatively large overshoot as the field strength is a maximum, but this is soon reduced to acceptable limits. The final perigee pass shown here has an overshoot, but in the opposite sense.

It is important to note that the software used here uses the very simple algorithm described above and there are no feedback/forward loops employed. If these were to be included then it should be possible to control the oscillation of the spin axis, but detailed control algorithms are not considered to be within the scope of this work. The continuous motion of the spin axis during the torquing period is undesirable because of power wastage and could be reduced by employing a 'dead-band' for the spacecraft attitude. If the SAA were to fall within this dead-band then the current would be switched off, therefore reducing this power wastage. Another way to reduce the magnitude of the oscillation is to reduce the step size between SAA calculations. For the software simulation the SAA was evaluated every 5° step in eccentric anomaly, and so if the current is in the wrong direction then the attitude will deteriorate for about 3 minutes before the precession is reversed, whereas, if the step size was smaller the error would

be reduced. The magnitude of the step for the actual spacecraft is dependent on the ability of the software and sensors to evaluate the SAA, but it is likely to be of the order of 1 minute before a noticeable change in attitude can be detected.

The next Figure (Figure 2.9) shows the effect of operating the coil for a complete 2 hr torquing region around perigee. The diagram shows a 'worst case' scenario when the spin axis is pointing away from the sun after release from Ariane. It can be seen that the correct attitude is attained during the second perigee pass (P2), with 60° of precession during the first pass, P1. This value is significantly less than the value estimated in Section 2.3.2, the difference being due to the estimated value of mean field strength for the perigee pass. From Figure 2.9 and Equation 3 a better estimate of the value of B_m can be made. This value should be 3600nT, the inaccuracy of the estimate being due to the plot in Figure 2.4 using the eccentric anomaly on the x-axis. If time was used then this would have the effect of narrowing the peak in the graph.

2.5 Summary

The work in this chapter is aimed at describing the STRV-1 satellite in detail. The first section is an introduction to the mission objectives of STRV and defines the orbit parameters which are used throughout the report and for the software simulations. The attitude control system is then discussed. Beginning with the sensors, requirements and an initial copper magnetorquer coil design (which were supplied by the DRA) a study was carried out into the development of the ACS as a whole. It was discovered that the use of aluminium rather than copper would give either greater precessional capability or a mass saving over a similar copper coil. An aluminium coil has now been implemented into the STRV design.

Further hardware studies were carried out and it was decided that a magnetometer was an unnecessary piece of equipment on the satellite so that the mission could proceed satisfactorily without it. Finally in this Chapter, software

was used to implement a simple hill-climbing control algorithm which showed the effect of operating the magnetorquer coil. This last section disclosed inaccuracies in the initial estimate of the Earth's magnetic field strength [Ref 9]. Care should be taken when estimating averages from graphs.

3 AEROTORQUE PREDICTIONS

3.1 Introduction

As a spacecraft passes through the upper atmosphere it will encounter drag forces due to the interaction of the atmospheric molecules and the surface of the spacecraft (see Section 1.3). The torques induced by these forces will be examined in this chapter and will be known as aerotorques.

In GTO, as in any orbit, the velocity, v, of a satellite is given by the vis-viva energy equation as

$$v = \left\{2\mu\left(\frac{1}{R} - \frac{1}{2a}\right)\right\}^{1/2} , \qquad (13)$$

where R is the distance from the occupied focus of the orbit to the spacecraft, a is the semi-major axis and μ is the Earth's gravitational constant.

At the perigee R is a minimum and so the velocity is higher than at any other point in the orbit. Also the atmospheric density (ρ_{at}) is a maximum at perigee and consequently these factors imply that the aerotorques will be at their largest in this region.

It is possible for atmospheric models to be used to predict the density variations over a wide range of altitudes, but the accuracy of these predictions is generally poor ($\pm 15\%$ [Ref 16]). Also the value of density (ρ_{at}) is a function of many parameters, varying from the time in the 11 year solar cycle to the local solar time at the point considered. Some of these models are extremely complicated and Roble [Ref 17] indicates that one model in particular, the Thermosphere/Ionosphere General Circulation Model (TIGCM), takes 20 minutes of CRAY-Y-MP 8/64 run time to simulate one day. This is clearly unsuitable for implementation on a PC and so the King-Hele exponential model [Ref 18] was

used with a constant density scale height, H_p, to evaluate the density at any point around the orbit.

So, given the density at perigee, ρ_p, King-Hele [Ref 18] gives the density to be

$$\rho(E) = \rho_p \exp\{-\beta(1-\cos E)\}\ , \qquad (14)$$

where $\rho(E)$ is the density as a function of the eccentric anomaly, (see Figure 2.5 for definition of E), and ß $= ae/H_p$. Here H_p is the density scale height at perigee.

To reduce simulation run times the aerotorque analysis was limited to the region of the orbit where the density is greater than 1% of the density at perigee. For example, if we assume a relatively high value of solar activity ($F_{10.7} \approx 250$), the Jacchia 77 model [Ref 19] can be used to give a density for the perigee as 4.54×10^{-10} kg/m^3.

$\rho(E)$ now equals $0.01\rho_p$ and so using Equation 14 gives a region relating to $-8° < E < +8°$ or, in terms of the true anomaly, θ, between $\pm$ 20°.

Kepler's Equation gives

$$t = 2\pi\sqrt{\frac{a^3}{\mu}}\,(E - e\sin E)\ , \qquad (15)$$

and using this we find that this interval of time lasts for only 7.58 minutes (approx 1.2% of total orbit period), and so the aerotorque perturbations can be treated as an impulsive change to the spacecraft attitude.

The attitude of the spacecraft is defined by its right ascension and declination as shown in Figure 3.2, where X, Y and Z are the directions in the geocentric

inertial reference frame. It is more convenient in this analysis to use a reference frame based upon the perigee of the orbit. This will be known as the perigee reference frame, where $\underline{\xi}_p$ is along the vector from the Earth to the perigee point (r_p), $\underline{\eta}_p$ is along the spacecraft velocity vector at perigee (tangential to orbit) and $\underline{\zeta}_p$ is normal to the orbit plane and completes the right handed set of axes. See Figure 3.3. The direction of the spacecraft spin axis can now be written as

$$\hat{\underline{z}} = z_1\underline{\xi}_p + z_2\underline{\eta}_p + z_3\underline{\zeta}_p \,, \qquad (16)$$

using the standard matrix transformation given in Appendix A, where the z_i terms represent the direction cosines of the $\hat{\underline{z}}$ vector.

3.2 Instantaneous Torques

The model developed by Van der Ha for MARECS-A in Refs 1 and 20 uses an approach based upon the momentum accommodation coefficients (MAC's) σ_n and σ_t as defined by Schaaf and Chambre [Ref 3] and described in Section 1.3. These MAC's are a measure of how the gas molecules of the atmosphere and the molecules of the spacecraft surface interact with each other, hence the term gas-surface interaction. The MAC's determine the forces acting on a spacecraft and so detailed knowledge of them would aid in drag calculations for station keeping, attitude control and orbit decay predictions. There are several models available for describing the gas surface interaction which Crowther [Ref 21] examines, and an experiment for determining the MAC's is proposed in Chapter 6.

The Van der Ha model can be used directly for STRV-1 as it, like the MARECS-A spacecraft, can be described as a 'box-like satellite in GTO'. The main difference between the two spacecraft is the size of the box. STRV-1 has the dimensions as shown in Figure 2.1 and the mass distribution will be such that the z axis is the axis of maximum moment of inertia. The instantaneous torque

acting on the satellite is given in Ref 1 and after evaluating the vector cross products this can be written as

$$\underline{T}(E) = \frac{-\rho_p(\mu/a)\,F(E)\exp[-\beta(1-\cos E)]}{(1-e\cos E)^2}\,(-z_3 s\cos E\ \underline{\xi}_p - z_3\sin E\ \underline{\eta}_p + (z_1 s\cos E + z_2\sin E)\ \underline{\zeta}_p)\ , \quad (17)$$

where

$$F(E) = b_0(1-e^2\cos^2 E)/f(E) + b_1(1-e^2\cos^2 E)^{1/2} + b_2 f(E) + b_3(z_2 s\cos E - z_1\sin E)\ , \quad (18)$$

$$f(E) = \{(s\sin\lambda_p\cos E + \cos\lambda_p\cos\mu_p\sin E)^2 + \sin^2\mu_p\sin^2 E\}^{1/2} \quad (19)$$

and

$$s = (1-e^2)^{1/2}\ . \quad (20)$$

Here the b_i (i=0-3) coefficients are known as the shape coefficients and are given in Appendix B. The angles λ_p and μ_p are known as the cone and clock angles respectively (Figure 3.4) and the z_i coefficients are related to these angles by Ref 1,

$$\left.\begin{aligned} z_1 &= \sin\lambda_p\cos\mu_p\ , \\ z_2 &= \cos\lambda_p\ , \\ z_3 &= \sin\lambda_p\sin\mu_p\ . \end{aligned}\right\} \quad (21)$$

Hence, using these relationships, we can re-write f(E) as

$$f(E) = \left\{ s^2 (1 - z_2^2) \cos^2 E + \left[1 + \frac{z_2^2 z_1^2 - z_1^2}{1 - z_2^2} \right] \sin^2 E + \right.$$

$$\left. + \; 2 s \sin E \cos E \, z_1 z_2 \right\}^{1/2} \qquad (22)$$

which removes any need to calculate the angles λ_p and μ_p . The MAC's are not shown in the expression for the torque (Equation 17), but they are contained within the b_i (i = 0-3) terms as shown in Appendix B. Because of this, the magnitudes of the torques and attitude deviations calculated in later sections are dependent on the re-emission model used for the GSI. It will be assumed in the next sections that there is near-diffuse re-emission with the MAC's given by σ_n = σ_t = 0.9.

3.3 Predicted Torques

Due to the relaxed attitude constraints imposed on STRV-1 (Section 2.3.1), it is, in theory, possible to pass through perigee in any orientation at some time in the mission. With different proportions of each face being exposed to the flow in each orientation there will obviously be different magnitudes of torque induced, and so it is necessary to examine all possibilities. Figure 3.5 shows the magnitude of the instantaneous torques as the satellite passes through perigee, and Figure 3.6 shows the principle governing the aerotorques. The numbers in Figure 3.5 indicate the angle, λ_p, which separates the spin axis and the velocity vector. The case where the spin axis and the velocity vector are aligned (λ_p = 0°) will now be described in detail.

As the satellite approaches perigee (θ < -20°) the density of the atmosphere is so small as to make the torques negligible. The analysis here starts at θ = -20°, and as the true anomaly is reduced, the magnitude of the torques

increase with the rise in density. At about θ = -6° the torque reaches a maximum and begins to decay. This is because the moment arm is reducing (between the centre of pressure and the centre of mass) and this now dominates the magnitude of the predicted torque. When the satellite is actually at perigee the top face is normal to the flow and so the centre of pressure is on the spin axis, thus there is no moment arm and the torque is zero. As STRV moves away from perigee the scenario is reversed; that is the moment arm increases, the density decreases and the torque is in the opposite sense.

When the spin axis and velocity vector are not aligned and λ increases, it can be seen that there is no longer zero torque at θ = 0° (Figures 3.5 and 3.7). The drag force now has a moment arm at perigee and the position of zero torque moves towards θ = +20°, until λ_p = 11°. With

$$\tan\psi = \frac{\tan E}{(1-e^2)^{1/2}} \quad . \qquad (23)$$

(see Figure 3.1 for definition of ψ) and E = 8° (θ = 20°) then ψ = 11° and so when λ_p > 11° the spin axis is not aligned with the velocity vector in the section of the orbit we are examining and therefore the torque graphs do not pass through zero.

The value of λ_p then had to be altered to cover the complete range of incidence angles. This was done by fixing the right ascension (RA) and varying the declination (DEC) through 180 degrees. The RA was then increased in steps of 10 degrees and the process repeated, until all possible attitudes were examined. See Figs 3.8 - 3.25. The largest torques occurred in Figure 3.15 (RA = 70°, DEC = 180°) and Figure 3.19 (RA = 110°, DEC = 0°). In the analysis here, the orbit parameters (ω, Ω and i) were chosen so that RA = 180°, DEC = 0° was the direction of the perigee velocity vector. This meant that the configurations which indicated the largest torques (T approximately 67×10^{-5}Nm) both had a value of λ_p = 70°.

3.4 Attitude Perturbations

It is now possible to integrate the instantaneous torques over the perigee region and the predominant effect will be to change the direction of the satellite's angular momentum vector. Energy dissipation effects will then cause the spin axis to align itself with the new angular momentum direction, thus altering the spacecraft's attitude. The component of torque along the spin vector will cause a small change in the spin rate. This is not discussed here, but it is covered in Chapter 5.

The spin axis direction after a perigee pass is given by Van der Ha [Ref 1] to be

$$z^{+} = (z_1 + \epsilon z_3)\,\underline{\xi}_p + z_2\,\underline{\eta}_p + (z_3 - \epsilon z_1)\,\underline{\zeta}_p \ . \qquad (24)$$

Here ϵ is the angular rotation about the $\underline{\eta}_p$ direction (perigee velocity vector), that is

$$\epsilon = \frac{\rho_p \gamma_{10} \sqrt{2\pi\mu H_p / e}}{H} \ , \qquad (25)$$

where γ_{10} can be written as

$$\gamma_{10} = (1+e)\left\{b_0 (1-z_2^2)^{-1/2} + b_1 + b_2 (1-z_2^2)^{1/2} + b_3 z_2\right\} \ . \qquad (26)$$

The effect on the spacecraft's attitude can now be evaluated by using Equations (16), (24), Figure 3.26 and the Cosine Rule.

The change in orientation can be calculated as

$$\Delta \underline{z} = \epsilon z_3 \underline{\xi}_p + 0 \underline{\eta}_p - \epsilon z_1 \underline{\zeta}_p \ , \qquad (27)$$

and the magnitude of the perturbation is then given by

$$|\Delta \underline{z}| = \epsilon \, (z_3^2 + z_1^2)^{1/2} \qquad (28)$$

or

$$|\Delta \underline{z}| = \epsilon \, (1 - z_2^2)^{1/2} \ . \qquad (29)$$

Equation (29) is now expressed only in terms of z_2 and so writing $|\Delta \underline{z}|$ as $f(z_2)$, elimination of ϵ gives

$$f(z_2) = K\{b_0 + b_1 (1 - z_2^2)^{1/2} + b_2 (1 - z_2^2) + b_3 z_2 (1 - z_2^2)^{1/2}\} \qquad (30)$$

where

$$K = \frac{\rho_p \sqrt{2\pi\mu H_p / e}}{H} (1 + e) \ . \qquad (31)$$

$f(z_2)$ is now the length of the vector joining up the end points of the spin vectors before and after the perturbation (see Figure 3.26). The angle the spin axis moves through is given using the Cosine Rule as

$$|f(z_2)|^2 = |\hat{\underline{z}}|^2 + |\underline{z}^+|^2 - 2 |\hat{\underline{z}}| \, |\underline{z}^+| \cos\Theta \qquad (32)$$

But by definition $|\hat{\underline{z}}| = 1$, and we can say that

$$|\underline{z}^+| = (1 + \epsilon^2 \{1 - z_2^2\})^{1/2} \ . \qquad (33)$$

The z_2 term can take any value from -1 to +1 and so $(z_2)^2$ always lies between 0 and +1. In these two extremes the spin vector either lies along the perigee velocity vector ($z_2 = 1$) or the two vectors are perpendicular ($z_2 = 0$). When z_2 is 1

then $|\underline{z}^+|$ is also 1, and when z_2 is 0, $|\underline{z}^+|$ is 1.0006. Therefore, by assuming that $\hat{\underline{z}}$ and z^+ are both unit vectors (to 0.06% accuracy) we can say that

$$\Theta = \cos^{-1}\left\{1 - \frac{|f(z_2)|^2}{2}\right\} . \qquad (34)$$

As $f(z_2)$ is a function of spacecraft attitude, the rotation which will occur during a perigee pass is therefore dependent on the initial orientation. If we can find when $f(z_2)$ is a maximum then it will be possible to determine the maximum predicted orientation change. $f(z_2)$ is either a maximum or minimum when the differential of (30) is zero, that is

$$f'(z_2) = 0 = K\{-b_1 z_2 (1-z_2^2)^{-1/2} - 2b_2 z_2 + b_3 (1-z_2^2)^{1/2} - b_3 z_2^2 (1-z_2^2)^{-1/2}\} \qquad (35)$$

This cannot be solved analytically and so a graphical solution was sought. $f(z_2)$ and $f'(z_2)$ are shown in Figure 3.27, and there are two solutions to Equation 35, the first at $z_2 = -0.943$ corresponds to a local minimum and the second at $z_2 = 0.340$. The latter case is the global maximum of $f(z_2)$ and since $f(z_2)$ is independent of both z_1 and z_3 there are an infinite number of attitudes which will give the maximum perturbation, all with a z_2 value of 0.34. Hence the maximum perturbation to STRV will occur if the perigee passage orientation lies with the spin axis anywhere on a cone, about the $\underline{\eta}_p$ vector, with a half angle of λ_p equal to $\cos^{-1}(0.340) = 70°$; see Figure 3.28, this agrees with the solution found in Section 3.3.

It should be noted here that this value of cone half angle was calculated for the specific case of the STRV satellite. The cone angle is a function of many different spacecraft parameters such as the areas of the side panels (A_1 & A_2), areas of the top and bottom panels (A_0) and the position of the centre of mass

with respect to the geometric centre of the body (R_z). It is also a function of the re-emission model assumed.

Here we have used STRV dimensions with a centre of mass offset of R_z = 5cm, and the MAC's have been chosen to represent near diffuse re-emission (MAC's = 0.9). If we expected specular reflection from the surface (MAC's = 0) then the maximum perturbation would occur when $z_2 = 0.0$. This would relate to a half angle of 90°; that is the spin axis would lie anywhere in the plane perpendicular to the perigee velocity vector. See Table 2.

TABLE 2

CONE HALF ANGLES

σ_n	σ_t	Reflection Type	z_2	λ_p
0.0	0.0	SPECULAR	0.0	90°
0.5	0.5	INTERMEDIATE	0.2	78°
0.9	0.9	NEAR DIFFUSE	0.34	70°

From this table we can see how the maximum deviation occurs at different orientations for various re-emission types. The magnitude of these perturbations can now be predicted using Equation 34. If we assume three initial orientations of z_2 = 0, 0.34 and 1.0 (ie λ_p = 90°, 70° and 0°), we can predict the expected change in attitude using both the specular and diffuse extremes.

The predicted changes for each orientation and reflection type are shown in Table 3 overpage and, as can be seen, the case where the spin axis is normal to the perigee velocity vector gives the greatest difference between the expected changes. If perigee passage occurs when the spin axis is aligned with the perigee velocity vector (as described earlier) then the difference between the two attitude perturbations that we would expect will be minimal (0.007°).

TABLE 3

EXPECTED ORIENTATION CHANGES

Value of z_2 / Re-emission	0.0	0.34	1.0
SPECULAR	2.63°	2.32°	0.015°
NEAR DIFFUSE	2.01°	2.52°	0.008°

It is important to note that these angular changes are calculated assuming the STRV configuration with a spin rate of 10rpm and an offset between the centre of mass and the geometric centre of the body of 5cm.

3.5 Density Variations

No satellite orbit can ever be described as being purely Keplerian as there are many factors perturbing it, including the interaction with the Earth's atmosphere, which tends to reduce its size and circularise it, and the gravitational influence of the Moon and the Sun (known as Luni-Solar perturbations), which affects the perigee height.

The value of r_p can either be raised or lowered depending on the relative positions of the Moon and Sun at the launch. If it increases then this will have little effect on the attitude control of the satellite, but if lowered then the results could be catastrophic. As the satellite gets lower into the atmosphere the density increases and so, therefore, do the induced aerotorques. Figure 3.29 shows the effect on the magnitude of the torques of a decrease in perigee height. As can be seen there is little effect down to about 160km, but by the time 140km is reached the torques are becoming unacceptable. Any further decrease in height would cause large demands on the attitude control system (ACS), and the satellite would most likely begin to tumble and then re-enter the denser layers of the atmosphere.

Variations in the density at one particular height can also be a problem, this effect may not be as great as the height variations, but its effect can still be significant in terms of the ACS performance. Jacchia [Ref 19] shows that the density at 200km can vary from 8.45×10^{-10} kg/m^3 to 7.73×10^{-11} kg/m^3, depending on the current solar activity and local solar time. This change in density is equivalent to a lowering in height from 200km to 160km, and so the size of the torques can again be seen in Fig 3.29.

3.6 Summary

The major perturbation to the spacecraft's attitude is expected to be the torques produced by the aerodynamic forces acting on the satellite's surfaces. These torques are known as aerotorques and have been discussed in detail in this chapter. The first section introduces these torques and describes the part of the orbit which will be used for the later analysis. This region consists of an 8° band either side of perigee ($|E| < 8°$) where the atmospheric density is more than 1% of its maximum value for the orbit.

Section 3.2 develops a model used by Van der Ha [Refs 1 and 20] which predicts the instantaneous torques acting on a box-like satellite. The work here focuses on developing the expressions so that the torque on the satellite can be written in terms of the spin axis components z_1, z_2 and z_3 rather than the cone and clock angles λ_p and μ_p. Software was then used to generate plots of these torques and these are described in the next Section 3.3. It was necessary to examine all possible attitudes for a perigee pass because of the relaxed attitude constraints of the STRV-1 mission and plots of Aerotorque versus True Anomaly are given for each orientation. The maximum torque of 67×10^{-5}Nm occurred when there was an angle between the velocity vector and spin axis of 70°.

The effect of these torques was then examined and an expression was developed which describes the magnitude of the perturbation in terms of the spacecraft dimensions, gas-surface interaction model used and the initial

spacecraft orientation. The only component of the initial orientation to appear in this expression is the z_2 component which implies that the magnitude of the perturbation is independent of both z_1 and z_3. This expression was then differentiated to find where the maximum spin axis deviation would occur. The result is dependent on the spacecraft used and the GSI model, but the answer obtained from this analysis for STRV-1 agrees with the result from the previous section; the maximum torque (and hence perturbation) occurs when there is an angle of 70° between the spin axis and velocity vector.

Finally in this chapter, the effect of the variation of the atmospheric density was examined. There are two causes of changing density, these are a lowering of the perigee altitude and varying the solar activity or local solar time. A perigee height of less than 140km is likely to cause unacceptable aerotorques because of the increase in density and this could give rise to problems controlling the spacecraft's attitude. Similarly, varying solar parameters will cause the torques to vary by significant amounts.

The work throughout this chapter is aimed at determining the magnitude of the expected aerotorque perturbations so that the ACS actuators can be designed to satisfactorily control the spin axis direction. It should be possible to control the spacecraft for the entire mission with the magnetorquer described in Chapter 2 providing the perigee height does not fall below 160km. The next chapter will now discuss the verification of the software that produced these aerotorque perturbations.

4 AEROTORQUE VERIFICATION

4.1 Introduction

Before the software used in the previous chapter can be used for the prediction of aerotorque perturbations in the ground station for the STRV mission it is necessary to verify the results using data from other spacecraft. Data from the MARECS-A GTO phase used in Ref 1 was employed to validate the coding of the software. Because the code was developed from a model used by Van der Ha it should be possible to reproduce his results. Perturbations in the solar aspect angle (SAA) for the Explorer 45 satellite were obtained and used to independently verify the predictions made.

Data were also obtained from the SKYNET 4C GTO mission phase and the results of software predictions are compared with the actual spacecraft data. It is noted here that the Earth sensors limit the accuracy of the spin axis declination measurements. Finally, an independent method using the classical drag coefficient will be used to confirm the validity of the software.

4.2 Real Spacecraft Data

4.2.1 MARECS-A

MARECS-A was launched by an Ariane booster on December 20 1981 into an Ariane geostationary transfer orbit (GTO) with a perigee altitude of 199.94km and eccentricity of 0.730. Ref 1 gives details of the orbit and predicts attitude changes for the three perigee passes prior to Apogee Motor Firing (AMF). MARECS-A is a much larger spacecraft than STRV-1, but the input files for the software were easily altered to represent a new configuration. The satellite was spinning at 65.3rpm and had an axial inertia of 352.7kgm^2. See Appendix C for full details of the input file.

The above data was entered and the software used to predict the induced torques on the spacecraft at perigee (θ = 0°) for varying angles of incidence (λ) and Figure 4.1 was produced. This graph is the same as the one given in Ref 1 and indicates that the software is at least coded correctly. Calculations for the SAA were then added to the programme and predictions made for the spin axis perturbations due to the aerotorques for 3 perigee passes. Figure 4.2 shows how the SAA varies over this 3 orbit period and can be compared with results from Ref 1.

The slope of this graph shows that the drift in SAA due to the motion of the Earth about the Sun is approximately 0.96°/day, and three distinct steps can be seen when the spacecraft passes through perigee, P1, P2 and P3. The magnitude of these steps is approximately -0.03° which are of the same order as those given in Ref 1. It should be noted that these checks are not independent because the model and data come from the same source, but they increase confidence in the software.

4.2.2 Explorer 45

Explorer 45 (SSS-A) data were obtained from Ref 12 and used to attempt to verify the software predictions. The SSS-1 orbit had a perigee height of 222.6km (120nmi), an eccentricity of 0.71374 and an inclination of 2.94°. The satellite was spin stabilised at 4rpm and had a moment of inertia (I) of 7.05kgm^2 about the +z axis. Appropriate input files were created for the software and a prediction of an attitude change of 0.33° was made. This differs by approximately 6.5% from the value of 0.31° estimated in Ref 12 which used the drag coefficient approach and set the value of C_D to 2.0. The software method used here assumed near diffuse re-emission and set the momentum accommodation coefficients (MAC's - Section 1.3) to 0.9 and work in Chapter 5 indicates that with this GSI model the C_D should be 2.23. This difference in the drag coefficient of at least 10% accounts for the slight under-estimation of the attitude perturbation and again suggests that the software predictions are satisfactory.

4.2.3 SKYNET 4C

4.2.3.1 SKYNET 4C predictions and actual data

SKYNET 4C data was obtained from the DRA to further test the aerotorque predictions using an independent source of data. SKYNET 4C is much larger than STRV-1, as was MARECS-A, but because it was launched from an Ariane 4 into GTO it was considered to be a good candidate to supply useful verification data.

The satellite was successfully released into GTO in August 1990. It remained in this orbit for only a short period and therefore only a small amount (5 orbits) of attitude data is available. Before the software could be used it was necessary to determine required dimensions from the SKYNET diagrams provided by DRA. The parameters given in Appendix C are all estimates used for the predictions, but errors due to possible variations are shown on the prediction graph (Figure 4.3) as error bands. Also shown on this graph are the values obtained for the right ascension (RA) and declination (DEC) of the spin axis whilst in GTO.

The graph of RA versus orbit number shows the predicted and actual values. Also shown is the position of an attitude manoeuvre which was carried out on orbit number 4. The effect of this manoeuvre can be seen clearly in the actual data, but is not modelled in the simulation, however, the results from the software are encouraging with both sets of values being similar. The prediction of DEC versus orbit looks, at first, to be inaccurate with the real attitude changing much faster than predicted by the software. But the errors involved with evaluating the DEC from sensor data must be considered.

4.2.3.2 SKYNET 4C sensor errors

The magnitude of the sensor errors gives rise to differing errors in the RA and DEC. Because of the low declination of the Ariane 4 GTO (i = 7°) the SAA

is very similar to the RA of the spin axis. The sun sensors used on SKYNET are 'cross-slit' sun sensors and are accurate to, at best, 0.03° and so it is possible to determine the RA with reasonable accuracy.

The DEC values however are subject to considerably larger errors in their reconstruction because of the method of measurement. This value relies on sensing the Earth. The Earth sensors are of a type known as 'infra red pencil beam' sensors which have a field of view of 1° and are designed to be sensitive to radiation with a wavelength of 14 microns. Unfortunately this type of sensor is also triggered by radiation at 16μm and this corresponds to emissions from CO_2. High altitude cloud (35km) emits radiation at this wavelength and so the presence of any such cloud will cause the sensors to trigger at the wrong time. This can cause a 0.3° error in the triggering of the pencil beam sensor, but is a common problem with infra red sensors.

The sensor characteristics combine to affect the final errors involved in the attitude reconstruction. The total 3 sigma errors are 0.5° in DEC and 0.25° in RA, and the distribution in not quite normal so the 1 sigma errors are 0.2° in DEC and 0.1° in RA. The 1σ errors are shown in Figure 4.3.

Another factor affecting the attitude of the spacecraft is the active nutation damping employed. This consists of small thrusters which fire automatically to reduce any nutation present and they can be activated up to 40 times per orbit. Each firing can cause 0.06° in attitude change and cannot be modelled unless the thruster characteristics and firing times are well known. This is the primary cause of differences between the predicted and observed values seen in the graphs. The information in this section came from Ref 22. The nature of the SKYNET 4C data consequently does not provide a good test for the prediction software.

4.3 Analytical Methods

Once the satellite data above had been used to verify the predictions made by the software it was decided to try and use methods derived from first principles to evaluate the magnitude of the expected torques and perturbations for the STRV configuration.

4.3.1 Instantaneous Torque Verification

To verify the torques predicted for the STRV satellite it was decided to use an approach based on the classical drag coefficient (C_D). Using this method it is possible to evaluate the force, and hence torque, on each face of STRV at a particular moment in time. The torque on each face can then be summed and integrated over a complete revolution of the spacecraft to give the average torque on the body as

$$\langle T \rangle = -\rho v^2 \left(\frac{2}{\pi} C_D R_Z A_1 \sin^2 \lambda_p + \frac{C_D}{4} (R_0 A_0 - R_1 A_1) \sin 2\lambda_p \right) \quad (36)$$

where ρ is the atmospheric density, v is the velocity of the spacecraft with respect to the oncoming flow and λ_p is the angle of incidence between the spin axis and the velocity vector. $R_{z,1,0}$ and $A_{1,0}$ are dimensions of the satellite as given in the Appendices. Equation 36 was then used to produce a graph of 'normalised torque' ($T/\rho v^2$) against the angle λ_p. This can be seen in Figure 4.4 along with the data produced using the software.

The curves are similar in shape with the software predicting slightly lower torque values than the analytic method, but the discrepancies can be attributed to differences between the values for C_D and the MAC's. The commonly accepted value of $C_D = 2.2$ was used and the MAC's were set to 0.9 to represent near diffuse re-emission. Figure 4.4 shows that there are differences between the two models and for near diffuse re-emission a slightly higher value of C_D should be

used (see Section 5.3.2). It should be pointed out here that both graphs have a maximum at approximately $\lambda_p = 70°$ which correlates to the predictions of the maximum torques made in Chapter 3.

4.3.2 Perturbation Verification

The above section indicates that the magnitude of the predicted torques for STRV are satisfactory and the final check to be made is for the size of the orientation change.

The rate of change of orientation of an axisymmetric spinning body $d\Phi/dt$ is defined as

$$\frac{d\Phi}{dt} = \frac{T}{L}, \qquad (37)$$

where T is the applied torque and L is the angular momentum of the body. Choosing an orientation where the torques were a maximum ($\lambda_p = 70°$) an average torque of 25×10^{-5}Nm was assumed to act over the entire perigee region of 7.58 minutes (Section 3.1). With a spin rate of 10rpm and a moment of inertia about the z axis of 2.5kgm^2 Equation 37 can be used to calculate the angle the spin axis will be moved through. This method indicates the perturbation will be 2.48°, which is only 1.6% different from the software calculated value of 2.52°. It should be noted however that this only checks the parts of the software associated with evaluating the attitude change as it relies on the programme generated values for the torque. It is therefore necessary to determine independently the instantaneous torques on the spacecraft.

4.4 Summary

This chapter focused on verifying the software predictions using as many sources as possible. Three spacecraft were used and the software generated

results that compared favourably with the perturbations that the satellites exhibited whilst in GTO. The MARECS-A data was used to validate the coding of the software but could not be relied upon for independent verification as it came from the same source as the initial model.

Both Explorer 45 (SSS-A) and SKYNET 4C data were used as independent checks and the SSS-A simulation gave very encouraging results. The SKYNET data did not, at first, appear as good as previous predictions, but after the sensing problems had been taken into account the results compared reasonably with the observations.

Finally, two approaches have been used aimed at verifying the actual values predicted for STRV-1. The ideal confirmation would, of course, be to use STRV attitude data but as yet the satellite is still being constructed. The methods here are aimed at first verifying the magnitude of the torques predicted and this is done by developing an expression from the classical drag coefficient C_D. Results from this work were compared with values obtained from the software and correlated well. The differences between the two methods indicated that it is not possible to draw direct comparisons between $C_D = 2.2$ and near diffuse re-emission (MAC's = 0.9). The second analytic verification was aimed at checking the magnitude of the attitude deviation using an average torque acting throughout the complete perigee passage. The result from this simple calculation was only 1.6% different from the value obtained from the software for a detailed STRV-1 simulation.

The validation of the software by the above methods indicates that the predicted values of both torques and perturbations can be used with confidence in the remaining work. Future work will now concentrate on developing the software so that it is possible to install it into the ground station for the STRV programme and use it to plan the attitude control strategy.

5 SPIN RATE DECAY

5.1 Introduction

The work in Chapter 2 is aimed at determining the hardware requirements for the STRV-1 satellite, primarily the critical parameters of the spin axis magnetorquer coil. As mentioned in Section 2.3 a spin plane coil is required to perform spin rate manoeuvres but such a coil has been omitted from the STRV design because of mass limitations. As the xenon on board is now the only means to achieve spin up after the release from Ariane, it is important to understand the extent of the spin rate decay throughout the mission. Spin decay is produced by two main mechanisms for a spacecraft the size and shape of STRV; induced eddy current effects and aerotorque effects.

5.2 Eddy Current Spin Decay

5.2.1 Introduction

When a conducting material moves through a magnetic field then a current is induced in the material which itself generates a magnetic field. The interaction of the two fields cause a force which tends to oppose the initial motion. This is summarised in Lenz's Law, which states,

The direction of an induced current (if one were to flow) is such that its effect would oppose the change in magnetic flux which gave rise to the current [Ref 23].

This force is called the Electromotive Force (EMF), and the currents induced into the material are known as eddy currents. The eddy currents induced into the shell of a spinning satellite create EMF's which tend to reduce the spin rate of the spacecraft.

5.2.2 Extension of circular orbit analysis

Shrivastava and Rajasingh [Ref 2] analyse the magnitude of the eddy current spin decay induced into a satellite in a 600km circular orbit. The spacecraft considered is the Indian satellite 'Aryabhata' which has an aluminium structure assumed to be spherical. This paper derives equations for the maximum and minimum spin rates of the satellite depending on its attitude with respect to the geomagnetic field. These are

$$\omega_{max} = \omega_0 \exp(-4Kt) \qquad (38)$$

and

$$\omega_{min} = \omega_0 \exp(-6.6Kt) \qquad (39)$$

respectively. Here the numerical parts of the above equations come from functions of the orbit parameters i (inclination) and θ (true anomaly) and also the offset between the Earth's geographic and geomagnetic North poles (See Ref 2 for the functions), and K is given by the expression

$$K = 86400 \frac{\sigma \pi r^4 s (M_e/R^3)^2}{6I} \text{ per day.} \qquad (40)$$

σ is the electrical conductivity of the spacecraft shell, s is its thickness and I is the moment of inertia about the z axis of the satellite of radius r. The M_e parameter is the Earth's magnetic dipole strength and R is the distance of the satellite from the centre of the Earth. If the orbit is not circular then the above expressions (Equations 38 and 39) are incorrect as K is not a constant because R varies with time. It is therefore necessary to move back a few steps and the equation for maximum spin rate can be written as

$$\int_{\omega_0}^{\omega_t} \frac{1}{\omega} d\omega = -4 \int_0^t K(t)\, dt \,, \qquad (41)$$

where

$$K = 86400 \frac{\sigma \pi r^4 s}{6I} \frac{M_e^2}{R(t)^6} \text{ per day.} \qquad (42)$$

with R(t) a function of time. Equation 41 can now be re-written as

$$\int_{\omega_0}^{\omega_t} \frac{1}{\omega_s} d\omega_s = -\frac{86400 C \sigma \pi r^4 s M_e^2}{6I} \int_0^t \frac{1}{R(t)^6} dt \,, \qquad (43)$$

where C is a function of the orbit and attitude parameters and is 4 for the maximum spin rate case and 6.6 for the minimum case. The problem now is how to integrate on the right hand side of Equation 43.

If we let

$$Int = \int_0^t \frac{1}{R(t)^6} dt \qquad (44)$$

and we use the fact that R = a(1 - e cosE), we can write

$$Int = \frac{1}{a^6} \int_0^t \frac{1}{(1 - e \cos E)^6} dt \,. \qquad (45)$$

We also have that

$$R \frac{dE}{dt} = \sqrt{\frac{\mu}{a}} \,, \qquad (46)$$

and so by combining (45) and (46) we get

$$Int = \frac{1}{a^6} \sqrt{\frac{a}{\mu}} \int_{E=0}^{E=E_1} \frac{1}{(1 - e \cos E)^5} dE \,. \qquad (47)$$

Equation 43 can now be used to give the spin rate of the satellite as

$$\omega_t = \omega_0 \exp\left[-\frac{86400 C \sigma \pi r^4 s M_e^2}{6 I} \frac{1}{a^6} \sqrt{\frac{a}{\mu}} \int_0^{E_1} \frac{1}{(1-e\cos E)^5} dE\right] . \quad (48)$$

5.3 Aerotorque Spin Decay

5.3.1 Drag coefficient approach

The aerodynamic force acting on a surface of area S and unit normal $\hat{n}$ is given by

$$F = \frac{1}{2} \rho v^2 S C_D (\hat{n} \cdot \hat{v}) (-\hat{v}) , \quad (49)$$

where v is the velocity of the surface relative to the atmosphere.
Initially the special case where the spin axis is perpendicular to the velocity vector was examined; see Figure 5.1. This expression can be re-written for each face of the satellite, for example for face i in Figure 5.1 we have

$$F_i = \frac{1}{2} \rho v_i^2 S_i C_D (\hat{n}_i \cdot \hat{v}_i) (-\hat{v}_i) , \quad (50)$$

where the subscript indicates the face to which the expression relates.

For this initial analysis the force was assumed to act at the centre of pressure (CoP) of each face. This implies the additional assumption that the air-relative velocity of surface i is uniform. In reality the velocity of a particular element of the surface is a function of its distance from the spin axis, by virtue of the rotation. However, accepting this assumption for the moment, the velocity of the CoP for the i^{th} face is given by

$$\underline{v}_i = \underline{v}_0 + (\underline{\omega}_s \times \underline{r}_i) \qquad (51)$$

where $\underline{r}_i$ is the position vector of the centre of pressure of the i^{th} face from the spin axis, $\underline{v}_0$ is the linear velocity of the spacecraft and $\underline{\omega}$ is its angular velocity. Figure 5.1 and Equation 51 can be used to write the velocity of the CoP of faces 1 and 2 as

$$\underline{v}_1 = (v_0 + \omega_s R\sin\theta_1)\underline{i} - \omega_s R\cos\theta_1 \underline{j} \qquad (52)$$

and

$$\underline{v}_2 = (v_0 - \omega_s R\cos\theta_1)\underline{i} - \omega_s R\sin\theta_1 \underline{j} \qquad (53)$$

Using Equations 50, 52 & 53 we can write the forces on faces 1 and 2 as

$$\underline{F}_1 = -\frac{1}{2}\rho S_1 C_D\left[(v_0^2\cos\theta_1 + v_0\omega_s R\sin\theta_1\cos\theta_1)\underline{i} - v_0\omega_s R\cos^2\theta_1 \underline{j}\right] \qquad (54)$$

and

$$\underline{F}_2 = -\frac{1}{2}\rho S_2 C_D\left[(v_0^2\sin\theta_1 - v_0\omega_s R\sin\theta_1\cos\theta_1)\underline{i} - v_0\omega_s R\sin^2\theta_1 \underline{j}\right] \qquad (55)$$

Now we know that the torque contributed by each face can be written as

$$\underline{T}_i = \underline{r}_i \times \underline{F}_i \qquad (56)$$

and so the total torque is

$$\underline{T} = \underline{T}_1 + \underline{T}_2 \ . \qquad (57)$$

The combination of the above results gives an expression for the instantaneous torque on the satellite as

$$\underline{T} = \frac{1}{2}\rho S C_D v_0 \omega_s R^2 \{\sin^3\theta_1 + \cos^3\theta_1 + \\ + \sin\theta_1 \cos\theta_1 (\sin\theta_1 + \cos\theta_1)\}\underline{k} \qquad (58)$$

Now the average torque over one complete revolution is

$$\langle \underline{T} \rangle = \frac{1}{2\pi} 4 \int_0^{\pi/2} \underline{T}\, d\theta_1 \qquad (59)$$

so that

$$\langle \underline{T} \rangle = \frac{2}{\pi}\rho S C_D v_0 \omega_s R^2 \underline{k} \ . \qquad (60)$$

The spin decay is governed by the angular momentum equation

$$\frac{d\underline{H}}{dt} = \langle \underline{T} \rangle \qquad (61)$$

and since the spacecraft is axisymmetric $\underline{H} = I\underline{\omega}$. Hence we have the result

$$\frac{d\omega}{dt} = \frac{2}{I\pi}\rho S C_D v_0 \omega_s R^2 = \omega_s \Gamma \ . \qquad (62)$$

For a circular orbit, the solution of this is simple as Γ is a constant. This gives

$$\omega_s = \omega_0 \exp(\Gamma) \ . \qquad (63)$$

When considering an elliptic orbit however, the solution is more complicated as both the velocity (v) and density (ρ) vary with time. If these parameters are written in terms of the eccentric anomaly, then Γ can be written as

$$\Gamma = -K_1 \rho_p a \sqrt{\frac{a}{\mu}} \int_{E=E_1}^{E=0} \exp\{-\beta(1-\cos E)\} \left\{ 2\left[\frac{\mu}{a(1-e\cos E)} - \frac{\mu}{2a} \right] \right\}^{1/2} (1-e\cos E)\, dE \quad (64)$$

where

$$K_1 = \frac{2}{I\pi} S C_D R^2 \quad . \quad (65)$$

The method used here ignores the changing velocity across the face of the satellite, but gives a useful first estimate using the drag coefficient approach. The results of this analysis are discussed in Section 5.4.

5.3.2 Accommodation coefficient approach

The torques on the spacecraft were then evaluated in terms of the accommodation coefficients using similar assumptions as above, that is, the velocity across each face of the satellite is equal to the velocity of the centre of pressure of that face and the force for that face acts at the centre of pressure. There was a problem with this second assumption as the normal component of the force on the surface (P_i) acted through the centre of mass of the body (see Figure 5.2) and therefore did not contribute to the torque. This meant that the parameter σ_n did not appear in the final expression and it was clear that the simplifying assumption made in Section 5.3.1 would not render useful results in this case.

To overcome this difficulty it was decided to divide the face into elements and evaluate the torque due to each one. This would eliminate both of the above assumptions, allowing the velocity of each element to be calculated separately.

Figure 5.3 can be used to define the normals to faces 1 and 2 as

$$\hat{n}_1 = \cos\theta_1 \underline{i} + \sin\theta_1 \underline{j} \qquad (66)$$

and

$$\hat{n}_2 = \sin\theta_1 \underline{i} - \cos\theta_1 \underline{j} \; . \qquad (67)$$

The position vector from the centre of the body to an element on face 1 is given by

$$\underline{r}_1 = R\hat{n}_1 + a\hat{n}_2 \qquad (68)$$

or

$$\underline{r}_1 = (R\cos\theta_1 + a\sin\theta_1)\underline{i} + (R\sin\theta_1 - a\cos\theta_1)\underline{j} \; . \qquad (69)$$

The velocity of this element is then given as

$$\underline{v}_1 = (\underline{v}_0 + \omega_s R\sin\theta_1 - \omega_s a\cos\theta_1)\underline{i} - (-\omega_s R\cos\theta_1 + \omega_s a\sin\theta_1)\underline{j} \; . \qquad (70)$$

The pressure and shear stress on the element are denoted by P and τ respectively (See Ref 24 for full definitions), and Van der Ha [Ref 20] simplified these to

$$P = (2-\sigma_n)\,[2\cos^2\theta_i + (v_m/v)^2] + \sigma_n\sqrt{\pi}\,(v_w/v)\cos\theta_i \qquad (71)$$

and

$$\tau = 2\sigma_t \cos\theta_i \sin\theta_i \; . \qquad (72)$$

These simplifications are based on the molecular speed ratio v/v_m for spacecraft in GTO. As STRV and MARECS-A are in the same orbit the speed ratio will be between 16 and 11 for both satellites (assuming an ambient atmospheric temperature between 500K and 1500K) and so the same simplifications apply.

The force on the element is therefore

$$\Delta \underline{F}_1 = (\underline{P}_1 + \underline{\tau}_1) S \ , \qquad (73)$$

where S is the area of the element ($S = \Delta a h$; h = height of satellite). From Figures 5.2 and 5.3, it can be seen that

$$\underline{P}_1 = P_1(-\hat{\underline{n}}_1) \qquad \text{and} \qquad \underline{\tau}_1 = \tau_1(-\hat{\underline{n}}_2) \ , \qquad (74)$$

so

$$\Delta \underline{F}_1 = -\Delta a h[(P\cos\theta_1 + \tau_1 \sin\theta_1)\underline{i} + (P_1 \sin\theta_1 - \tau_1 \cos\theta_1)\underline{j}] \ . \qquad (75)$$

Now the torque on the element becomes

$$\Delta \underline{T}_1 = -\Delta a h(P_1 a - \tau_1 R)\underline{k} \ . \qquad (76)$$

If we now use the normalised pressure and shear stress (P^* and τ^*) we get

$$\Delta \underline{T}_1 = -\frac{1}{2}\rho v_1^2 \Delta a h(P_1^* a - \tau_1^* R)\underline{k} \qquad (77)$$

where

$$P_1^* = P_1 / \frac{1}{2}\rho v_1^2 \ , \qquad \tau_1^* = \tau_1 / \frac{1}{2}\rho v_1^2 \ . \qquad (78)$$

Substitution for v_1^2 and integration across face 1 of the body from a = -R to a = +R, gives the torque due to that face as

$$\underline{T}_1 = \frac{1}{2}\rho S\left[\frac{2}{3}P_1^* R^2 v_0 \omega_s \cos\theta_1 + \tau_1^* R v_0^2 + \frac{4}{3}\tau_1^* R^3 \omega_s^2 + 2\tau_1^* R^2 v_0 \omega_s \sin\theta_1\right]\underline{k} \cdot \quad (79)$$

A similar analysis for face 2 of the body results with the expression

$$\underline{T}_2 = \frac{1}{2}\rho S\left[\frac{2}{3}P_2^* R^2 v_0 \omega_s \sin\theta_1 - \tau_2^* R v_0^2 - \frac{4}{3}\tau_2^* R^3 \omega_s^2 + 2\tau_2^* R^2 v_0 \omega_s \cos\theta_1\right]\underline{k} \cdot \quad (80)$$

The total instantaneous torque on the body is then given by the sum of the components. ie $\underline{T} = \underline{T}_1 + \underline{T}_2$. But $\tau_1^* = \tau_2^*$, and so after some manipulation we get

$$\underline{T} = \rho S v_0 \omega_s R^2\{d_1(\cos^3\theta_1 + \sin^3\theta_1) + d_2(\cos\theta_1 + \sin\theta_1) + d_3 + d_4(\sin^2\theta_1\cos\theta_1 + \cos^2\theta_1\sin\theta_1)\}\underline{k} \cdot \quad (81)$$

where

$$\left.\begin{aligned} d_1 &= \frac{2}{3}(2-\sigma_n) \\ d_2 &= \frac{(2-\sigma_n)}{3}\left(\frac{v_m}{v}\right)^2 \\ d_3 &= \frac{\sigma_n\sqrt{\pi}}{3}\left(\frac{v_w}{v}\right) \\ d_4 &= 2\sigma_t \ . \end{aligned}\right\} \quad (82)$$

The average torque over one complete revolution can again be evaluated using Equation 59 and the final result for the spin decay torque on a box-like satellite configuration is given by

$$\langle \underline{T} \rangle = \frac{2}{\pi}\rho s v_0 \omega_s R^2 \left(\frac{8}{9}(2-\sigma_n) + \frac{2}{3}(2-\sigma_n)\left(\frac{v_m}{v}\right)^2 + \frac{\pi\sqrt{\pi}}{6}\sigma_n \frac{v_w}{v} + \frac{4}{3}\sigma_t \right) \underline{k} \ . \qquad (83)$$

If this expression is equated to Equation 60 and a value of 0.9 used for both σ_n and σ_t (near diffuse re-emission), then this results with a value for the drag coefficient of 2.23. Comparing this result with the generally accepted value of $C_D = 2.2$ gives confidence that the expressions are of the correct form.

This equation is of the same form as Equation 60 and the spin rate can again be determined using

$$\omega_s = \omega_0 \exp(\Gamma) \ , \qquad (84)$$

but this time Γ is written as

$$\Gamma = -K_2 \rho_p a \sqrt{\frac{a}{\mu}} \int_{E=E_1}^{E=0} \exp\{-\beta(1-\cos E)\} \ x \left\{ 2\left[\frac{\mu}{a(1-e\cos E)} - \frac{\mu}{2a} \right] \right\}^{1/2} (1-e\cos E)\, dE \ , \qquad (85)$$

where

$$K_2 = \frac{2}{I\pi} S R^2 \left(\frac{8}{9}(2-\sigma_n) + \frac{2}{3}(2-\sigma_n)\left(\frac{v_m}{v}\right)^2 + \frac{\pi\sqrt{\pi}}{6}\sigma_n \frac{v_w}{v} + \frac{4}{3}\sigma_t \right) \underline{k} \ . \qquad (86)$$

5.4 Spin Decay Predictions

5.4.1 Eddy Currents

To predict the spin decay of STRV in GTO due to eddy currents requires the evaluation of the integral in Equation 48. As it is a complicated expression it was decided to carry out the integration numerically using routines from Ref 25. Once the software had been debugged, a check was made to verify the calculations. This was to use data from the Aryabhata satellite [Ref 2] and produce a time history of the spin rate. Figure 5.4 was produced and is identical to figure 2 in Ref 2 and so indicated that the software was working correctly in this simpler case.

The next step was to use the data for STRV-1 as the input file. This was carried out and Figure 5.5 was the result. This graph shows two lines, one for the maximum spin rate and the other for the minimum; the spin rate should lie between these two lines depending on the spacecraft's attitude with respect to the Earth's magnetic field lines. It should be noted that the maximum final spin rate relates to the minimum spin decay and vice-versa.

Although the attitude constraints for STRV are not stringent, work at DRA (Farnborough) has indicated that it should be possible to keep the spin axis perpendicular to the orbit plane. If this is the case, then the spin axis will lie roughly in the 'best orientation' as far as spin decay is concerned (ie the spin decay will be minimal). This is because the $\pm$X and $\pm$Y faces will be almost parallel to the field lines and therefore will not be crossed by them. If we consider the other case, with the spin axis in the orbit plane then the side faces will continually cut the field lines and hence larger eddy currents will be induced.

The magnitude of the induced currents (and hence the spin decay) is dependent on the conductivity of the outer shell of the spacecraft. Because of the physical make up of the Carbon/PEEK structure it is difficult to measure the

conductivity for STRV, but a value of $\sigma_{STRV} = 4x10^7 ohm^{-1}m^{-1}$ was used for the generation of Figure 5.5. The true value is likely to be less than this as the value for aluminium is $3.2x10^7 ohm^{-1}m^{-1}$. Figure 5.6 was produced using the conductivity as a variable to indicate how the final spin rate after 365 days would vary with different values of σ.

As can be seen, if the spin axis is in the optimum attitude then knowledge of the conductivity has little effect on the predicted final spin rate, but if the attitude were to be near the maximum spin decay attitude then the final spin rate could vary from $\approx$9.5rpm to $\approx$6.5rpm, depending on the shell's conductivity.

5.4.2 Aerotorques

Most authors who investigate the spin decay of spacecraft in elliptic orbits neglect the effect of the aerotorques and consider only the eddy current effects. As the aerotorques are the major perturbation to the STRV's attitude it was thought necessary to examine the spin decay caused by this mechanism. The software used to make the predictions for the eddy current spin decay in Section 5.4.1 was altered to evaluate the integral of Equation 85 and used to determine the spin decay due to the aerodynamic effects. Figure 5.7 was produced and shows the spin rate of STRV during the year long mission.

It can be seen from this diagram that the spin rate will fall to 9.8rpm in 365 days because of the aerotorques. This result is derived for the case where the spin axis is perpendicular to the velocity vector (See Section 5.3.2) as this is thought to be the worst case (maximum) for aerotorque spin decay, but the best orientation (minimum) for eddy current spin decay. The two values are of the same order of magnitude and this shows that the eddy currents are likely to be the greater cause of spin decay, possibly reducing the spin rate to 6.5rpm in the year long mission. Even so, the assumption that the aerotorques are negligible should be treated with caution as in some circumstances the effects from both mechanisms can be of the same order of magnitude

5.5 Summary

This chapter investigates the two main mechanisms thought to cause spin decay of satellites in orbit, aerotorques and eddy current torques. Expressions are derived for the two cases for a satellite in an elliptic orbit, where variations in orbital velocity, atmospheric density and geomagnetic field strength cannot be assumed constant. The effects of these torques are evaluated numerically and it appears that the eddy current effects are usually more significant, possibly causing the spin rate of STRV-1 to fall to 6.5rpm in the year long mission. If the spacecraft is in a 'bad' orientation for eddy current spin decay, then knowledge of the value of the conductivity of the satellite's shell is needed to predict the final spin rate.

The results from the analysis in this chapter indicate that the omission of a spin plane magnetorquer coil from the STRV-1 hardware definition should not cause problems with on-board experiments as a final spin rate of around 6.5rpm is predicted. The experiment primarily concerned with spin decay is the Neutraliser Experiment as described in Section 2.2, as this would be jeopordised if excessive xenon was required to perform 'top-up' manoeuvres to the spin rate. Should it be necessary to increase the spin rate back to 10rpm to reduce attitude perturbations then the small amount of gas required should not adversly affect this experiment.

6 GSI PARAMETERS EXPERIMENT

6.1 Introduction

The gas surface interaction (GSI) parameters are defined in the Introduction (Chapter 1) and are a measure of how the molecules of the upper atmosphere are accommodated to the spacecraft surfaces and the momentum exchange between the spacecraft and the atmospheric flow. The term 'accommodated' refers to the amount of time the molecules are in contact with the spacecraft, and this in turn determines how they are emitted from the surface. If the molecules are totally accommodated before re-emission then the reflected beam has a cosine velocity distribution and is said to be diffuse ($\sigma_n = \sigma_t = 1.0$), whereas if the molecules are not accommodated to the surface then the reflected beam is said to be specular in nature ($\sigma_n = \sigma_t = 0.0$). A specularly reflected beam has the same tangential momentum as the incident beam and the normal momentum component is reversed; analogous to a perfectly elastic ball bouncing on a hard surface (see Figure 1.1a & 1.1b).

Many authors and experimenters have tried to evaluate the type of re-emission using ground based facilities but with few conclusive results. Crowther [Ref 21] examines many of the current models available to describe the interactions taking place and Van der Ha [Refs 1 & 20] uses the Schaaf and Chambre model [Ref 3] to evaluate torques on the MARECS-A spacecraft. Throughout the literature, these and other authors [Refs 26, 27] indicate that the true nature of the particle re-emission is little understood, primarily because of uncertainties in the modelling process and difficulties in simulating the spacecraft environment in the laboratory. Better knowledge of the interaction process would improve satellite drag calculations and lifetime predictions and this would enable more accurate fuel estimates to be made prior to missions, therefore reducing the spacecraft mass.

The work in Chapter 3 extends the Van der Ha work to enable the magnitude of the attitude perturbation to be expressed as a function of the spin axis direction with respect to the perigee velocity vector direction and the momentum accommodation coefficients (MAC's). Chapter 5 develops expressions for the aerodynamic spin decay mechanisms from first principles. This Chapter proposes an orbital experiment to improve our present GSI knowledge using only general housekeeping data from the satellite and the predictions made in Chapters 3 and 5 along with a least squares differential correction method which will now be described.

6.2 Least Squares Differential Correction Method

Expressions to predict both the spin rate decay and the aerotorque attitude perturbations have been derived for a box-like satellite in terms of the accommodation coefficients (Chapters 3 and 5), and so if we can measure the changes from the spacecraft data then, in theory, it is possible to improve our initial estimate of the MAC's. To do this we can propose the use of a Least Squares Differential Correction (LSDC) Method.

First of all, we must have an initial estimate of the parameters involved in the problem (the MAC's). Then inputting this estimate into the software it is possible to predict theoretically how the attitude or spin rate will change. This can then be compared with actual measurements of the attitude and spin rate derived from flight data. This comparison will generate quantified differences between the predicted and observed changes, and these differences can be used in the LSDC procedure to generate corrections to the initial estimates of the GSI parameters. This process can be repeated iteratively to refine knowledge of these parameters. A brief description of the standard LSDC method follows (See Ref 28 for more detailed description).

Let the initial estimate of the parameters be denoted by $\Upsilon_{Nx1}^{(o)}$ where

$$\Upsilon^{(o)}_{Nx1} = \begin{pmatrix} \Upsilon_1 \\ \cdot \\ \cdot \\ \cdot \\ \Upsilon_N \end{pmatrix} \qquad (87)$$

The predicted change (in spin rate or spacecraft attitude) is then given by $\eta_K^{(p)}$, and the observed change is given by $\eta_K^{(ob)}$. From these two matrices it is possible to write the residuals $\Delta\eta_K$,

$$\Delta\eta_K^{(o)} = \eta_K^{(ob)} - \eta_K^{(p)} \ . \qquad (88)$$

Assuming that the residuals are small (ie. the initial estimate was a good one), then because the values of $\Delta\eta_K^{(o)}$ are functions of the initial estimate, we can write

$$\Delta\eta_K^{(o)} = \sum_{j=1}^{N} \frac{\partial\eta_K}{\partial\Upsilon_j} \Delta\Upsilon_j \ . \qquad (89)$$

If we write this in matrix form, Equation 89 becomes

$$\Delta\eta^{(o)}_{Kx1} = A_{KxN} \Delta\Upsilon_{Nx1} \ , \qquad (90)$$

where

$$\Delta\Upsilon_{Nx1} = \begin{pmatrix} \Delta\Upsilon_1 \\ \cdot \\ \cdot \\ \cdot \\ \Delta\Upsilon_N \end{pmatrix} , \qquad \Delta\eta^{(o)}_{Kx1} = \begin{pmatrix} \Delta\eta_1^{(o)} \\ \cdot \\ \cdot \\ \cdot \\ \Delta\eta_N^{(o)} \end{pmatrix} ,$$

and

$$A_{KxN} = \begin{pmatrix} \frac{\partial \eta_1}{\partial \Upsilon_1} & \cdots & \frac{\partial \eta_1}{\partial \Upsilon_N} \\ \vdots & & \vdots \\ \frac{\partial \eta_K}{\partial \Upsilon_1} & \cdots & \frac{\partial \eta_K}{\partial \Upsilon_N} \end{pmatrix} .$$

In the case here, the partial derivatives in matrix A represent how the magnitude of the observations (spin rate decay or attitude perturbation) vary with the estimated parameters (the MAC's). These partial derivatives can either be determined analytically or numerically.

There will obviously be some errors in our knowledge of the measured spacecraft attitude or spin rate and these must be included into Equation 90

$$\Delta \eta^{(o)}_{Kx1} = A_{KxN} \Delta \Upsilon_{Nx1} + E_{Kx1} . \qquad (91)$$

If K > N, that is we have more observations than unknowns then the system is over-determined and we must use a least squares method to find the solution. The most common way to do this is to minimise the sum of the squares of the weighted residual errors Φ_E, where

$$\Phi_E = E^T_{1xK} W^{-1}_{KxK} E_{Kx1} \qquad (92)$$

and W^{-1}_{KxK} is the diagonal weighting matrix shown overpage.

In this matrix, σ_K^2 is the variance of $\eta_K^{(o)}$. To minimise Φ_E we need $\partial\Phi/\partial(\Delta\Upsilon) = 0$, and so by combining the above equations we can show that

$$\Delta \Upsilon = (A^T W^{-1} A)^{-1} (A^T W^{-1} \Delta \eta^{(o)}) . \qquad (93)$$

The weighting matrix is

$$W^{-1} = \begin{pmatrix} \frac{1}{\sigma_1^2} & \cdots & 0 \\ \vdots & & \vdots \\ 0 & \cdots & \frac{1}{\sigma_K^2} \end{pmatrix} .$$

From this a new estimate of the values in the Υ matrix is given by

$$\Upsilon^{(1)} = \Upsilon^{(0)} + \Delta\Upsilon \, . \tag{94}$$

This process can now be repeated iteratively, refining our knowledge of Υ (the MAC's) until some specified convergence criterion is satisfied.

6.3 Perturbation Measurement Strategy

Before decisions can be made as to how or when the required measurements should be made it is necessary to determine whether it would be best to use measurements of attitude perturbations or spin rate decay as the mechanism by which to improve our estimate of the MAC's. The attitude method at first appears the better choice due to the larger change each orbit, approximately 2°, but the measurement of spin rate only requires the time between two sun sensor pulses to be measured and so this needs further examination.

6.3.1 Measurement of spin rate

As mentioned above, the measurement of spin rate only requires the time to be measured between two sun sensor outputs. No knowledge of the sensor alignment or accuracy is required and the only assumption is that the pulse produced each revolution is identical. For STRV-1 there is a clock running at

4MHz and so one revolution at 10rpm will correspond to $24x10^6$ counts. If near diffuse re-emission is assumed then Figure 5.7 indicates the spin rate due to aerotorques will fall by $2.4x10^{-4}$ rpm/orbit, and so per orbit period there will be 576 more counts for each revolution of the spacecraft about its spin axis. If specular reflection is assumed then the spin rate will fall slightly faster at the rate of $2.6x10^{-4}$rpm/orbit. This means that there would be 624 extra counts per orbit period, and this difference of only 48 counts corresponds to only 0.0002% of the initial count of $24x10^6$ and will be difficult to measure.

The above assumption of the sun sensor output being identical for each pulse is, in reality, unlikely to be true and so filtering out any errors in these measurements will induce further uncertainties. It is therefore unlikely that the spin decay will be of help for determining the GSI parameters.

A further factor against the use of spin decay to estimate the GSI is the conclusions of the work in Section 5.4.1. It was found that, even in an optimum orientation, the spin rate will fall to around 9.5rpm due to eddy current mechanisms alone, which is a decay rate of $6x10^{-4}$ rpm/orbit. Because of this it will not be possible to record the accumulated decay over a few orbits as the decay rate due to the eddy currents is around 2.5 times faster than the aerotorque mechanism and will dominate any measureable spin decay.

6.3.2 Attitude measurement

There are two optimum times when it would be possible to observe the attitude changes, the first would be during a perigee pass and the second would be during a ground station pass. Therefore, two methods of acquiring attitude measurements are proposed, corresponding to these optimum times.

The first method entails recording attitude sensor output frequently during a perigee pass which typically lasts 7.5 minutes (Section 3.1). For the LSDC procedure to produce results about 40 measurements of the spacecraft attitude will

be required. This means that sensor data will be needed approximately every 10 seconds during a particular pass which will then have to be stored in the OBC as perigee is usually out of ground station contact. These measurements will then have to be downloaded at a later time for the analysis to begin.

The second method involves downloading sensor data frequently in real time during a ground station pass. This would enable a more detailed attitude reconstruction to be carried out in retrospect on the ground using a least squares method to smooth out the observations. On the next ground station pass a similar procedure will be carried out and the difference in the attitude can be attributed to the action of the aerotorques during the intervening perigee pass. This can be repeated over a number of orbits so that we can obtain the required number of observations (>40).

The magnitude of the expected orientation change of STRV in a maximum perturbation configuration varies from 2.63° (Specular) to 2.01° (Diffuse), that is a difference of 0.62°, for a complete perigee pass. For the changes to be measureable requires that the attitude sensors are at least of this accuracy, and ideally they should be more accurate. The sensor system on STRV will allow the relative attitude (from one orbit to the next) to be known to $\pm 0.5°$ so to try to take multiple measurements of the attitude variation during a single pass will be difficult. About 40 measurements will be required, varying in steps of about 0.05°. It seems, therefore, that the first method of data gathering will not be suitable for the purpose of determining the GSI parameters, whereas the second method in conjunction with a least squares method could supply data of sufficient accuracy.

The two methods above describe ideal theoretical situations for recording data. The method which is likely to conform to the general housekeeping activities of the STRV mission will be a combination of both methods. Attitude sensing will primarily be undertaken away from perigee and if there is ground station contact the data will be downloaded in real time, as suggested in the

second method above. Unfortunately, there is an unstated assumption in the second method which implies there is adequate ground station coverage each orbit for the attitude to be determined. This is not the case, and on those orbits which do not have contact with Lasham (the ground station) the data will have to be stored for downloading later, as in the first method. To achieve the best accuracy for the attitude determination process it is desirable to have observations over a long time period of time as this gives favourable Earth-Sun geometries for the reconstruction [Ref 22]. Rather than storing attitude data over this complete period, which would require a large amount of OBC memory space, small subsets of the data will be stored along with the time of observation, thus allowing attitude reconstruction at a later time (see Figure 6.1).

6.4 Centre of Mass Position

The position of the centre of mass (CoM) of the spacecraft will obviously have a large effect on the predicted magnitude of the aerotorques. For the experiment a relatively large offset (R_z) between the CoM and the geometric centre of the body is required to produce perturbations large enough to measure. However, for the general attitude control operations it is best to have this dimension (R_z in Appendix C) as small as possible, preferably zero. If a serious proposal for this experiment is made then it is important to ensure an adequate value of R_z can be built into the design without compromising the attitude control activities. A 2.3° change (average of specular and diffuse predictions) was calculated for the spin axis direction using the STRV data. This assumed a 5cm offset between the CoM and the geometric centre of the body. The competing attitude control requirements demand a change in spin axis direction of no more than 1° per orbit, so to adhere to this an offset of no more than 2cm would be required. This has repercussions for the proposed experiment as passing through perigee in anything but an optimum orientation will result in an attitude change less than 1°. Consequently the difference between the specular and diffuse extremes will be much reduced and more difficult to distinguish.

6.5 Experiment Outline

6.5.1 Introduction

This section details an orbital experiment which could be carried out in the future using data either from STRV-1 or another spinning satellite. With some alteration it should be possible to adapt the ideas presented here to analyse data from three axis stabilised spacecraft.

Before any requests for a CoM offset are made or a serious proposal for an experiment submitted it is important to determine whether or not the sensor accuracies of the attitude control system (ACS) of the considered satellite will be adequate for the experiment to be carried out. To achieve this it is necessary to simulate the spacecraft attitude determination data and implement software which is likely to be used for the experiment. This will enable a 'simulated analysis' to be carried out and will give an estimate of the accuracy required of the spacecraft sensors.

6.5.2 Simulated data sets

As a first step a data set simulating the observed state of the spacecraft (simulated flight data) should be produced. This will represent the 'real' attitude of the satellite in inertial space in terms of the RA and DEC of the spin axis. To form this set the aerotorque prediction software can be used with the MAC's both equal to 0.9 which is the value assumed by many authors. This was carried out and the data in Table 4 (overpage) was generated using STRV data and an initial orientation of RA = 270° and DEC = 83°. With the particular orbit parameters as used here, this gives a SAA of 90° which is also included in the data.

Ideally the 'actual' angles for RA and DEC, given in Table 4, would be the values recorded on the ground, but in practice this will not be the case. The

'true' value will be corrupted by sensor and attitude determination errors so that we have

$$\text{observed} = \text{actual} + \text{errors} . \tag{95}$$

The magnitude of these errors will be dependent on the conditions for each observation and must be modelled. If, for example, the 1σ error on the final observation in Table 4 is $\pm 0.1°$, then there is a 67% probability (assuming normal distribution) that the observed value will lie in the range 93.61° to 93.81°. The magnitude and distribution of these errors are important for the error matrix in Equation 91 and are fundamental in determining if the satellite data are of use for the proposed GSI experiment. When these have been obtained it should be possible to develop a simulated flight data set based on Table 4 and Equation 95.

TABLE 4

'Actual' Attitude Variations using the MAC's = 0.9

(All angles in degrees)

Ecc. Anom.	RA	DEC	SAA
180.0	270.00	83.00	90.000
355.0	270.00	83.00	90.061
365.0	270.00	85.08	90.070
715.0	270.00	85.08	90.208
725.0	270.00	87.17	90.233
1075.0	270.00	87.17	90.387
1085.0	270.00	89.25	90.428
1435.0	270.00	89.25	90.598
1445.0	270.00	91.33	90.654
1795.0	270.00	91.33	90.839
1805.0	269.99	93.41	90.910

The attitude of the spin axis can then be theoretically predicted using the same method as above with an initial guess that the MAC's = 0.8 (see Table 5). The LSDC software will then be used to try and refine the initial guess of $\sigma_n = \sigma_t$

= 0.8 to the value of 0.9 used for the observed data. This procedure will have the effect of verifying the analysis software, but more importantly it will also determine the sensor accuracy required to achieve useful results from the GSI experiment.

TABLE 5

'Predicted' attitude variations using MAC's = 0.8

(All angles in degrees)

Ecc. Anom.	RA	DEC	SAA
180.0	270.00	83.00	90.000
355.0	270.00	83.00	90.061
365.0	270.00	85.14	90.070
715.0	270.00	85.14	90.209
725.0	270.00	87.28	90.235
1075.0	270.00	87.28	90.389
1085.0	270.00	89.43	90.431
1435.0	270.00	89.43	90.603
1445.0	270.00	91.57	90.660
1795.0	270.00	91.57	90.847
1805.0	269.99	93.71	90.920

As can be seen from these two tables, it is unlikely that the attitude sensors on STRV in particular will be able to give results to the required accuracy for a satisfactory outcome to the experiment. This is because for this arbitrary example the difference between the predicted and observed variations is only 0.3° whereas the attitude will only be reconstructed to $\pm 0.5°$. Alternatively, it may be possible to extend the analysis to more than the 5 perigee passes shown in the tables and allowing the perturbations to accumulate. Using this approach there would be a measureable attitude change after a number of orbits, but there may be problems with removing the effect of the variations in atmospheric density between perigee passes.

For further work to be carried out here it will be necessary to identify another spacecraft which could supply useful data.

6.5.3 Attitude Measurement Problem Areas

Two methods have been outlined in Section 6.3.2 to record attitude changes, the first involves measurements during a perigee pass. However the expected magnitude of each change is likely to be small and difficult to measure. The second involves taking measurements during a ground station pass. Mission analysis studies have shown that STRV will not be visible to the ground station each orbit, but it is still hoped to record the spacecraft attitude even when not in view. This will allow the attitude changes each orbit to be calculated and the aerotorque perturbation to be evaluated.

As the observations will be taken on separate orbits then the atmospheric density at perigee will vary each time and so it will be necessary to account for this when modelling the attitude changes. The problems and inaccuracies associated with predicting the state of the atmosphere are well known and therefore trying to predict the density during a perigee pass will induce significant errors [Refs 16 & 17]. Crowther [Ref 21] has shown that the change in the semi-major axis (a) of an elliptic orbit is predominantly due to drag effects and insensitive to the assumed nature of re-emission, so if these changes are measured then this will provide an opportunity to normalise the results and reduce the influence of the ill-determined density variation.

To a lesser extent, the variation of the spacecraft wall temperature each orbit will also alter the perturbations that are observed. This is because with a higher surface temperature, more momentum is carried away by the re-emitted particles, and hence the attitude change will be greater. If these effects are expected to be large then temperature sensor data from the satellite will also be needed to complete the analysis.

Finally, when evaluating the aerotorque perturbations it will be necessary to model any ACS actuations which occur during the perigee pass in question. The main actuators on STRV are magnetorquers and if these are controlled

autonomously in a closed loop system then it may be difficult to reconstruct the attitude changes due to their operation. The only way to overcome this problem would be to record all the ON/OFF times and download these along with the sensor data. A detailed magnetic field model would then be required on the ground to emulate the spin axis motion. A much simpler approach would be to switch the magnetorquers to off for the complete perigee pass so the full attitude change could be attributed to aerodynamic effects.

6.5.4 Further work

The proposal in the above sections still requires detailed work to be carried out before the experiment can be performed to improve our knowledge of the GSI. As suggested in Section 6.5.2 it is unlikely that STRV will provide useful data as the magnitude of the changes expected due to the different models are less than the accuracy of the attitude reconstruction process. This will not be known however until the 'simulated experiment' can be performed to assess sensor accuracies. It may therefore be necessary to identify other spacecraft with more accurate sensors before any further progress can be made. For each prospective satellite, a simulated experiment should be carried out which will determine the required accuracy of its sensors and centre of mass position to achieve satisfactory results. The LSDC procedure has only been outlined in this work and this will need extending into detailed software before the analysis can be carried out.

6.6 Summary

More detailed knowledge of the interaction between spacecraft surfaces and the rarefied upper atmosphere will aid in attitude perturbation predictions and satellite drag modelling. This will be of special importance to researchers when making predictions of re-entry times of uncontrolled spacecraft.

It is suggested that a least squares differential correction method could be employed using satellite attitude data to refine the values currently used for the momentum accommodation coefficients. Measurement strategies are outlined and it is noted that studies into the accuracy of the satellite sensor system would be required as part of any proposal for such an experiment.

As the perturbations given in this chapter are all maxima then, in reality, it is unlikely that STRV-1 will produce significant amounts of data to the required accuracy, but the analysis could still be carried out with data collected from other, more accurate, sources.

7 CONCLUSIONS

This thesis contains an overview of the perturbations induced in the spin vector of satellites whilst in elliptic orbits. The work is primarily based on geostationary transfer orbits and so both aerodynamic and magnetic field effects have been investigated. The aerodynamic torques acting on a spacecraft in such an orbit will be the main influence in changing the direction of the spin axis, whereas the spin rate will be affected mainly by eddy current effects. If the orbit has a higher perigee than the usual Ariane value of 200km then the aerotorques will have a much reduced effect in changing the attitude and eddy current spin decay effects would become the dominant perturbation.

The magnitude of the aerotorques are evaluated and the perturbations that they cause are predicted. For a 5cm offset between the CoM and the centre of the body and a spin rate of 10rpm the likely attitude change for STRV-1 will be of the order of 2° per perigee pass. However the ACS operational requirements will probably constrain the change to 1° per orbit and therefore a maximum CoM offset of 2cm is more likely. The software and theory used to make these predictions have been verified using flight data from other satellites (MARECS-A, Explorer 45, SKYNET 4C) and the design requirements of the attitude control hardware are examined.

Attitude manoeuvres using an aluminium spin axis coil are simulated using software and this shows that a possible 60° of precessional capability are available per perigee pass using the coil dimensions as calculated. An aluminium coil has since been included in the STRV design specifications. This has less than the planned capability of 90° per pass because of inaccuracies in estimating the mean value of the Earth's magnetic field strength during the torquing region of the orbit.

Two sources of spin decay have been identified for STRV, these are aerodynamic and induced eddy current effects. The eddy current mechanism was

found to be the more dominant effect throughout the complete orbit, possibly reducing the spin rate to 6.5rpm after the year long mission. Aerodynamic effects were found to be less of a problem with the spin rate only being reduced to 9.8rpm after one year in a worst case.

Finally, an experiment has been proposed which would use a least squares differential correction method to improve our understanding of the gas-surface interaction. It is suggested that either attitude perturbations or spin decay could be used for the investigation. However analysis of the magnitude of the aerodynamic spin decay shows that this is unlikely to provide useful results. The attitude perturbations provide more hope. If the spacecraft sensors are sufficiently accurate and the CoM offset is large enough, it should be possible to record the attitude each orbit and iteratively update our estimates of the GSI parameters. The STRV attitude can only be reconstructed to $\pm 0.5^{\circ}$ and this is unlikely to be good enough for the experiment to be carried out effectively. It is suggested that other satellite data are examined and another spacecraft targetted for the analysis to be continued.

8 REFERENCES

[1] Van der Ha J.C. "Attitude perturbations induced by free molecule flow interactions in perigee region", Acta Astronautica, Vol 13, No 6/7, pp301-309, 1986.

[2] Shrivastava S.K. & Rajasingh C.K. "Spin decay of 'Aryabhata'", Proc. Indian Academy Science Vol C Part 1. pp 141-147. March 1979.

[3] Schaaf S.A. & Chambre P.L. *Flow of rarefied gases*, Princeton University Press, 1961.

[4] Harris I.L. "An instrument to examine the effects of atomic oxygen in LEO", Proc COMADEM Symposium, Warsash, Hants, UK. 2nd - 4th July 1991.

[5] Greer W.A.D "Arc-jet studies of surface-induced luminescence relevant to spacecraft glow", PhD Thesis, Dept of Aero & Astro, Southampton University, Southampton, U.K. March 1991.

[6] Ryden K.A. et al "The Space Technology Research Vehicle (STRV-1)", Proc RAe Conference on Small Satellites, Culham, UK. 24th January 1991.

[7] Ryden K.A. & Markwell A.J. "Attitude control of a small spacecraft in an elliptical orbit" Presented at the 4th Annual USU/AIAA Conference on small satellites, 28-31 August 1990.

[8] Fearn D.G. et al "The development status of the Space Technology Research Vehicle" 42nd Congress of the International Astronautical Federation, October 5-11, 1991, Montreal, Canada. Paper Number IAF-91-008.

[9] Ryden K.A. "A Proposed Attitude Control System for a Small Spacecraft in an Elliptical Orbit" RAE Space Dept Working Paper No SP(89)WP52, Nov 1989.

[10] Wertz J.R. *Spacecraft attitude determination and control*, D Reidel Publishing Co. Dordrecht Holland, 1978.

[11] Flatley T.W, "Magnetic Attitude and Spin Control of the Small Scientific Satellite S^3-A" NASA TN D5572, Feb 1970, GSFC, Greenbelt, Md.

[12] Werking R.D, Beck J, Gardener D, Moyer P & Plett M "SSS-A Attitude Control Pre-Launch Analysis and Operations Plan" NASA Report.

[13] Kowalik H. "A spin and attitude control system for the ISIS-I and ISIS-B satellites", Preprints of the 3rd IFAC symposium on automatic control 3. Application Part 12. 1970. Journees d'electronique de Toulouse, France.

[14] Ferreira L,D. et al "Attitude Control Simulation of the Data Collecting Satellite SCD2" Presented at the 1st Brazilian Symp of Aerospace Technology, Sao Jose dos Campos, Brazil, 27-31 Aug 1990.

[15] Houchin P.P. "The Effect of Ariane 4 transfer Orbit Launch Epoch on Perigee Height" RAE Space Dept Working Paper No SP(90)WP22, May 1990.

[16] Hoots F. & France R. "Uncertainty estimation for satellite lifetime prediction", AAS/AIAA Astrodynamics Specialist Conference, 19-22 August 1991, Durango CO. Paper No. AAS 91-431.

[17] Roble R.G. "Global dynamic models of the Earth's upper atmosphere", AAS/AIAA Astrodynamics Specialist Conference, 19-22 August 1991, Durango CO. Paper No. AAS 91-489.

[18] King-Hele D.G. *Satellite orbits in an atmosphere*, Blackie, Glasgow, 1987.

[19] Jacchia L.G. "Thermospheric temperature, density & composition: New Models" Special Report 375, Smithsonian Astrophysical Observatory, March 15, 1977.

[20] Van der Ha J.C. "Approximate free-molecular flow torques on spinning satellites", The Journal of Astronautical Sciences, Vol 34, No 4, Oct-Dec 1986. pp 403-419.

[21] Crowther R. "The influence of the gas surface interaction on spacecraft orbital motion" PhD Thesis, Dept of Aero & Astro, Southampton University, Southampton, U.K. March 1989.

[22] Kelleher C. Space Dept. Defence Research Agency - Aerospace Division. Farnborough UK. Personal Communication.

[23] Whelan P.M. & Hodgson M.J. *Essential Principles of Physics*, J.W. Arrowsmith and Son, 1978.

[24] Bird G.A. *Molecular Gas Dynamics*, Oxford University Press, Oxford, UK. 1976.

[25] Press W.H, Flannery B.P, Teukolsky S.A & Vetterling W.T. *Numerical Recipes - The Art of Scientific Computing (FORTRAN Version)*, Cambridge University Press, Cambridge, UK. 1990.

[26] Boettcher R.D. "Analysis of free molecular effects on the attitude of satellites in Geostationary Transfer Orbit; Part 1 Theoretical Analysis" European Space Agency Contract Report No. DFVLR-IB 222-86 A 08. 1986.

[27] Knechtel E & Pitts W "Normal and tangential momentum accommodation for Earth satellite conditions" Astronautical Acta, Vol 18 pp 171-184, 1973.

[28] Vonbun K.O. & Kahn W.D. "Tracking systems, their mathematical models and their errors - Part I, Theory", NASA TN D1471. Goddard Space Flight Center, Greenbelt, Maryland. October 1962.

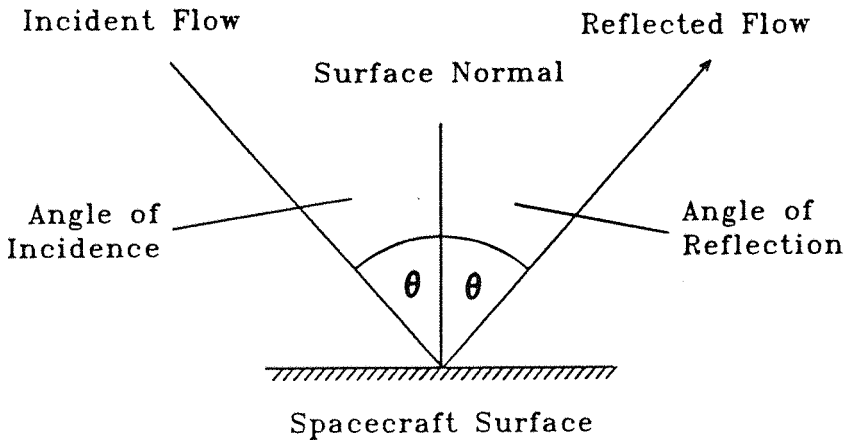

Figure 1.1a Specular Reflection

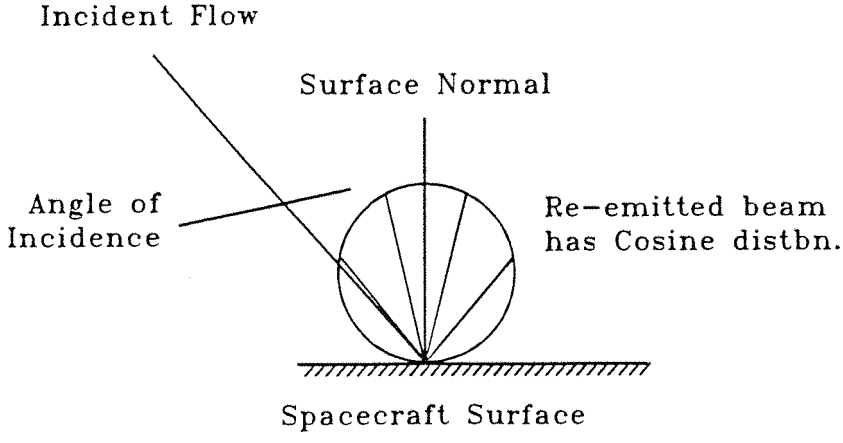

Figure 1.1b Diffuse Reflection

Figure 2.1
STRV-1

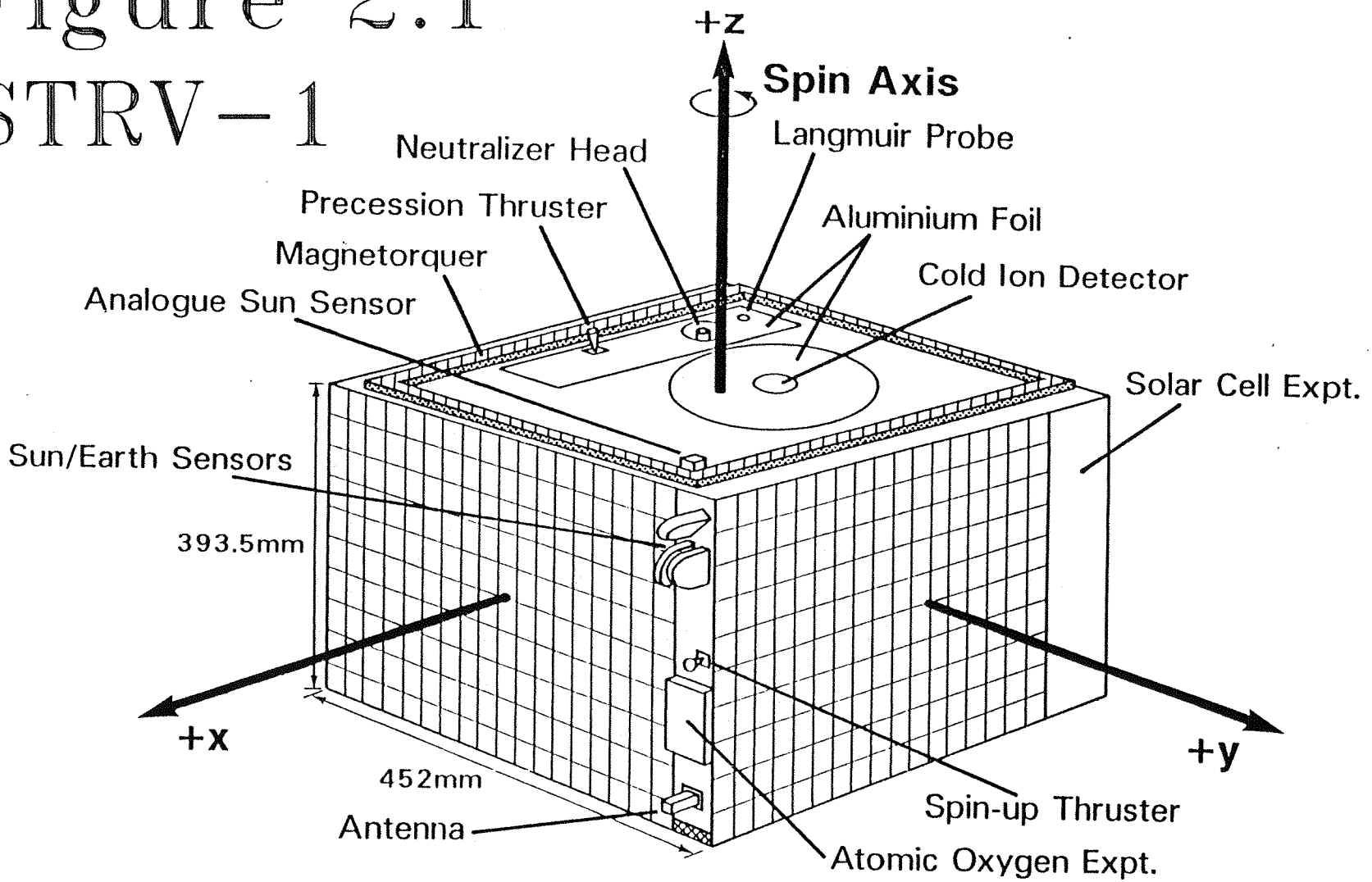

THE 'SUN-PERPENDICULAR' PLANE

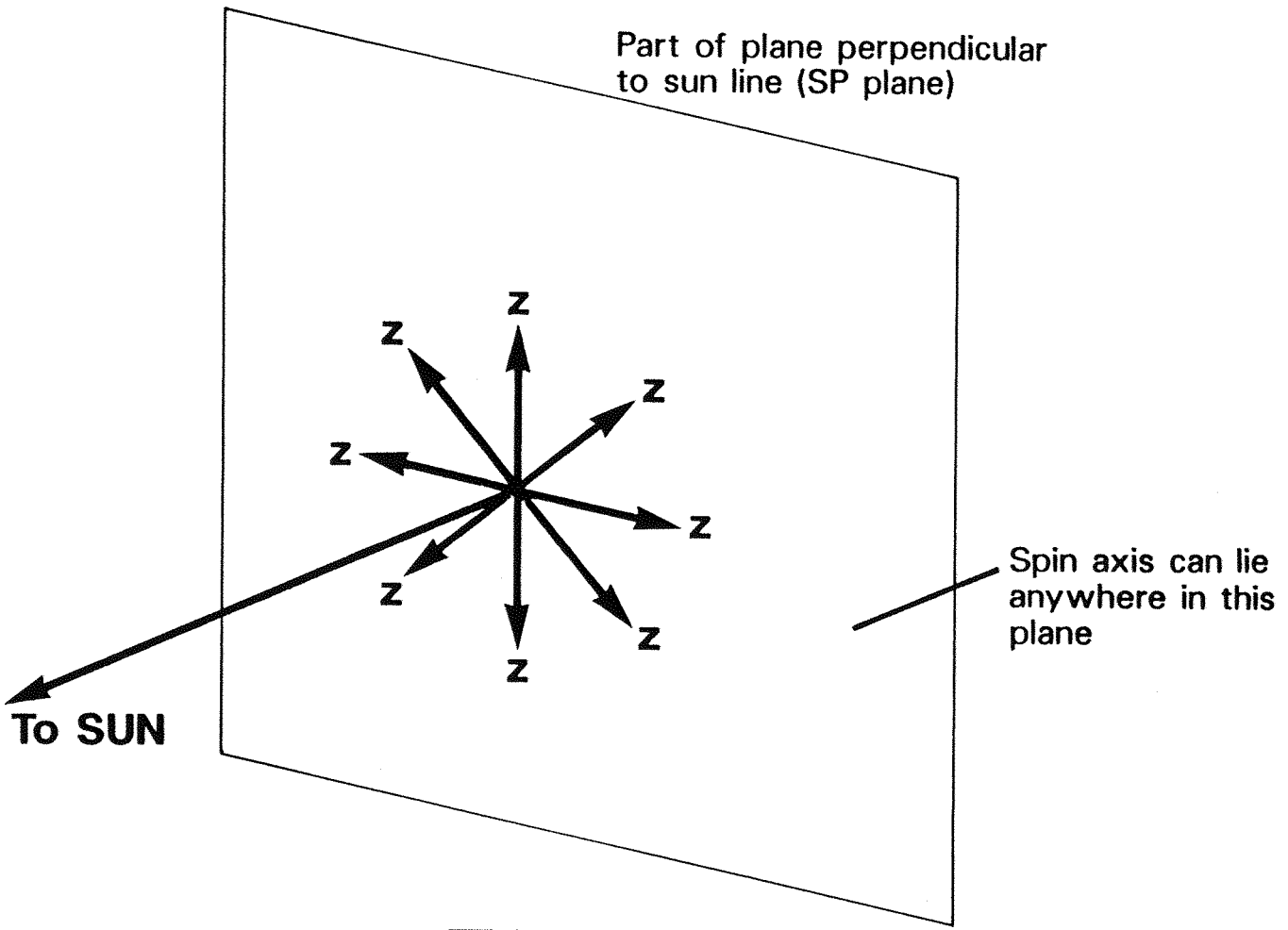

Figure 2.2

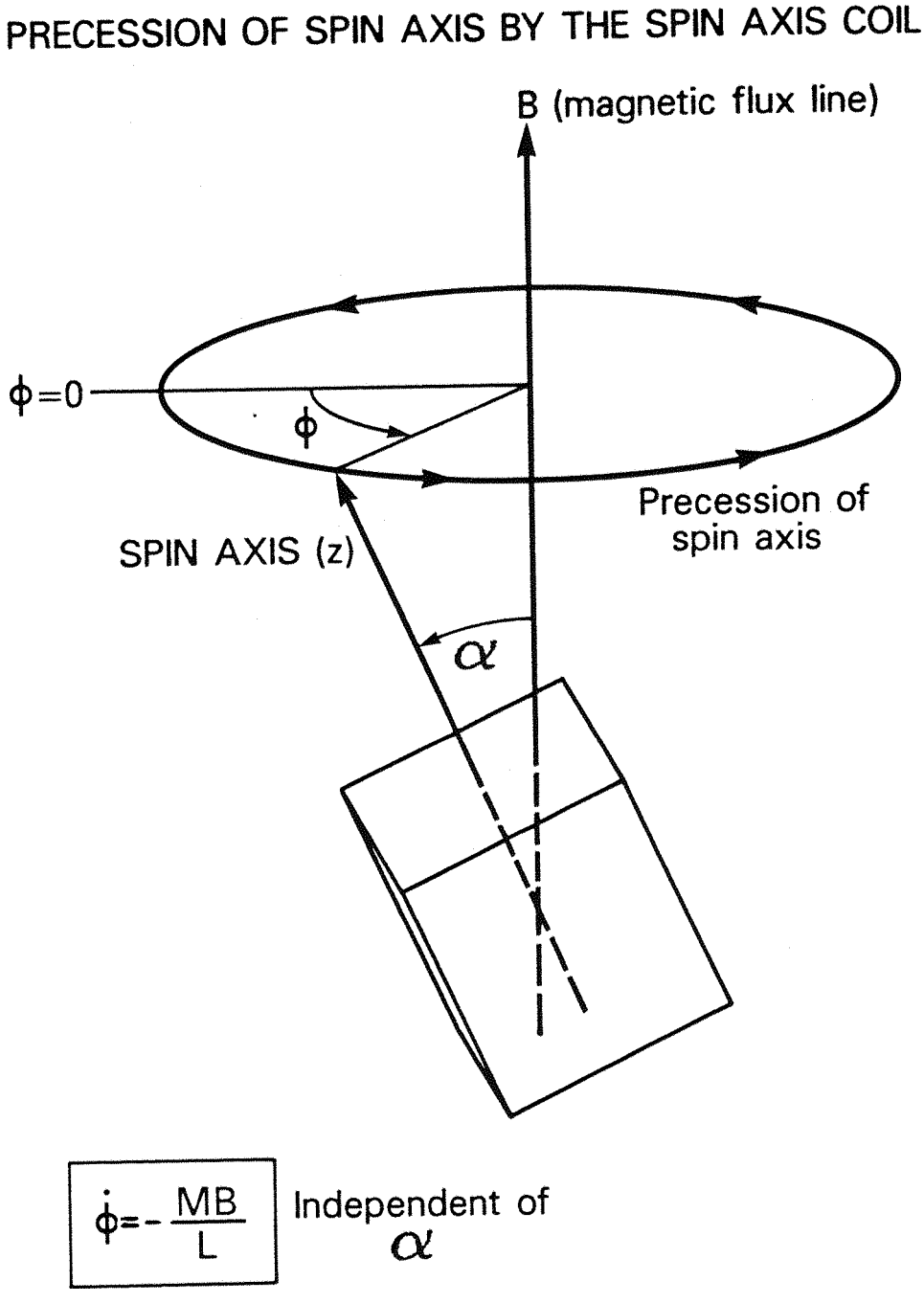
PRECESSION OF SPIN AXIS BY THE SPIN AXIS COIL
B (magnetic flux line)
ϕ=0
ϕ
Precession of spin axis
SPIN AXIS (z)
α
$\dot{\phi} = -\frac{MB}{L}$
Independent of α

Figure 2.3

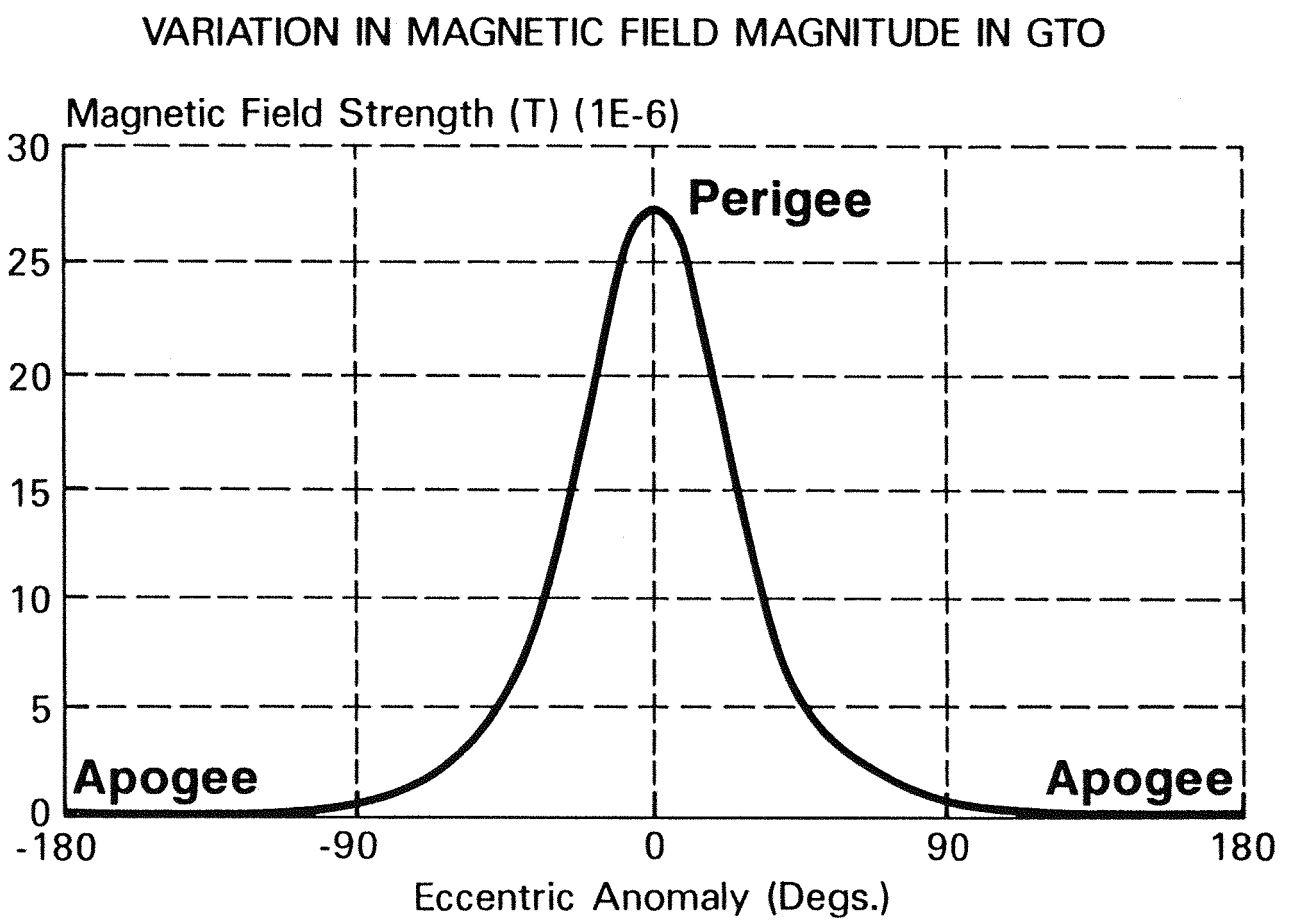
VARIATION IN MAGNETIC FIELD MAGNITUDE IN GTO
Magnetic Field Strength (T) (1E-6)
30
25
20
15
10
5
0
Perigee
Apogee
Apogee
-180
-90
0
90
180
Eccentric Anomaly (Degs.)

Figure 2.4

Eccentric Anomaly

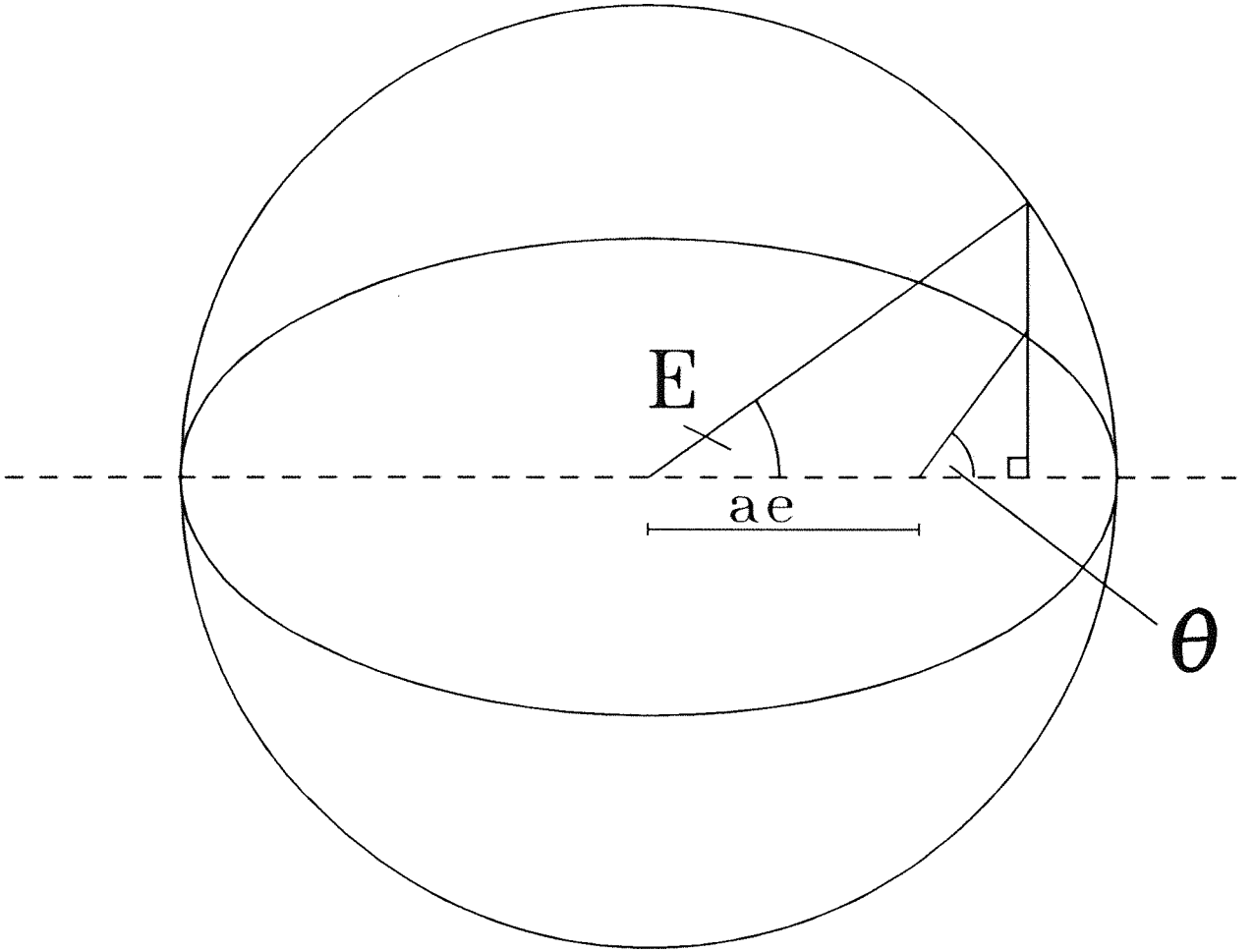

Figure 2.5

Time incremented orbit generator

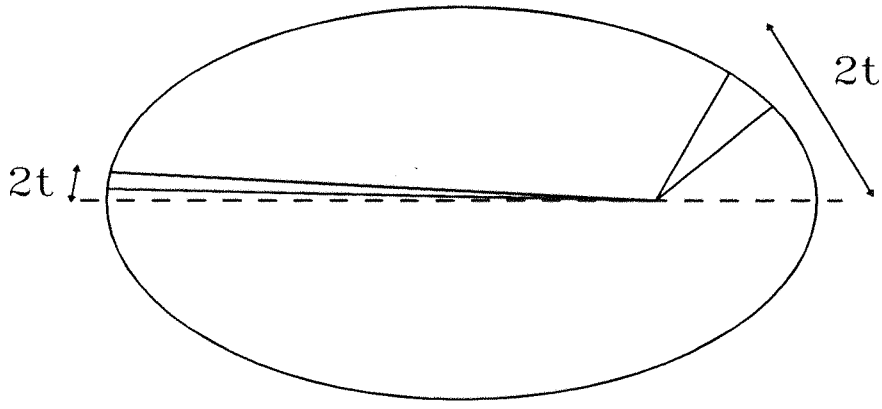

Figure 2.6

Modified orbit generator

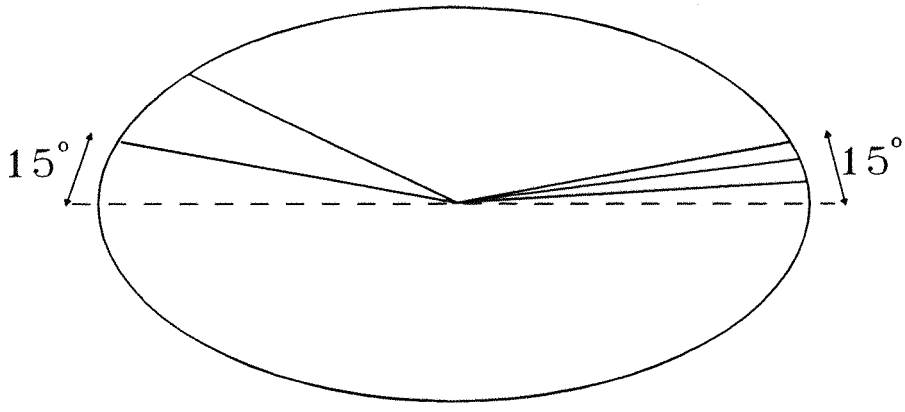

Figure 2.7

Solar Aspect Angle

STRV General Case FIGURE 2.8

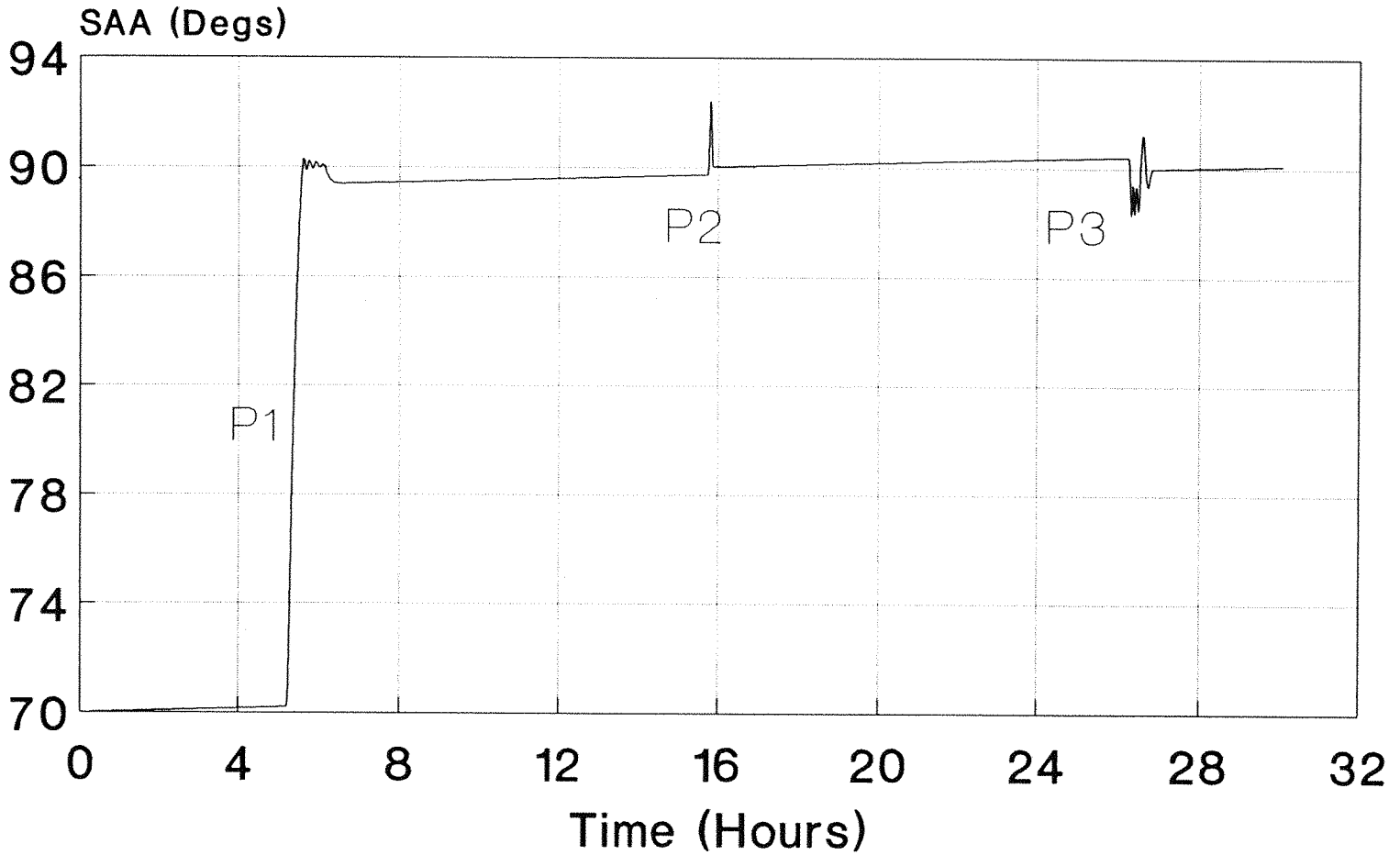

Solar Aspect Angle

STRV Worst Case FIGURE 2.9

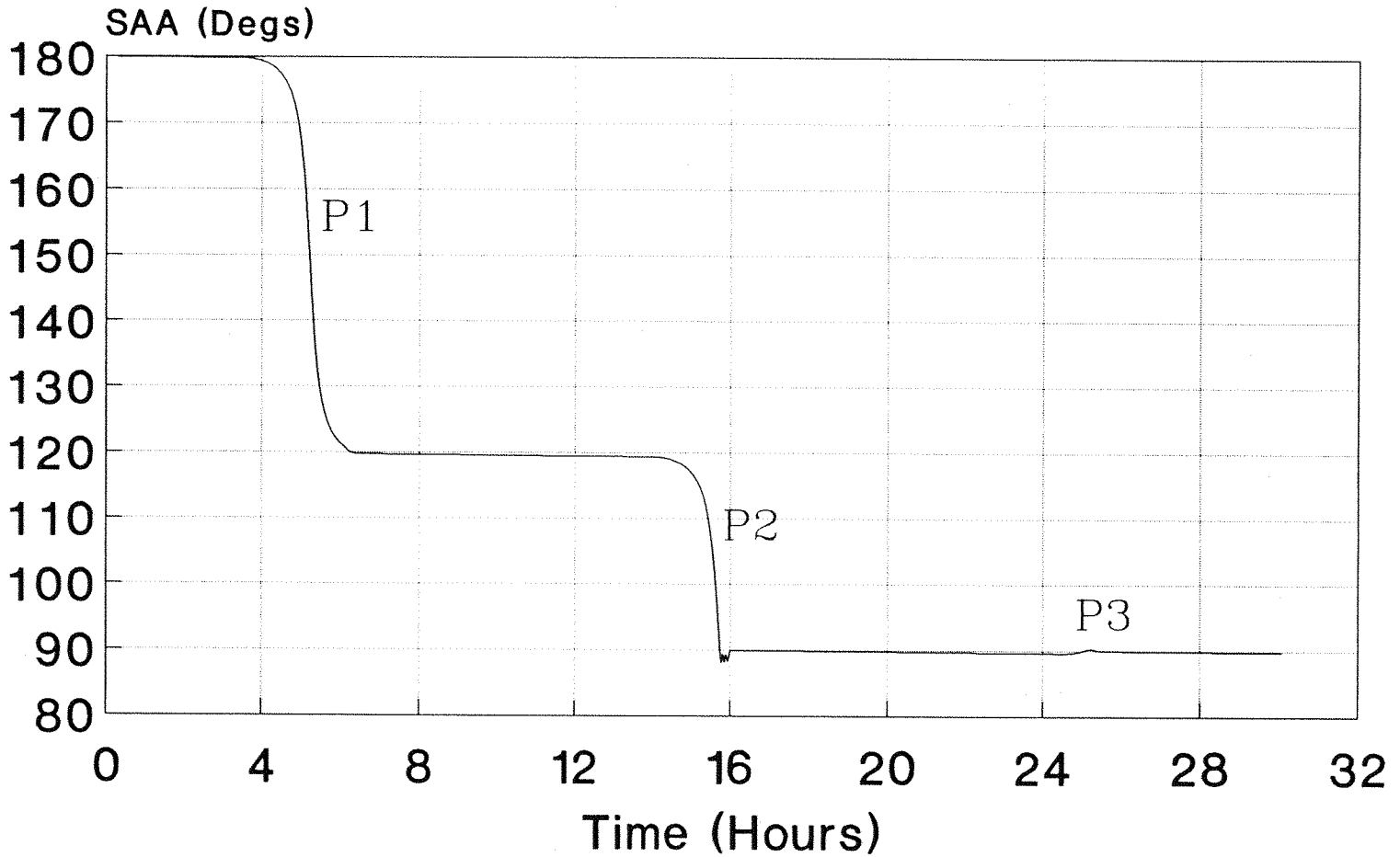

Figure 3.1

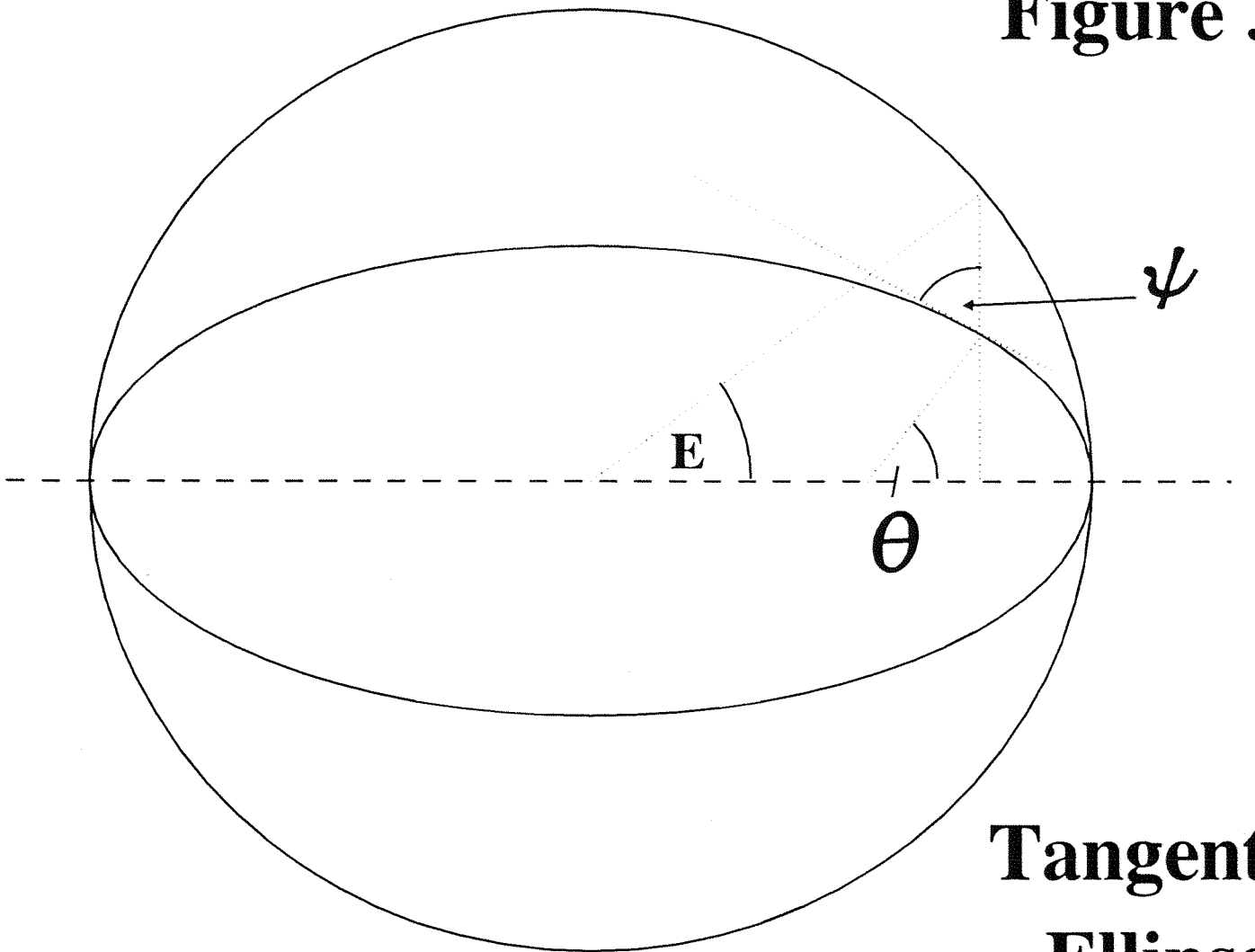

Tangent to Ellipse

Figure 3.2

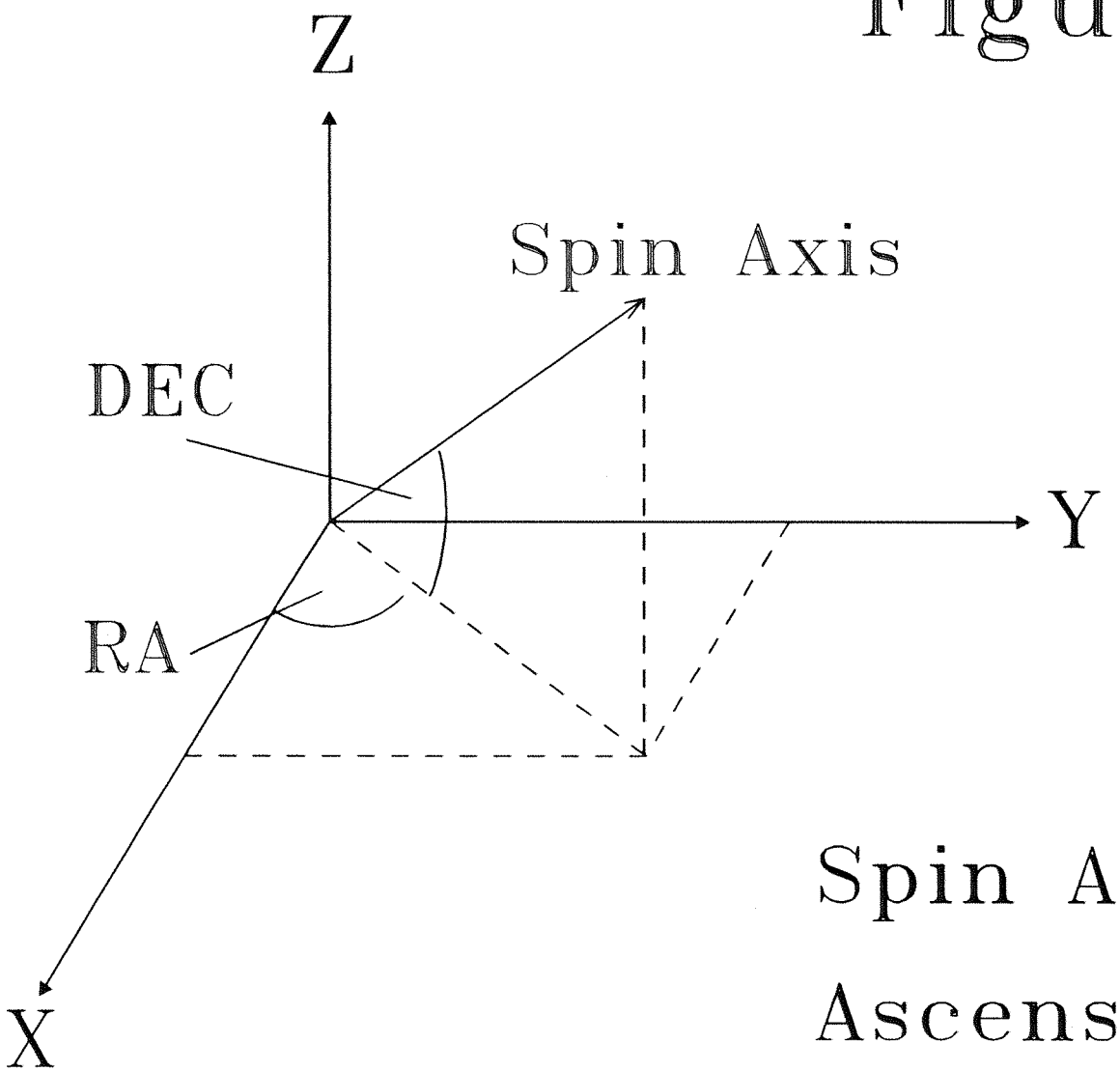

Spin Axis Right Ascension and Declination

PERIGEE
REFERENCE
FRAME

FIGURE 3.3

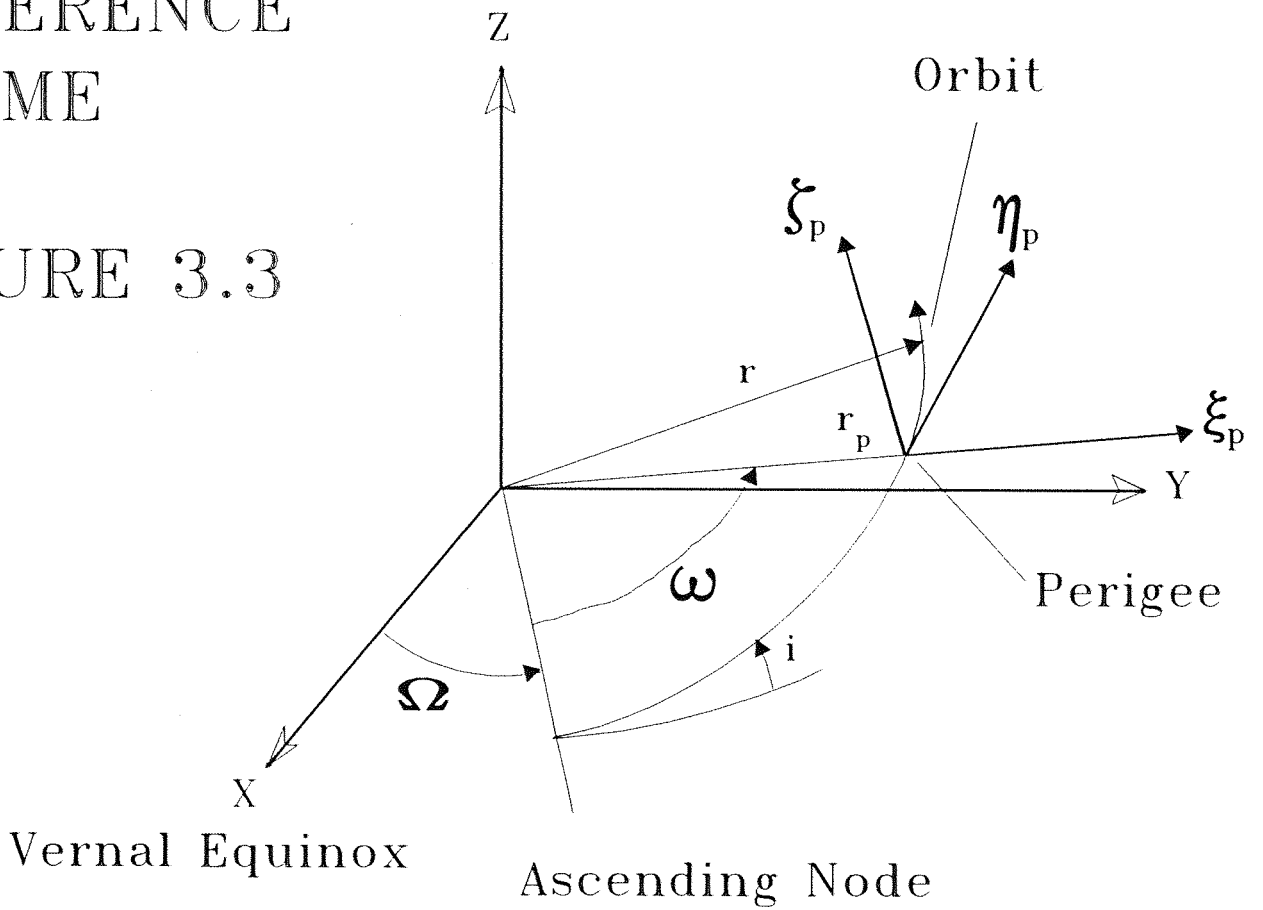

Cone and Clock Angles

FIGURE 3.4

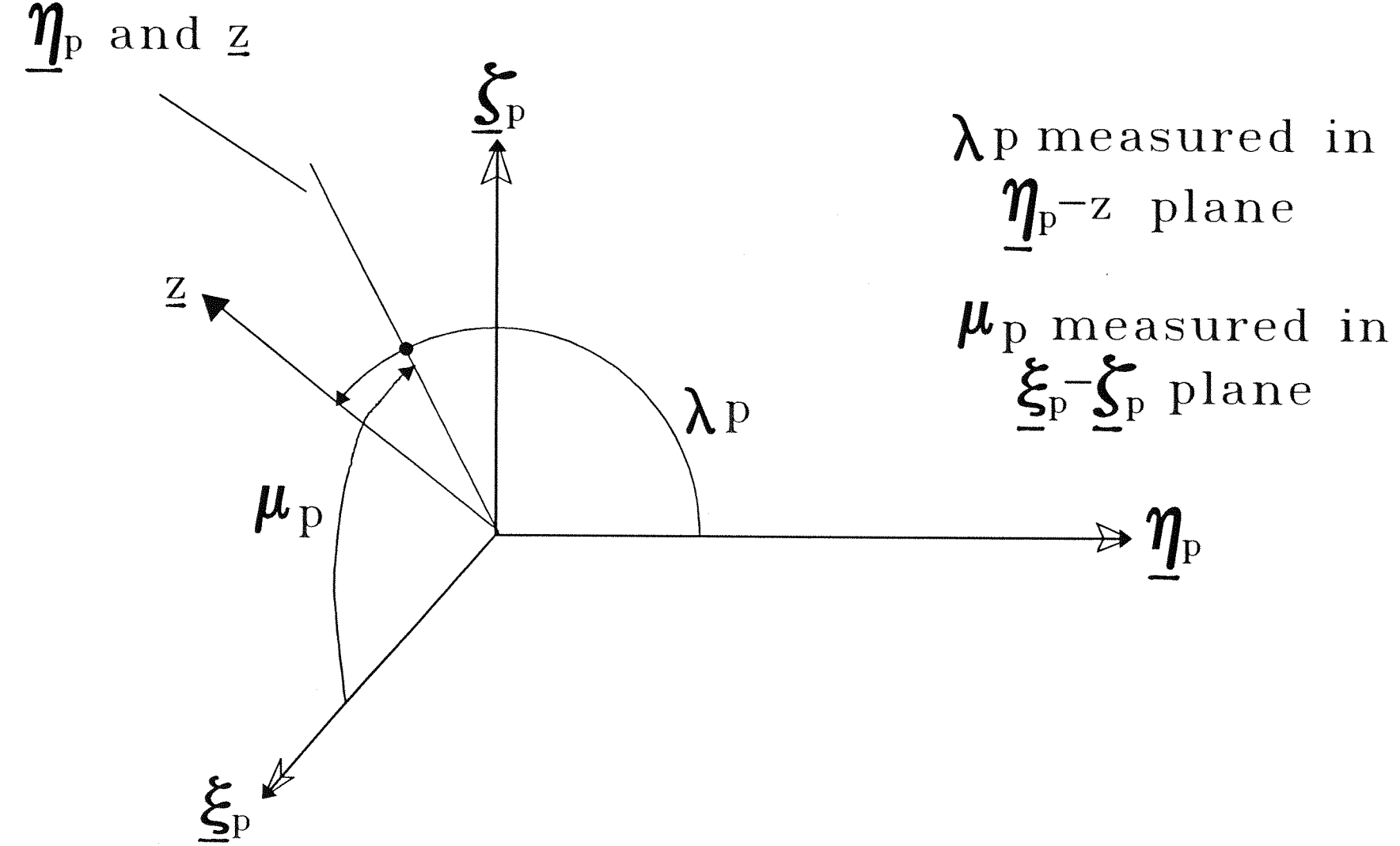

Aerotorques at Perigee
Figure 3.5

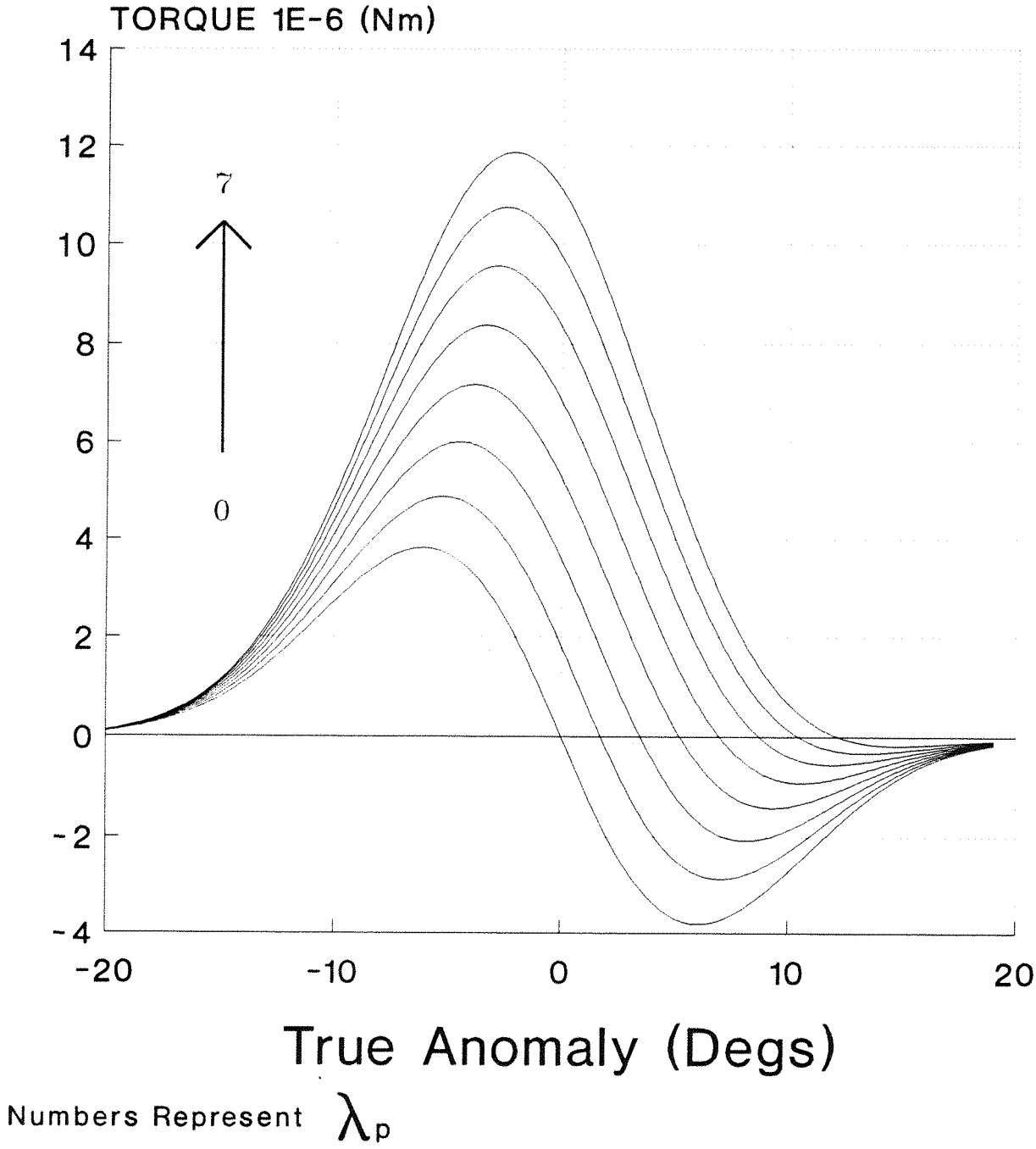

Numbers Represent λ_p

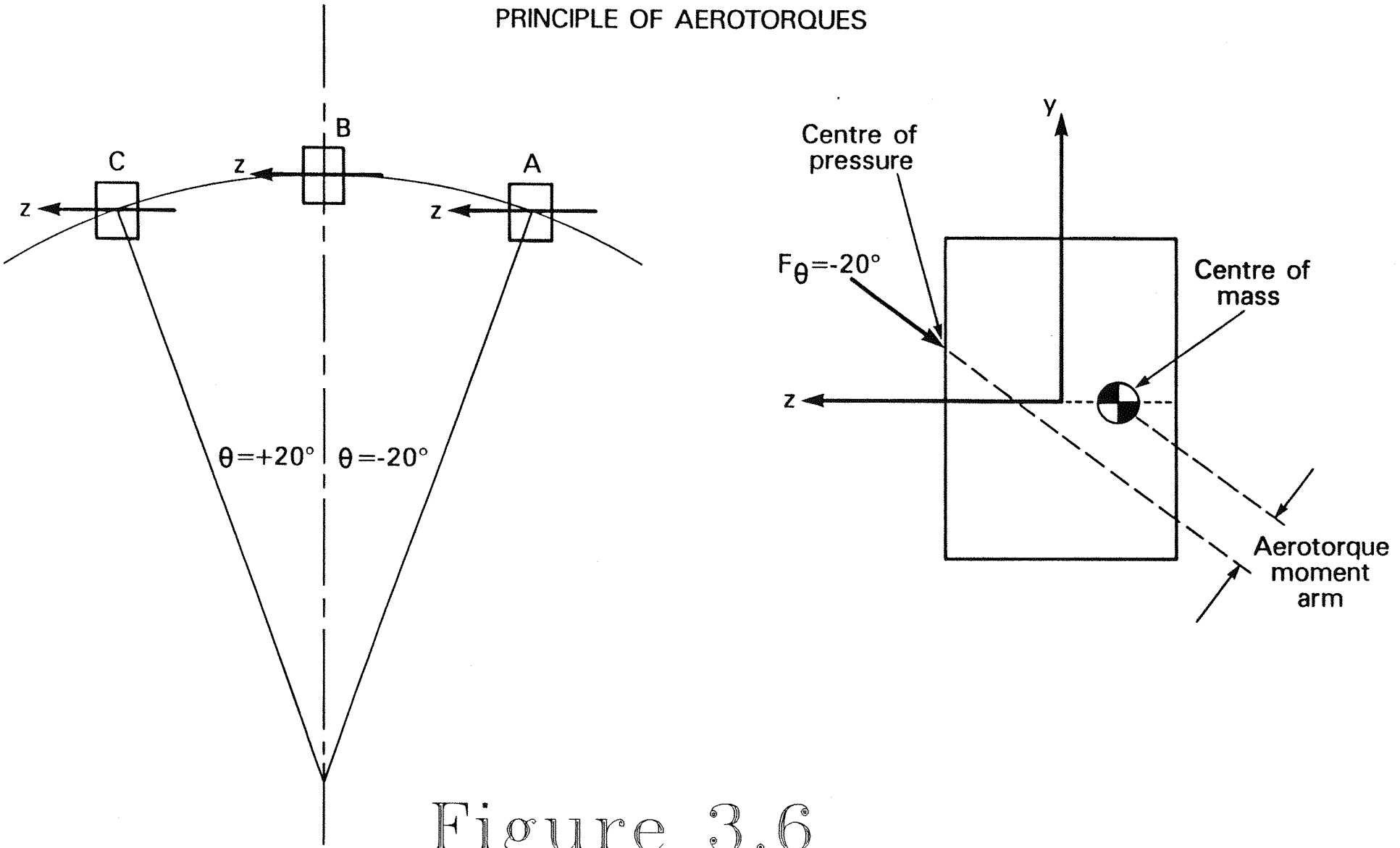
PRINCIPLE OF AEROTORQUES
B
C
A
z
z
z
θ=+20°
θ=-20°
y
Centre of pressure
Fθ=-20°
Centre of mass
z
Aerotorque moment arm

Figure 3.6

Aerotorques at Perigee

Figure 3.7

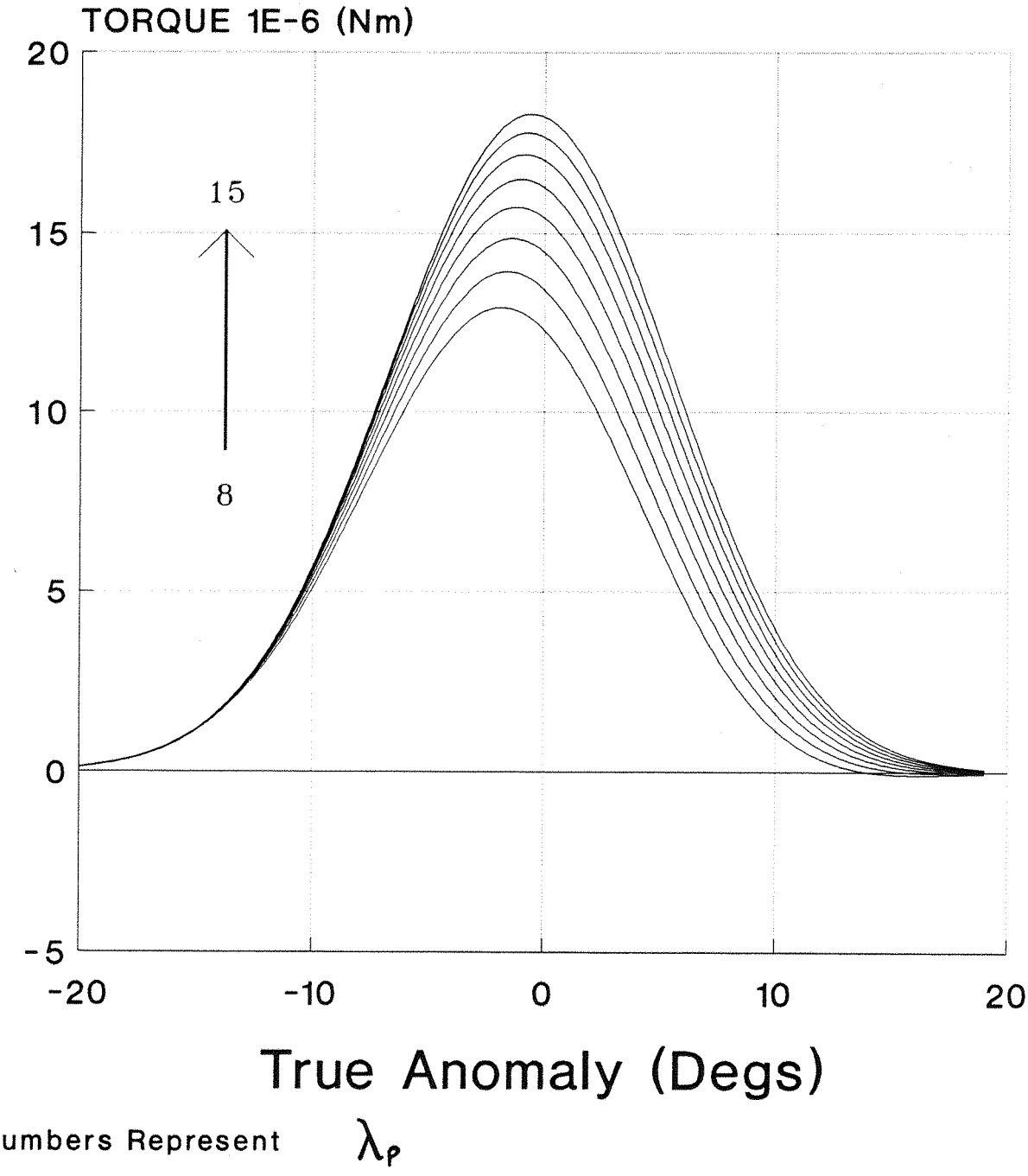

Numbers Represent λ_p

Perigee Aerotorques

RA0 Figure 3.8

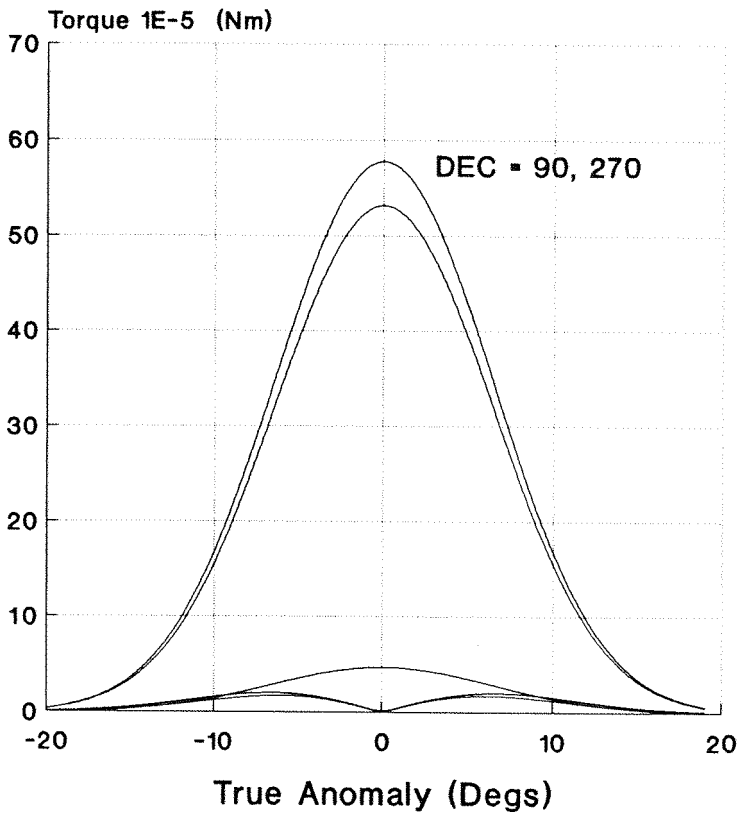

Perigee Aerotorques

RA10 Figure 3.9

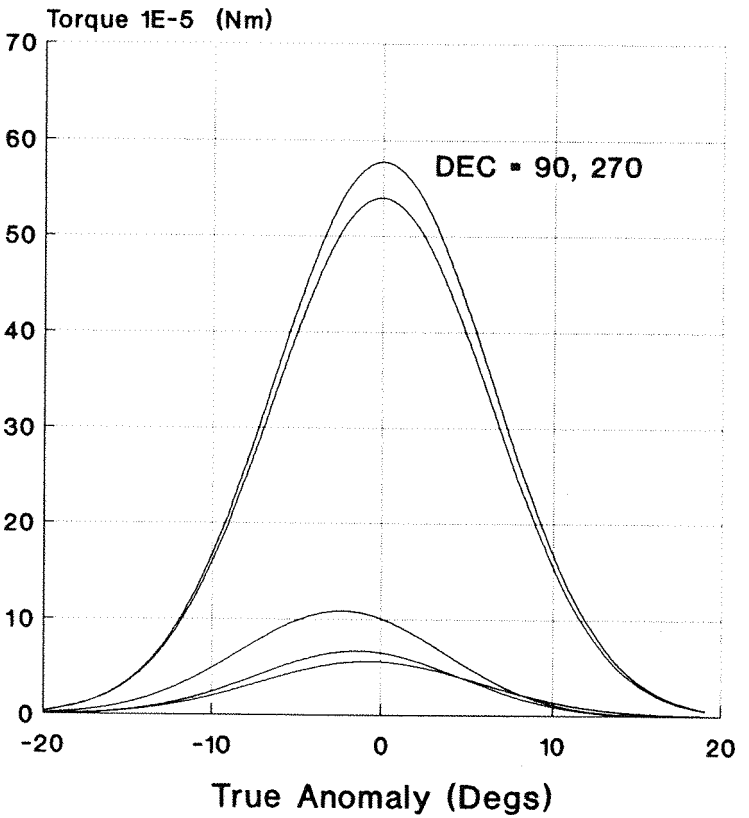

Perigee Aerotorques

RA20 Figure 3.10

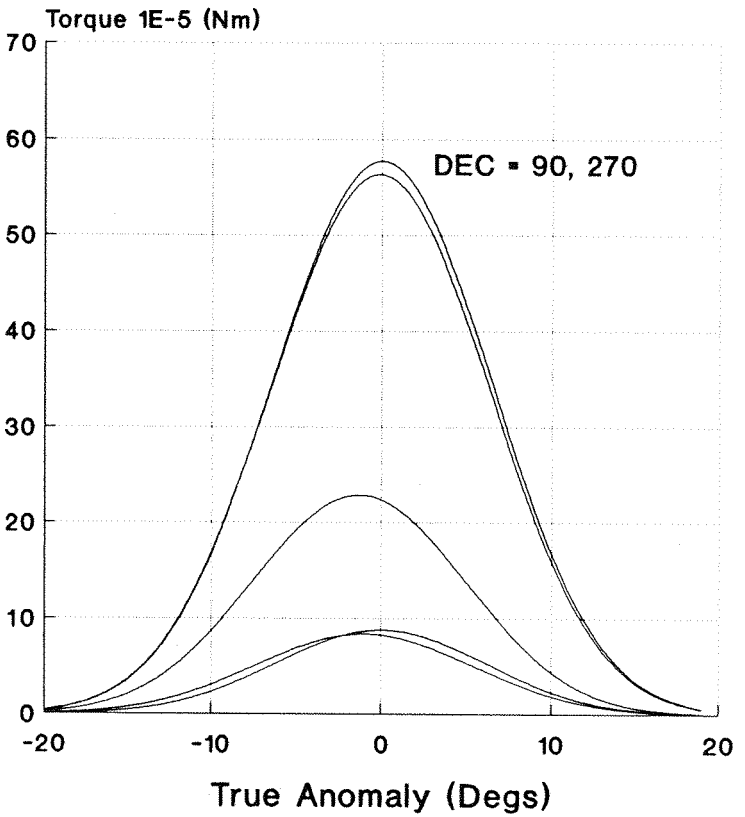

Perigee Aerotorques

RA30 Figure 3.11

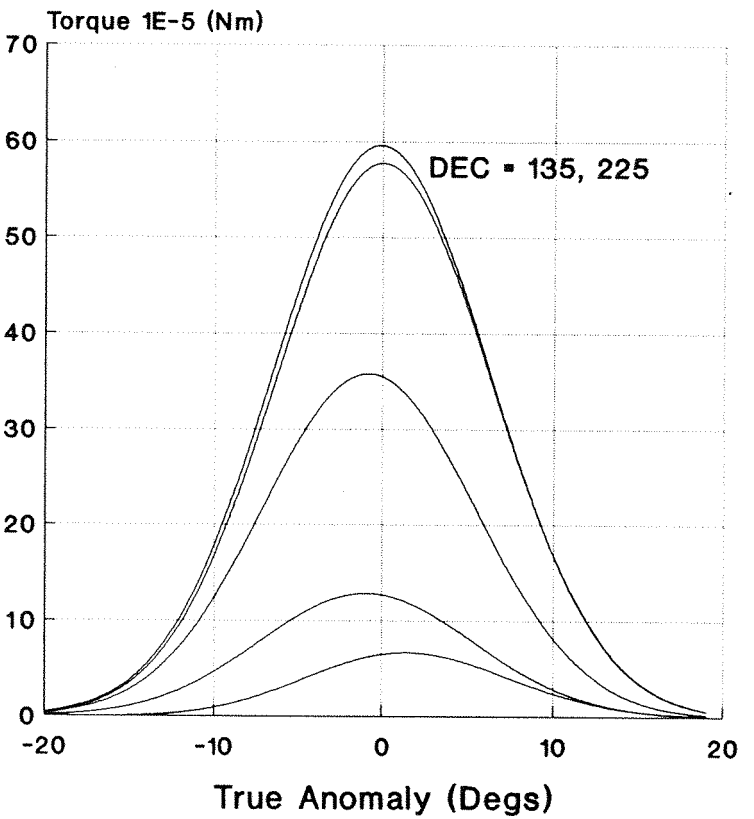

Perigee Aerotorques

RA40 Figure 3.12

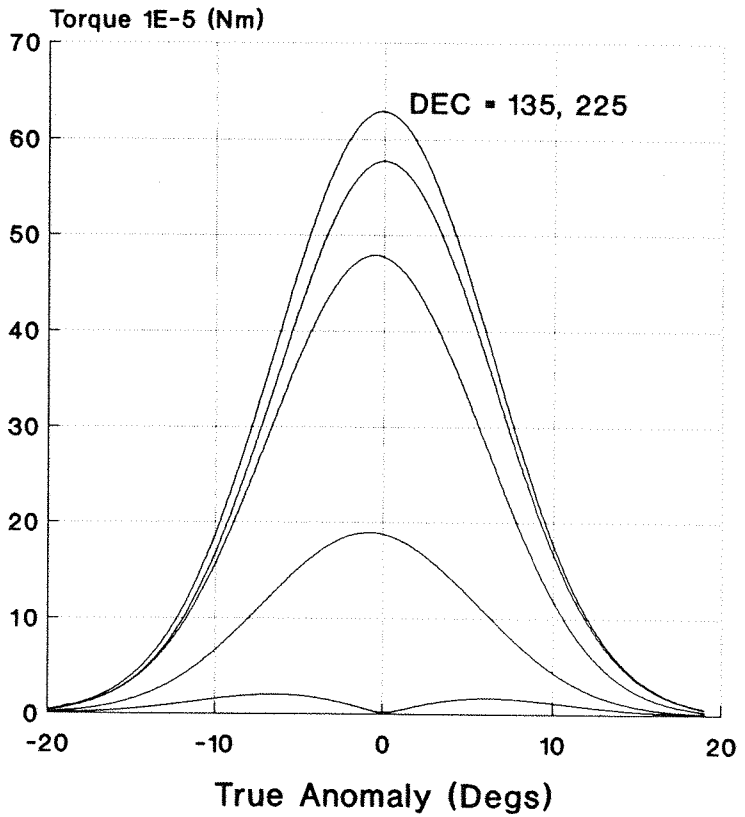

Perigee Aerotorques

RA50 Figure 3.13

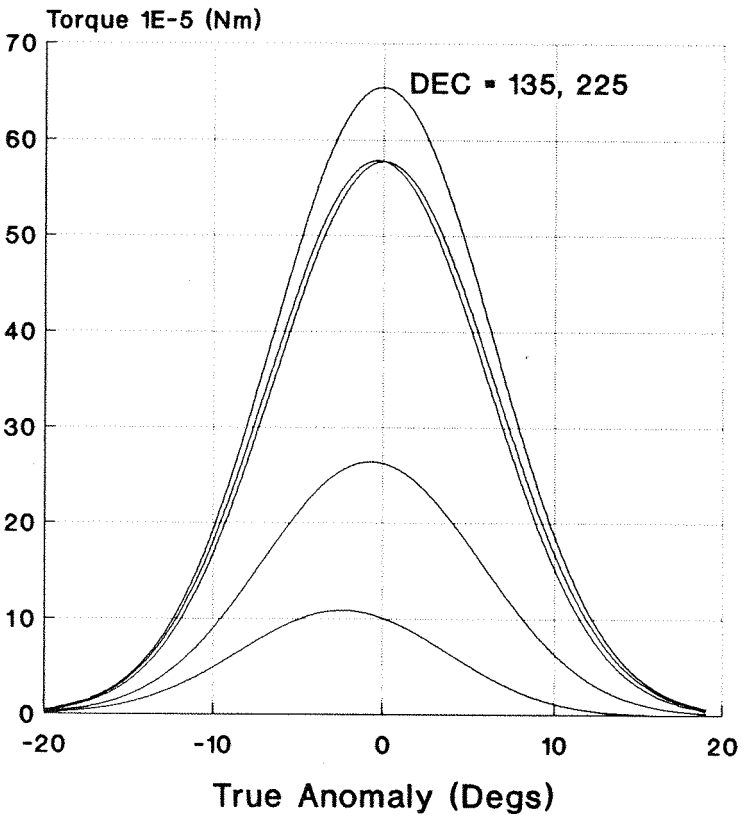

Perigee Aerotorques
RA60 Figure 3.14

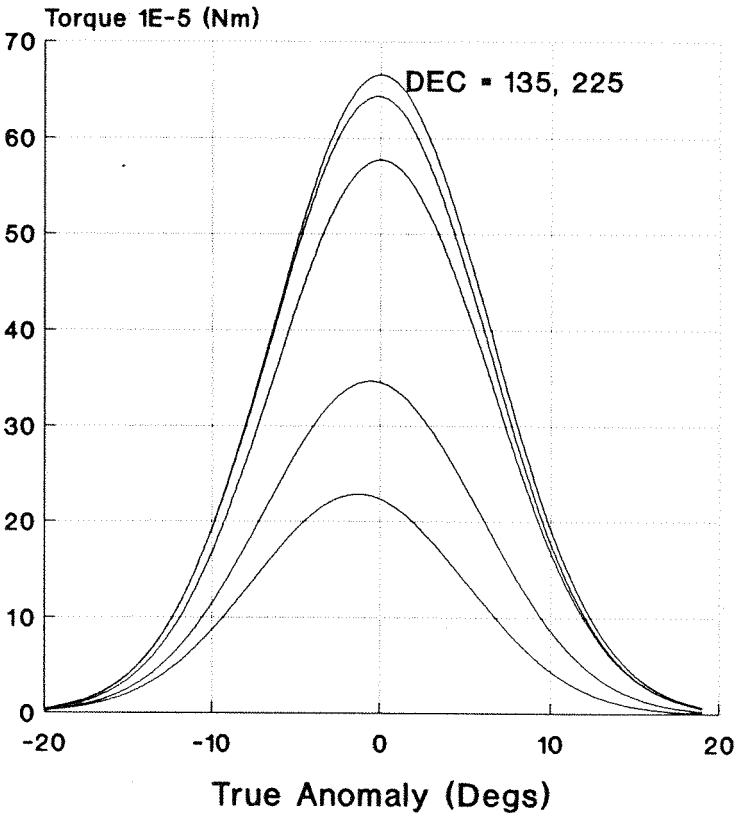

Perigee Aerotorques
RA70 Figure 3.15

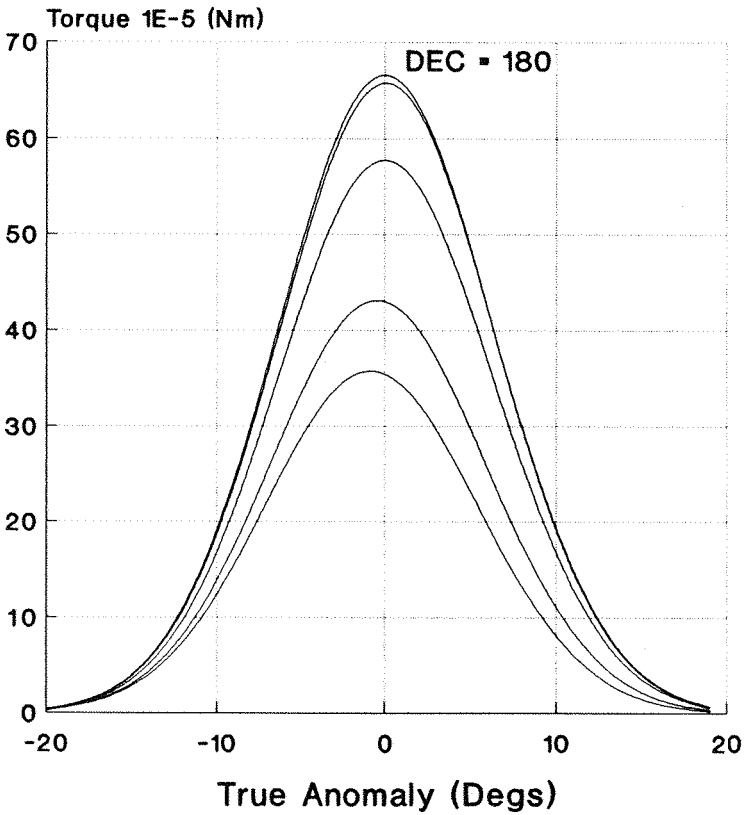

Perigee Aerotorques
RA80 Figure 3.16

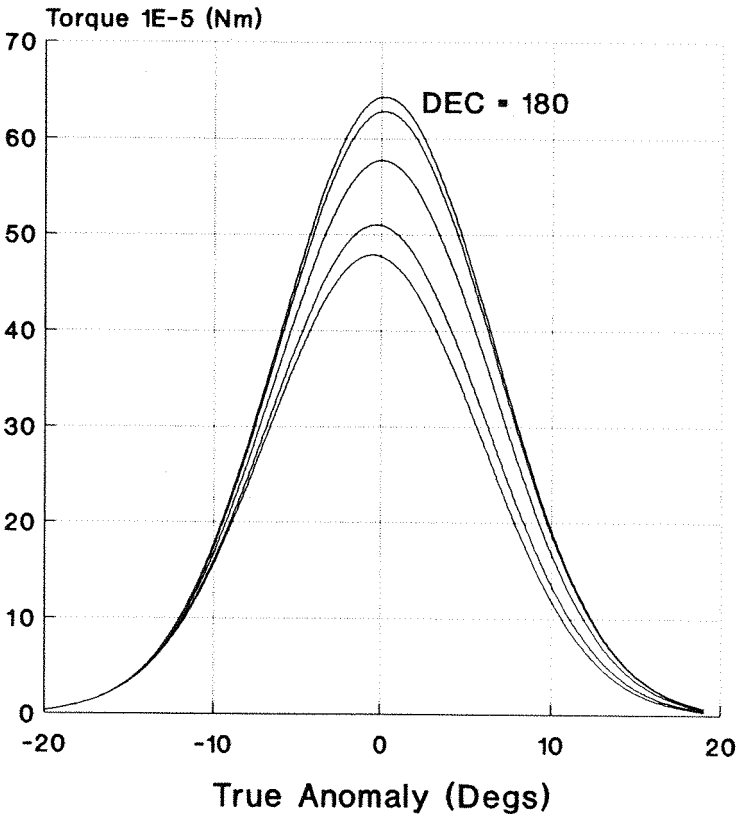

Perigee Aerotorques
RA90 Figure 3.17

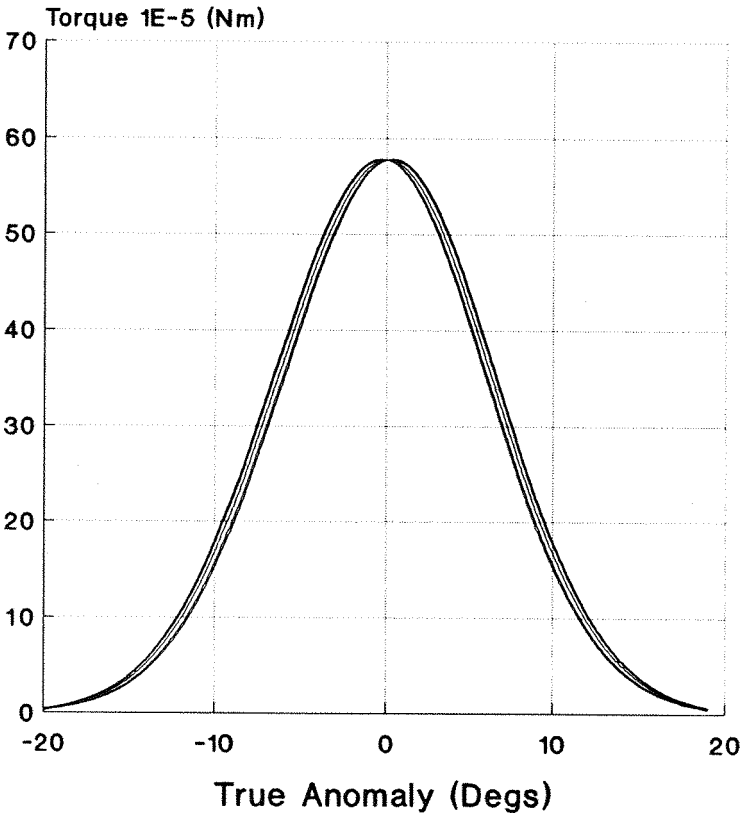

Perigee Aerotorques

RA100 Figure 3.18

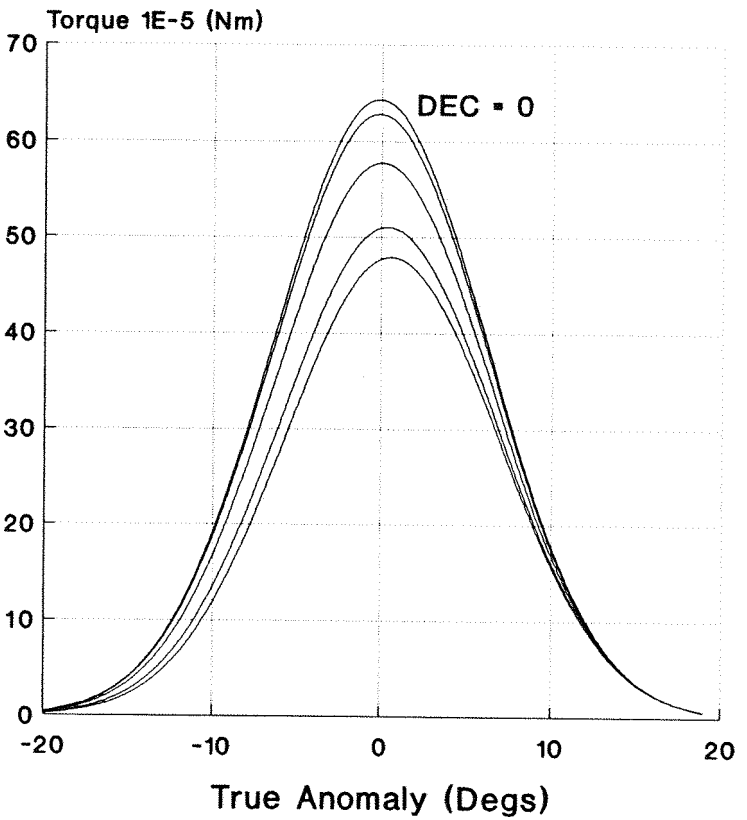

Perigee Aerotorques

RA110 Figure 3.19

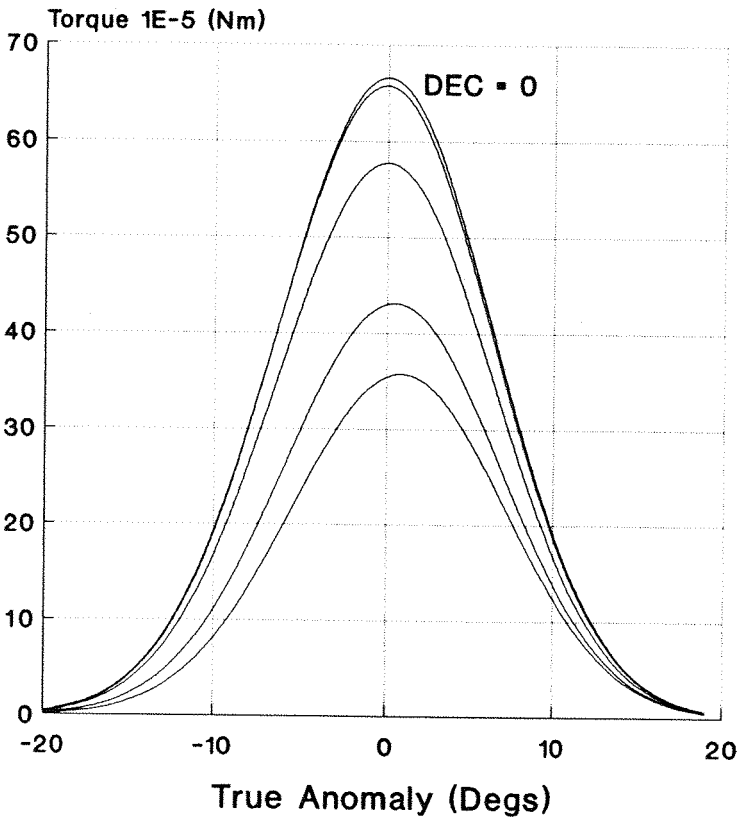

Perigee Aerotorques
RA120 Figure 3.20

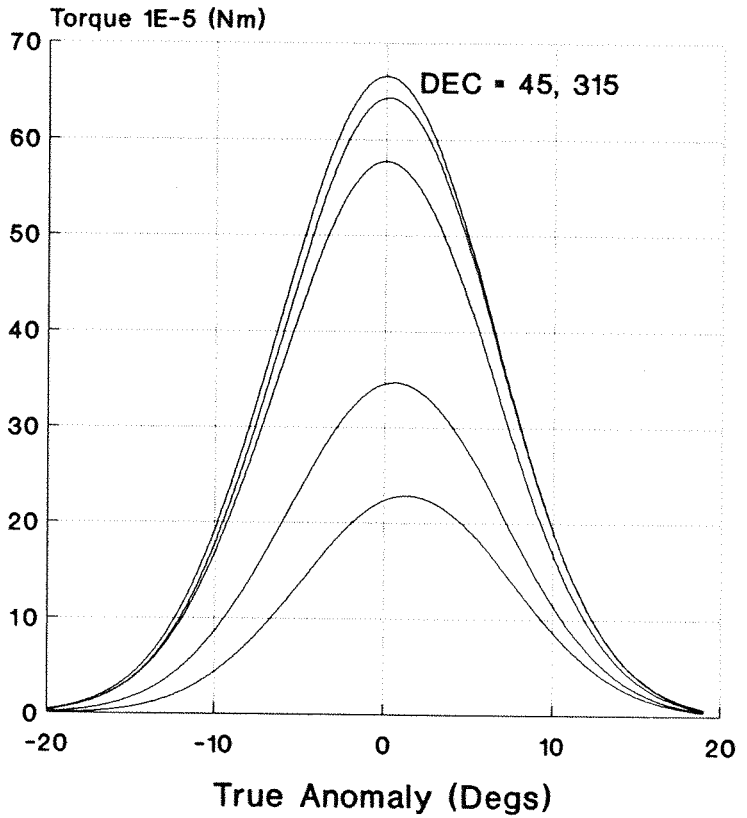

Perigee Aerotorques
RA130 Figure 3.21

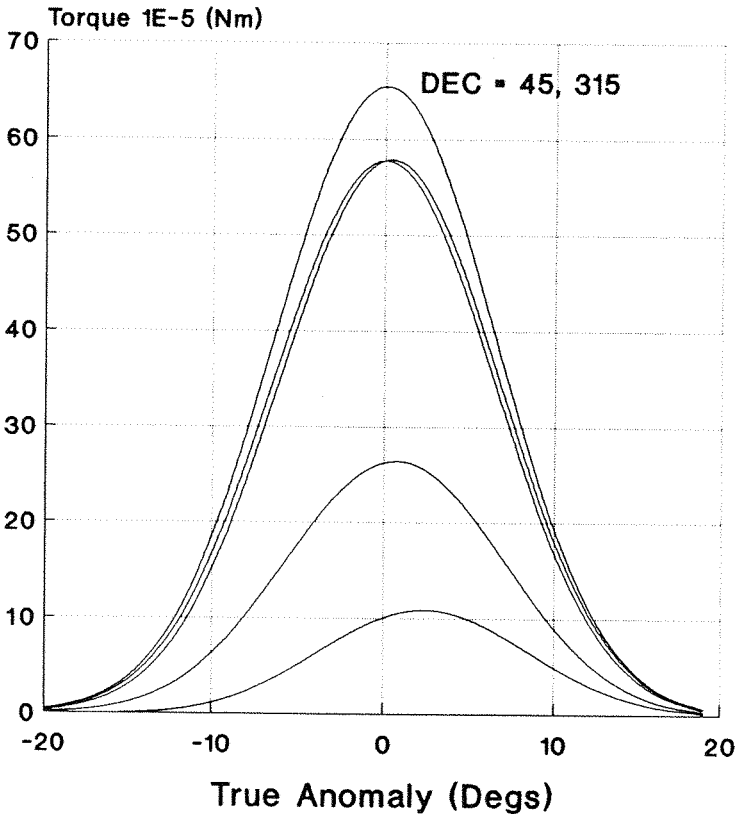

Perigee Aerotorques
RA140 Figure 3.22

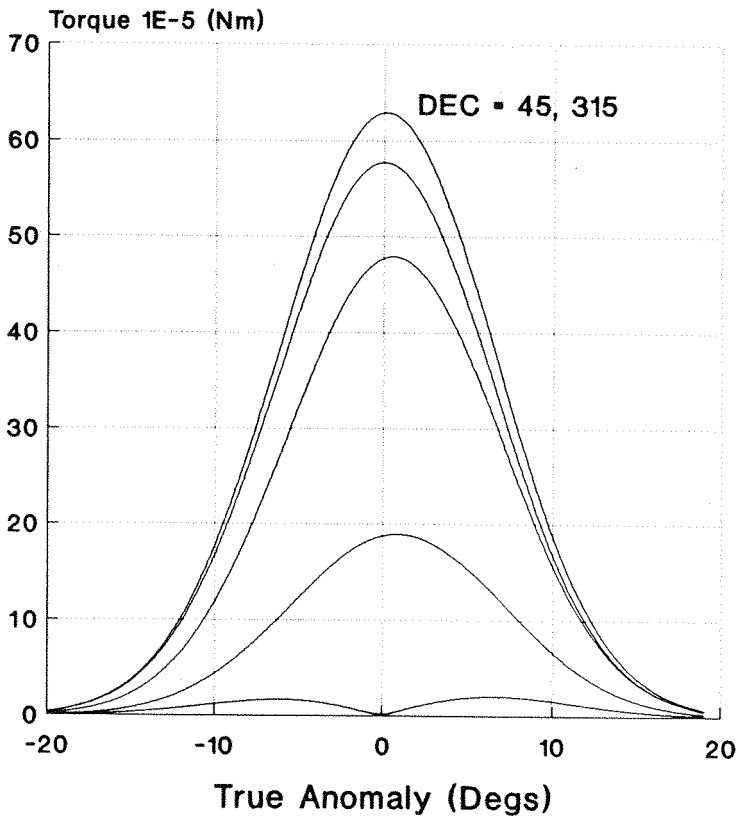

Perigee Aerotorques
RA150 Figure 3.23

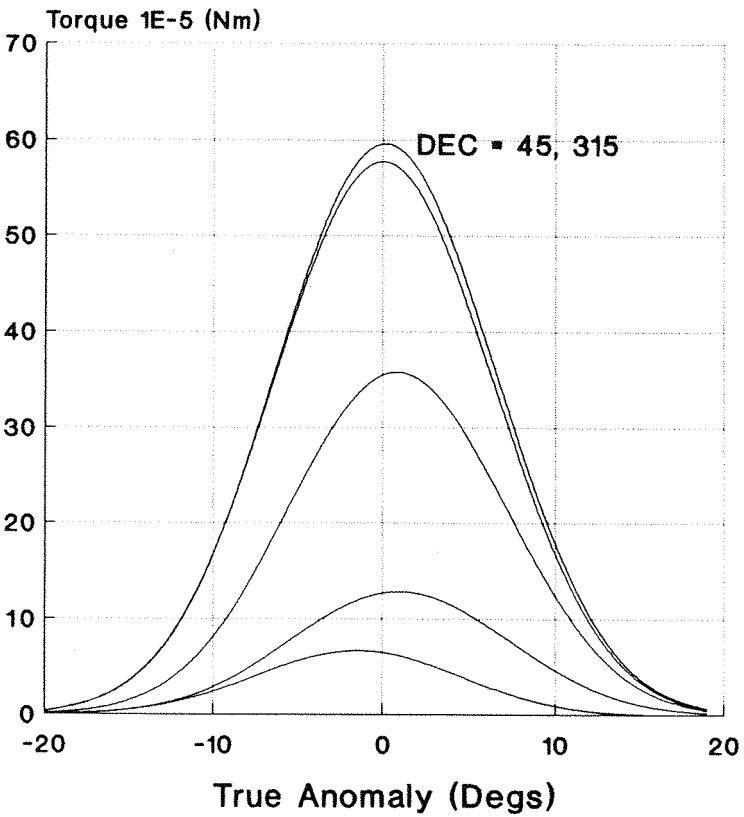

Perigee Aerotorques
RA160 Figure 3.24

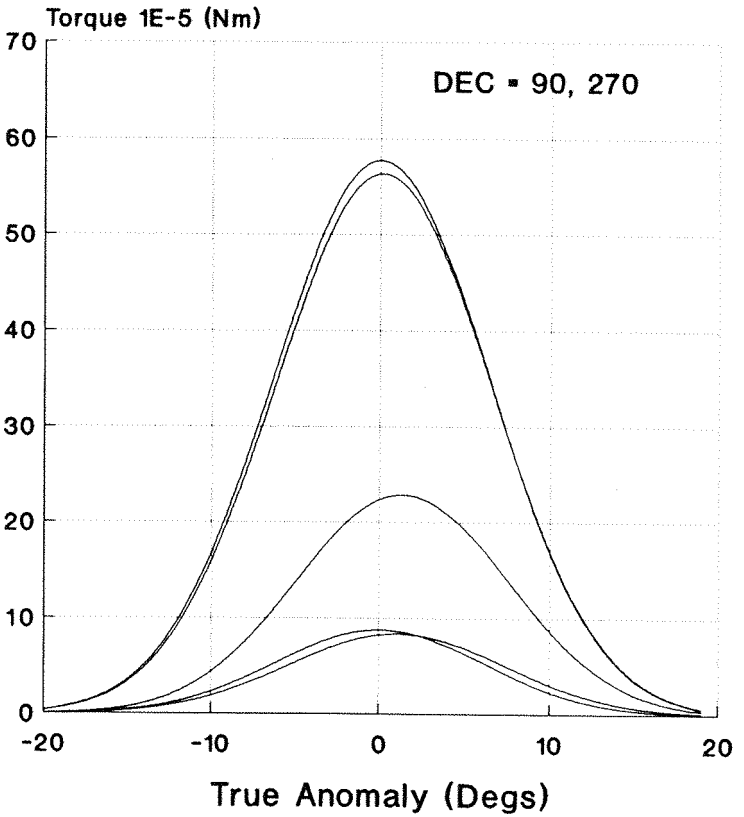

Perigee Aerotorques
RA170 Figure 3.25

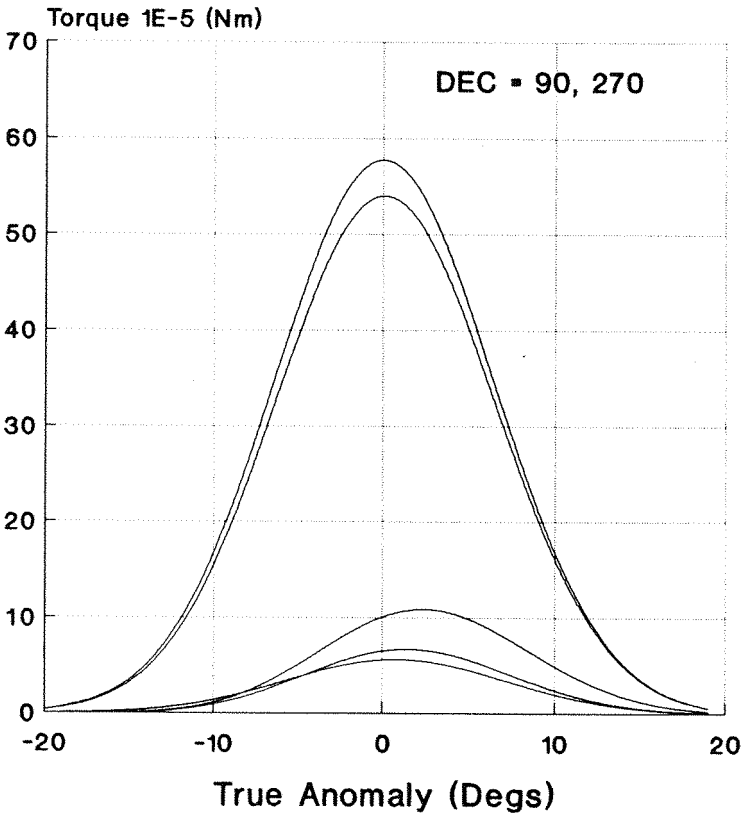

Change of Orientation

FIGURE 3.26

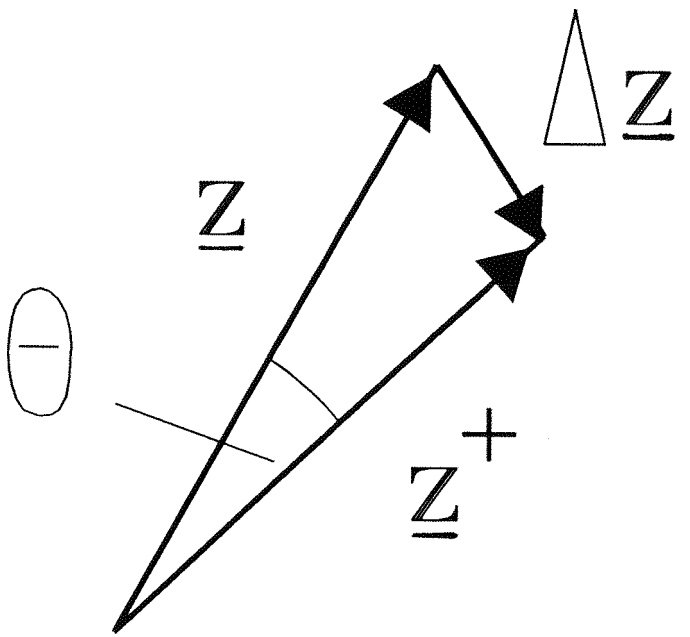

f(Z2) and f'(Z2) v Z2

Figure 3.27

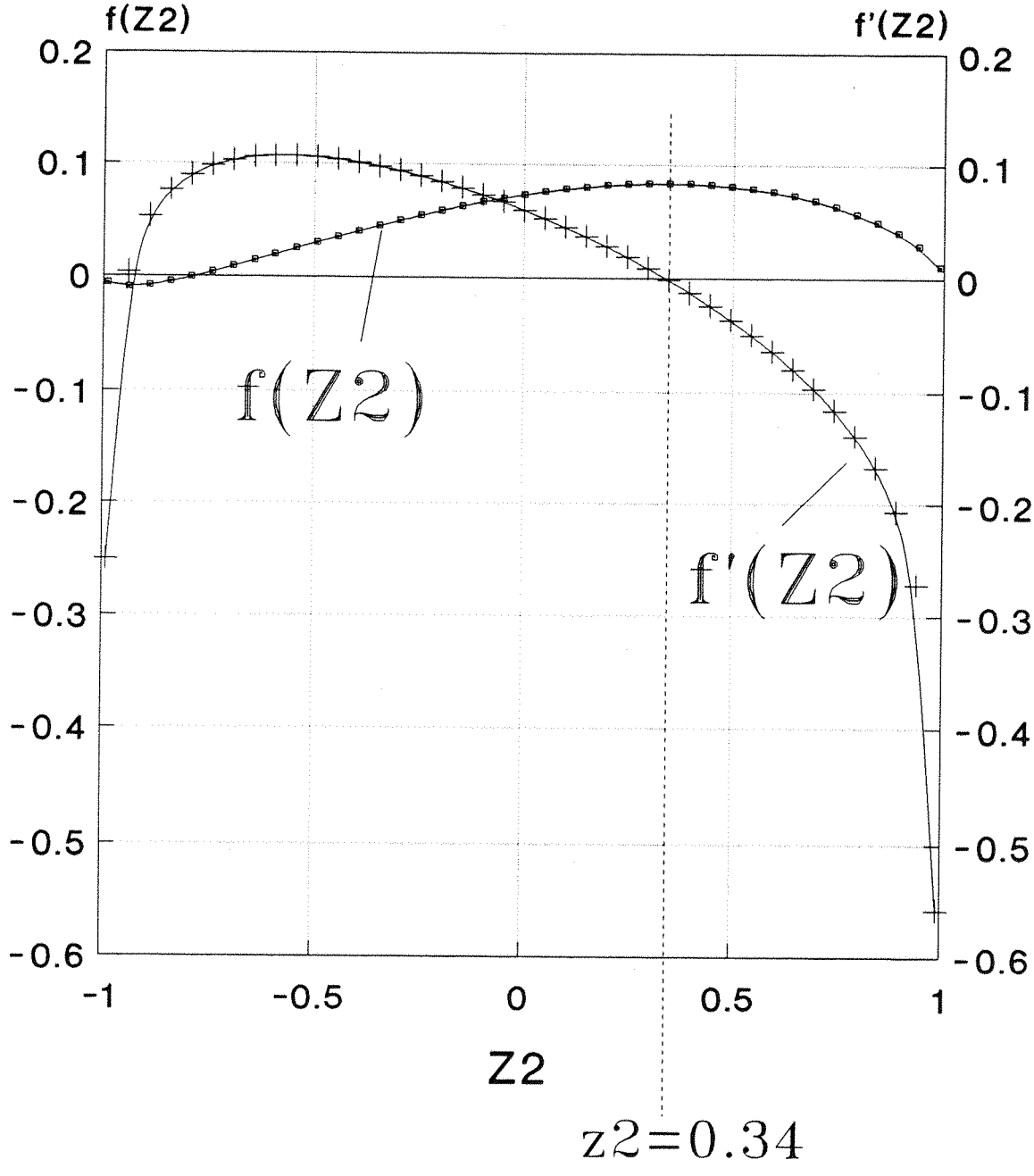

Spin Axis Cone

FIGURE 3.28

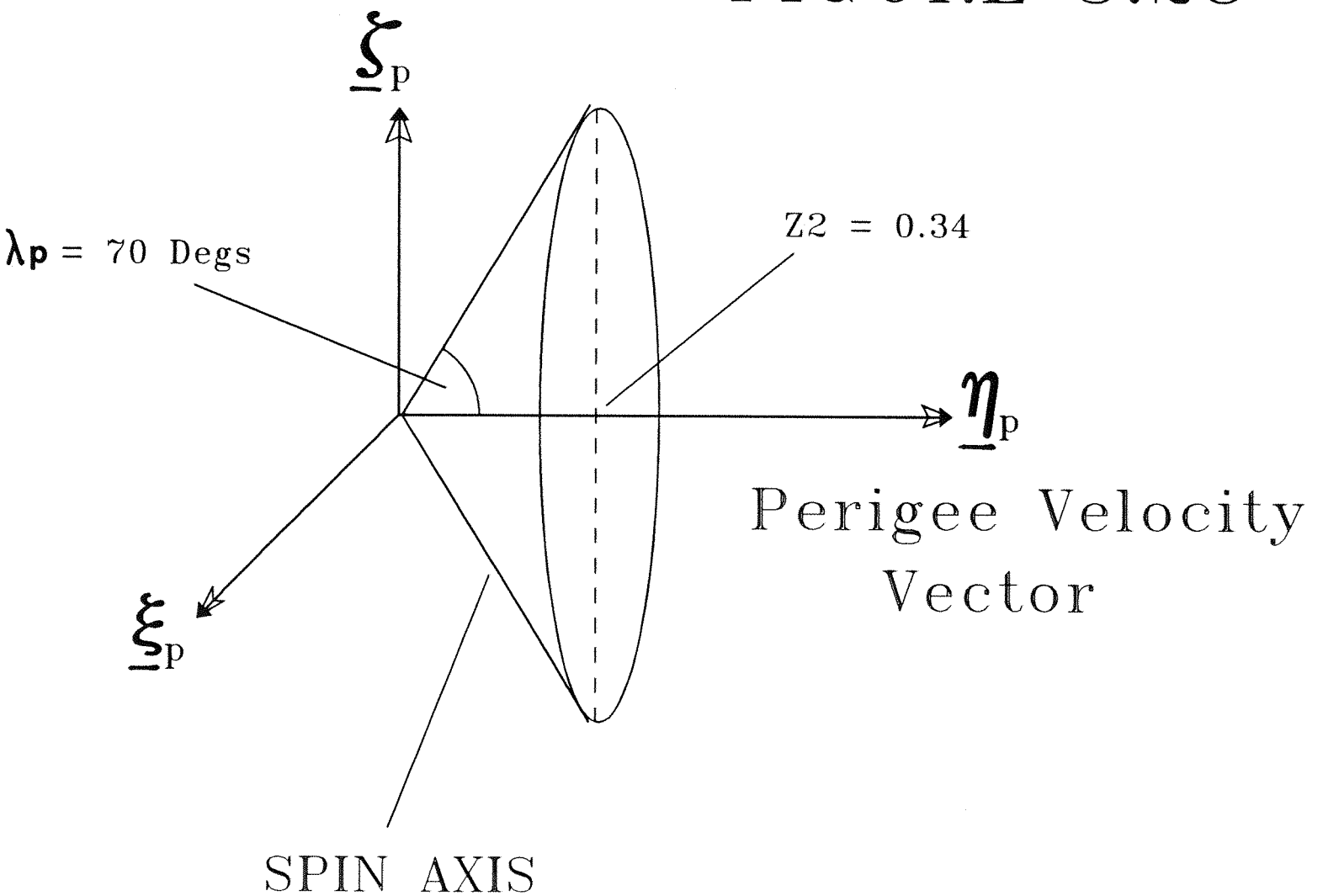

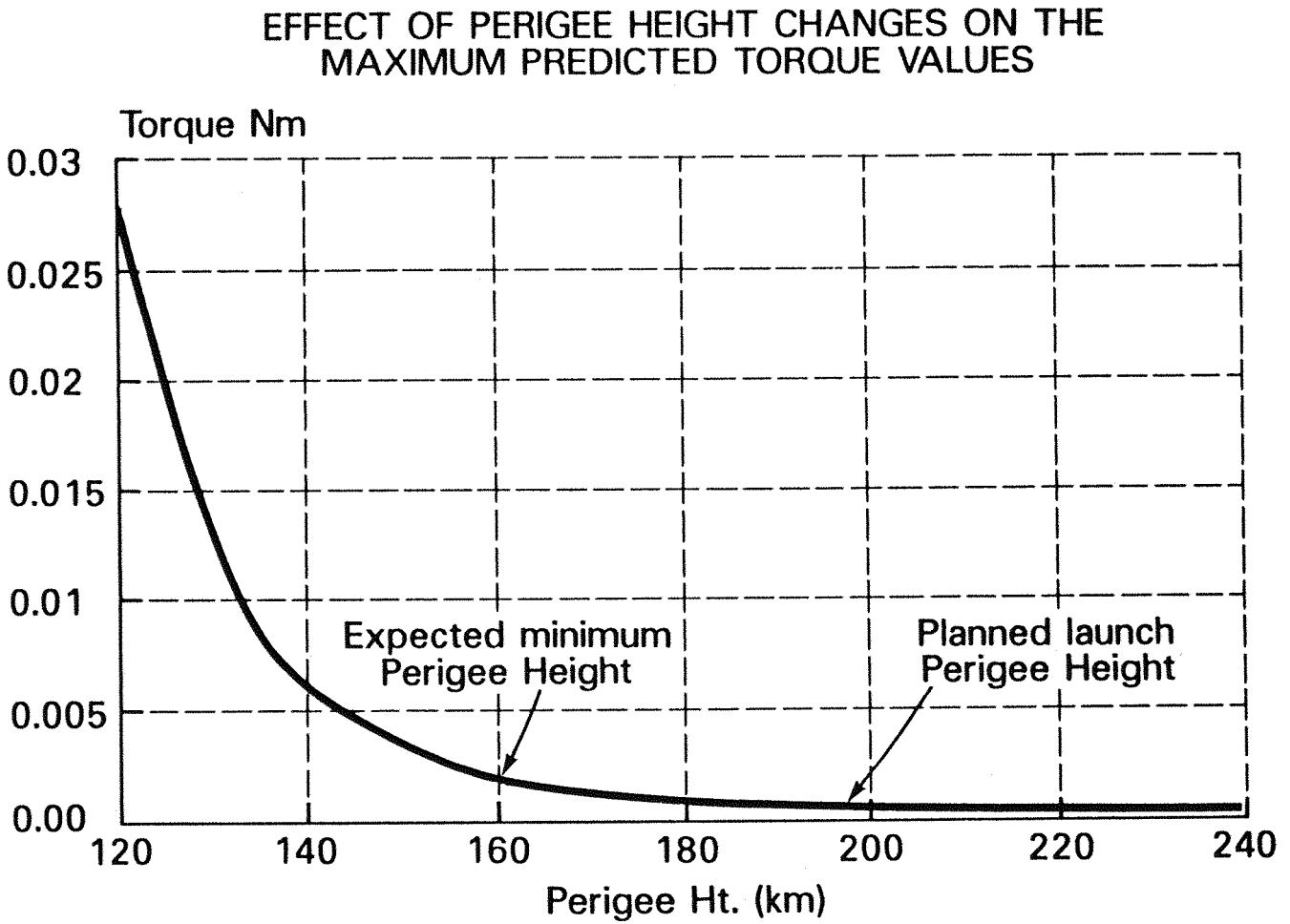
EFFECT OF PERIGEE HEIGHT CHANGES ON THE
MAXIMUM PREDICTED TORQUE VALUES
Torque Nm
0.03
0.025
0.02
0.015
0.01
0.005
0.00
Expected minimum
Perigee Height
Planned launch
Perigee Height
120
140
160
180
200
220
240
Perigee Ht. (km)

Figure 3.29

MARECS-A Normalized Data

Figure 4.1

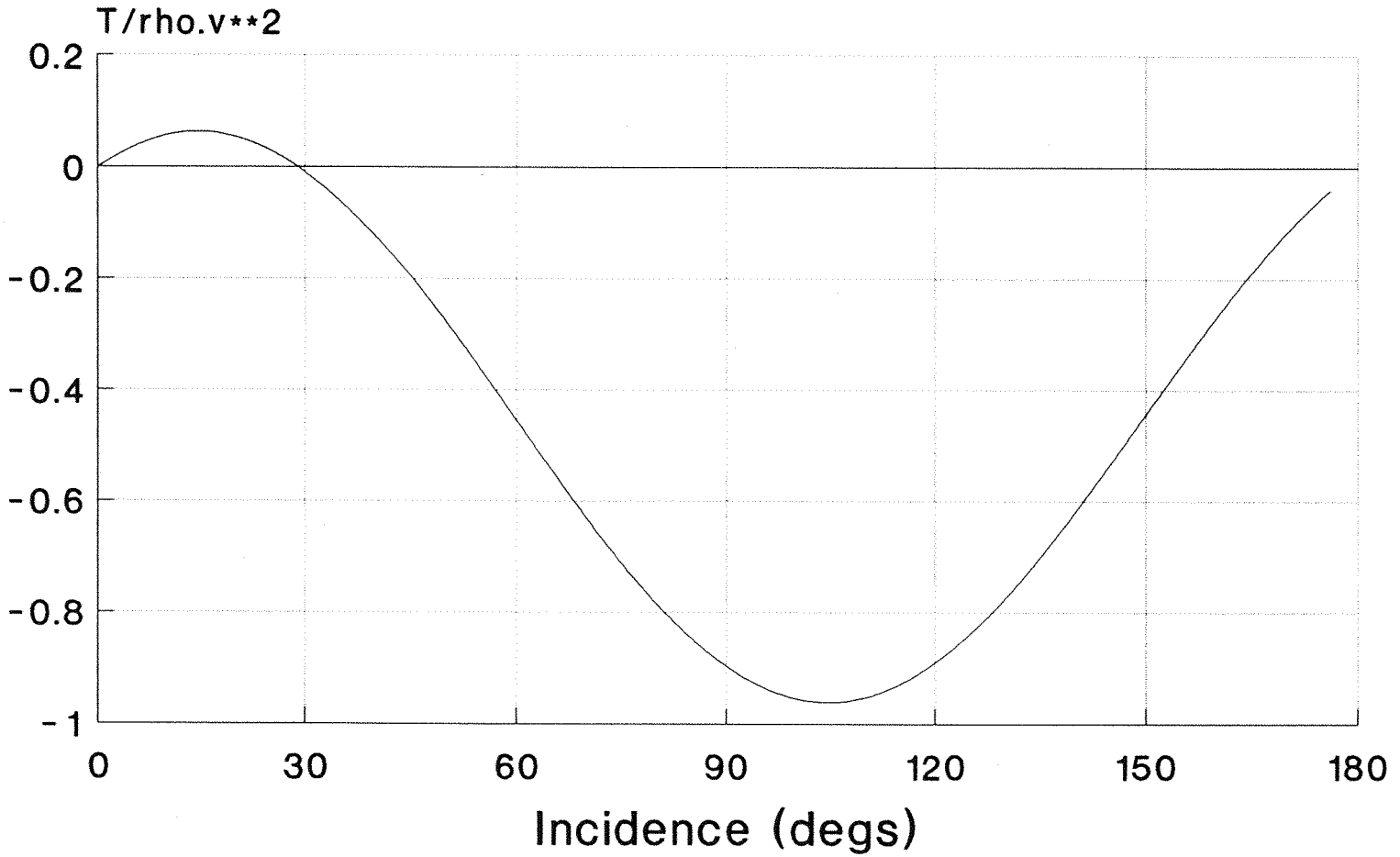

MARECS-A SAA Variation

Figure 4.2

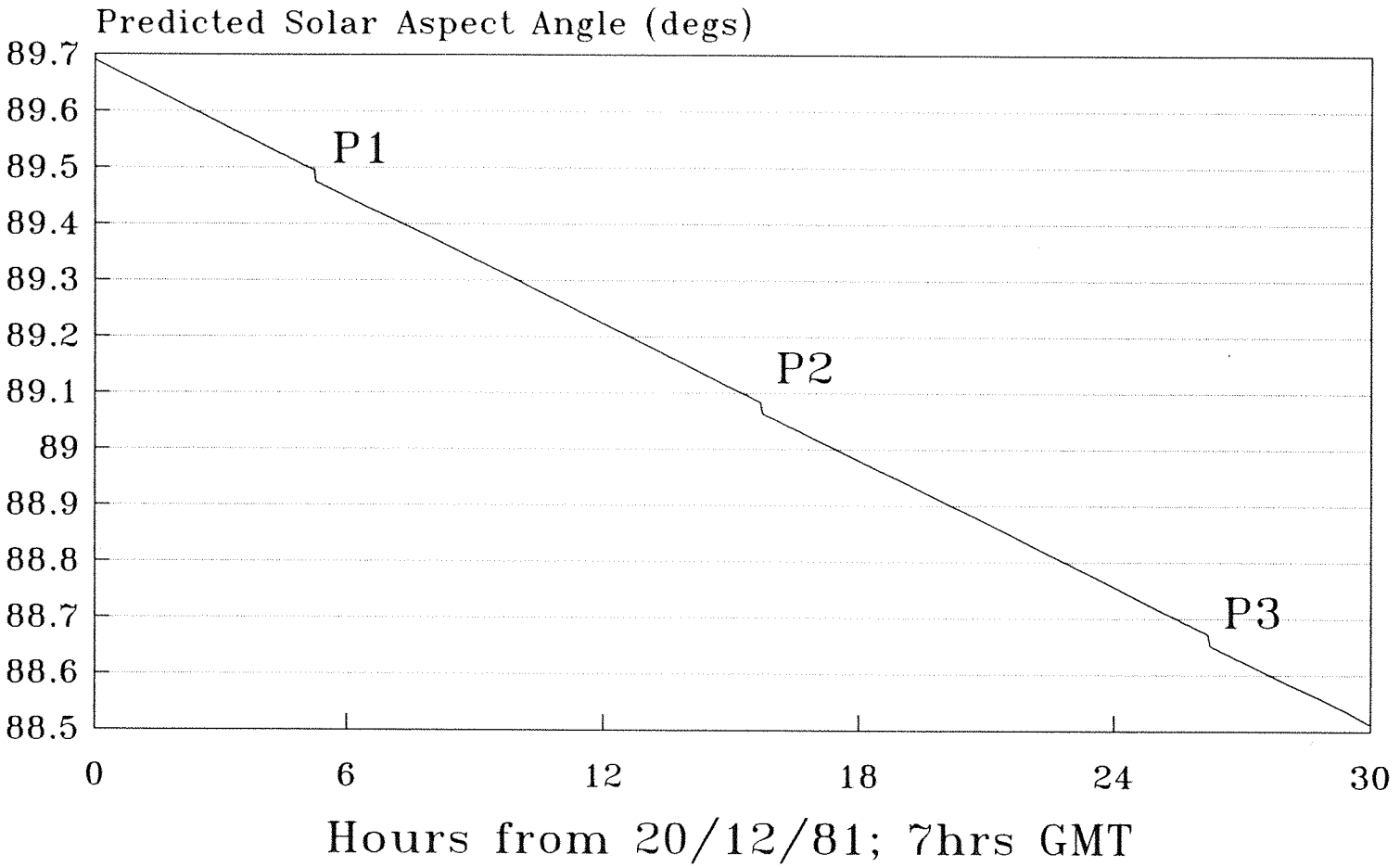

SKYNET 4C RA Data

Figure 4.3a

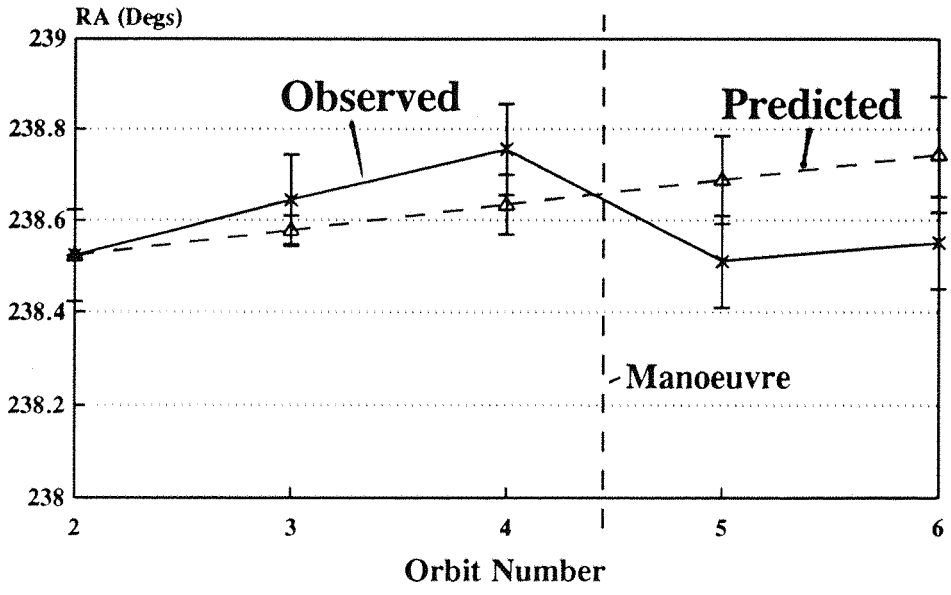

SKYNET 4C DEC Data

Figure 4.3b

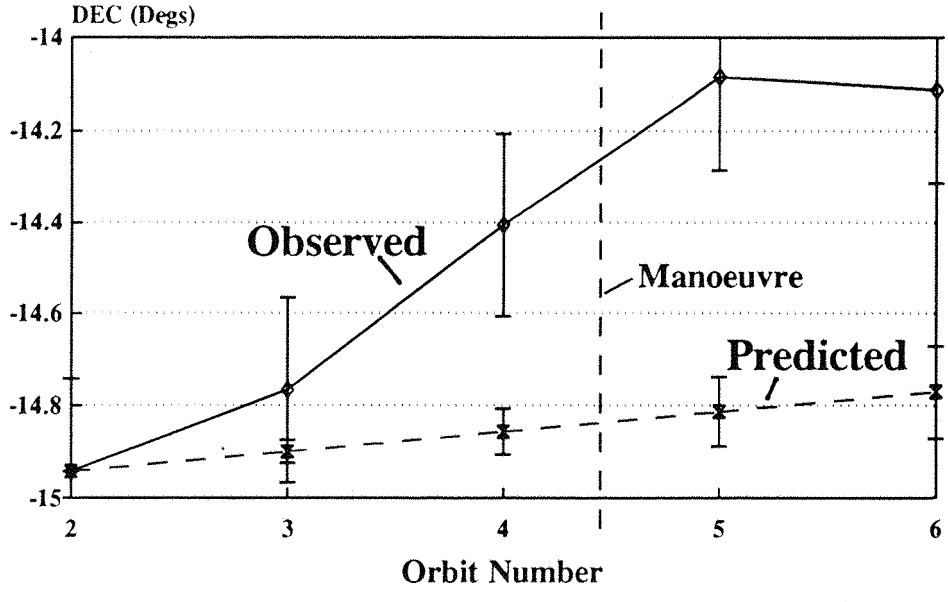

Torque Verification

Figure 4.4

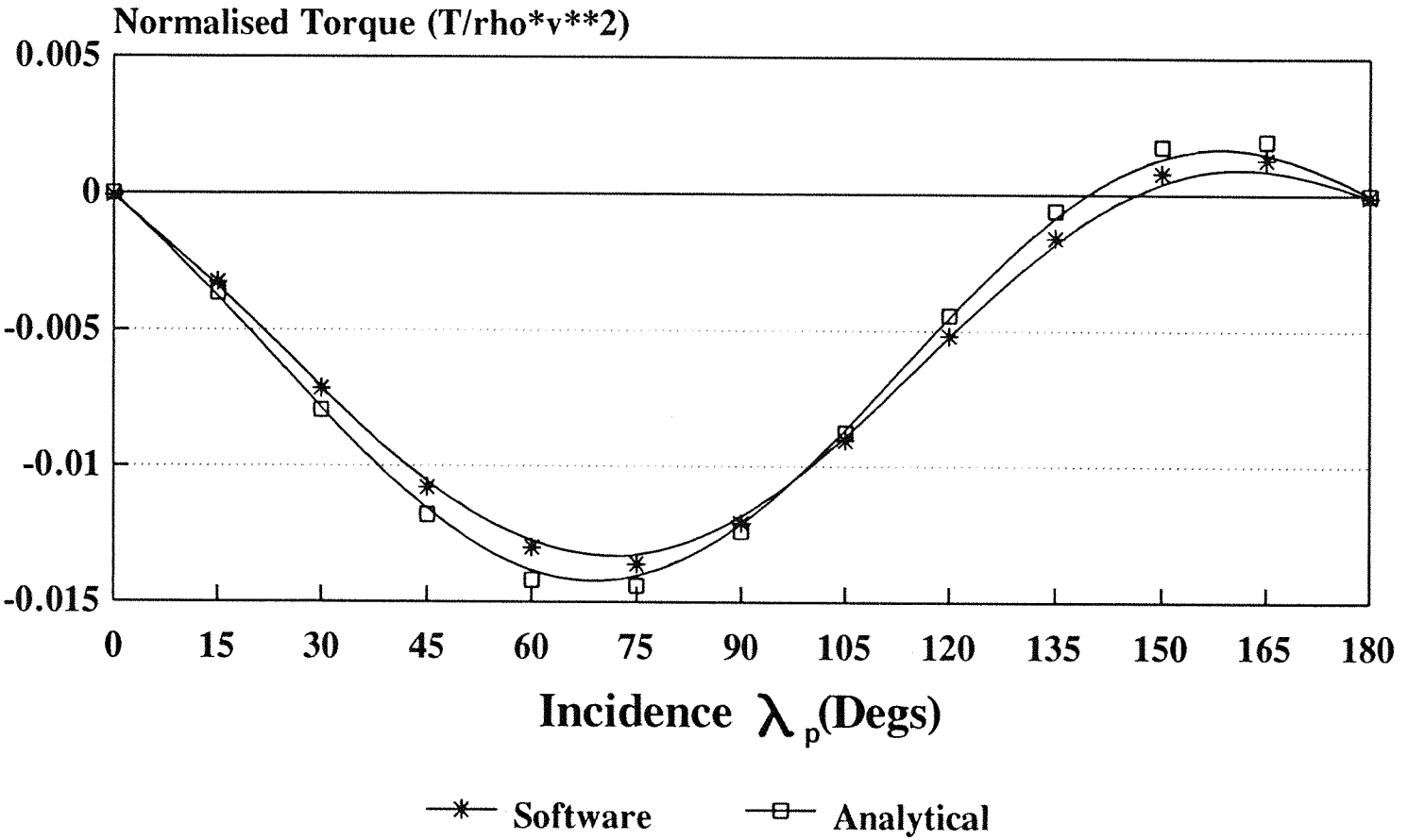

STRV Vectors and Angles

for Spin Decay (CD Method)

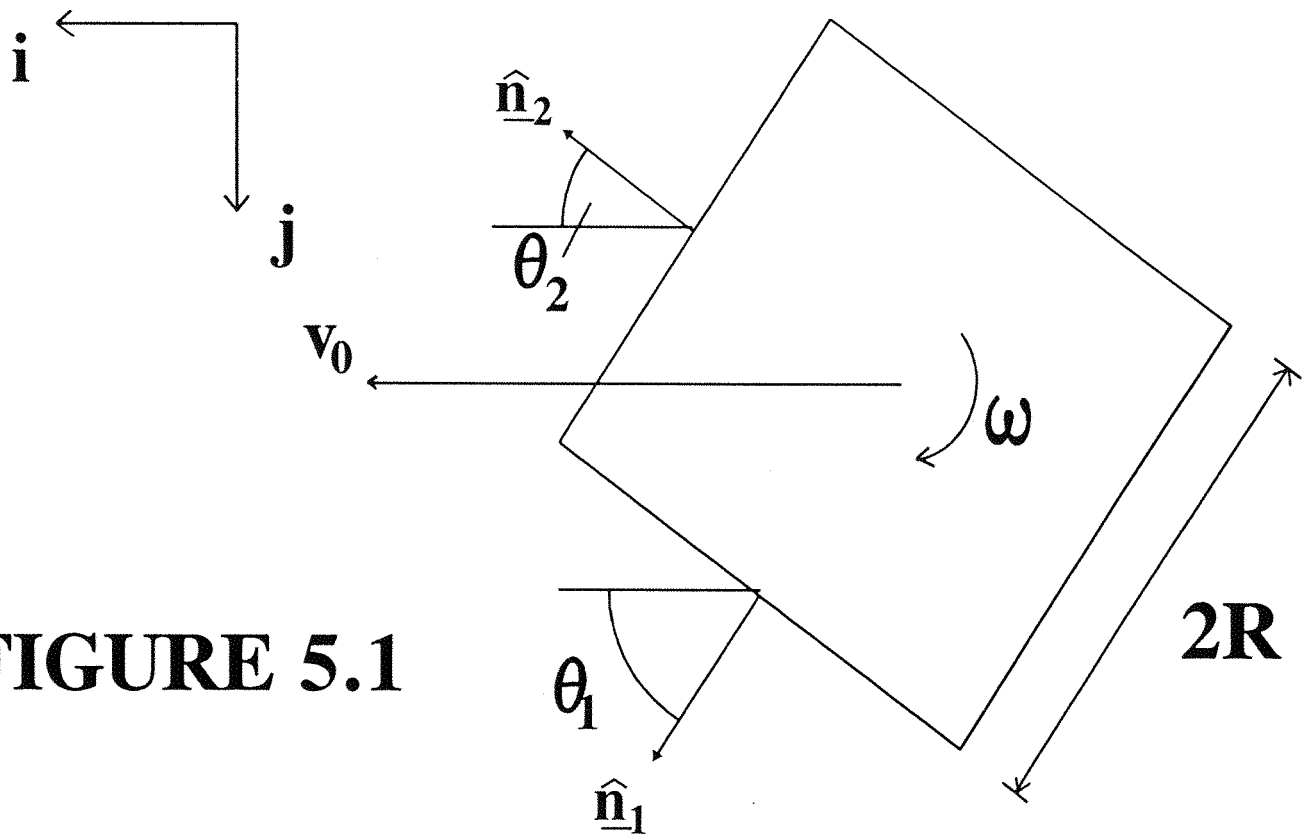

FIGURE 5.1

Pressure and Shear Stress on Surface

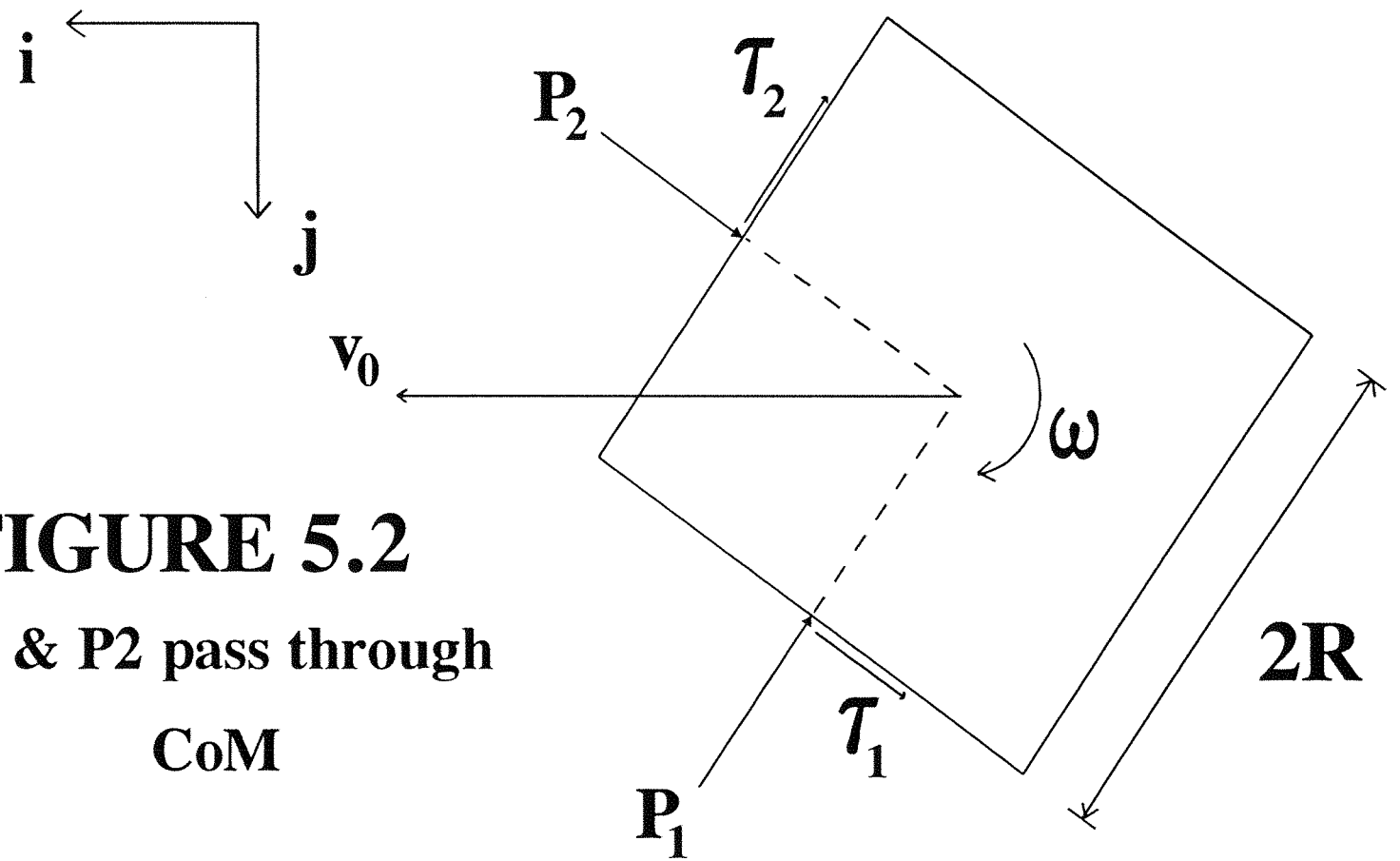

FIGURE 5.2

P1 & P2 pass through CoM

STRV Vectors for Spin Decay

Definition of Elements

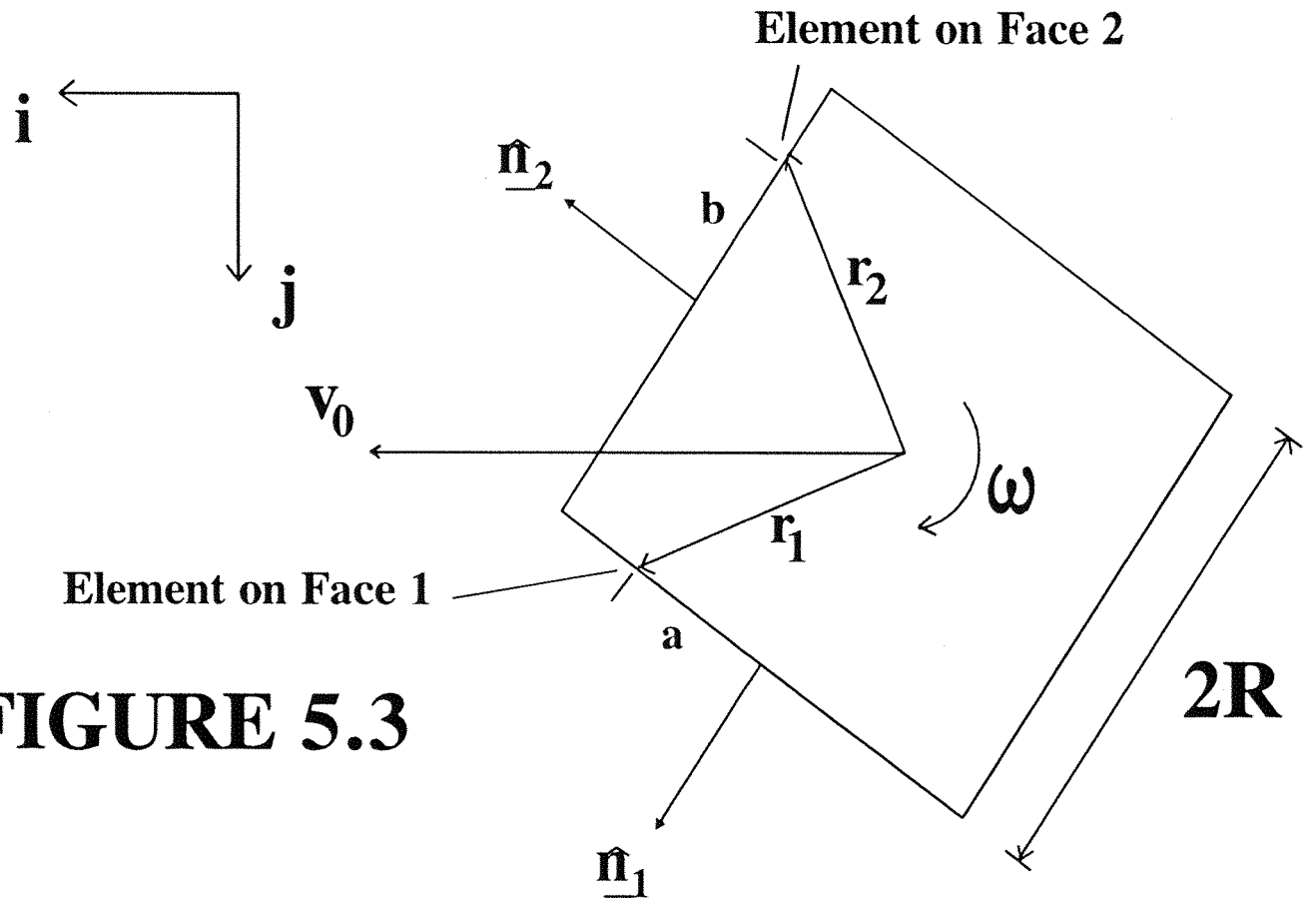

FIGURE 5.3

Spin Rate History
ARYABHATA

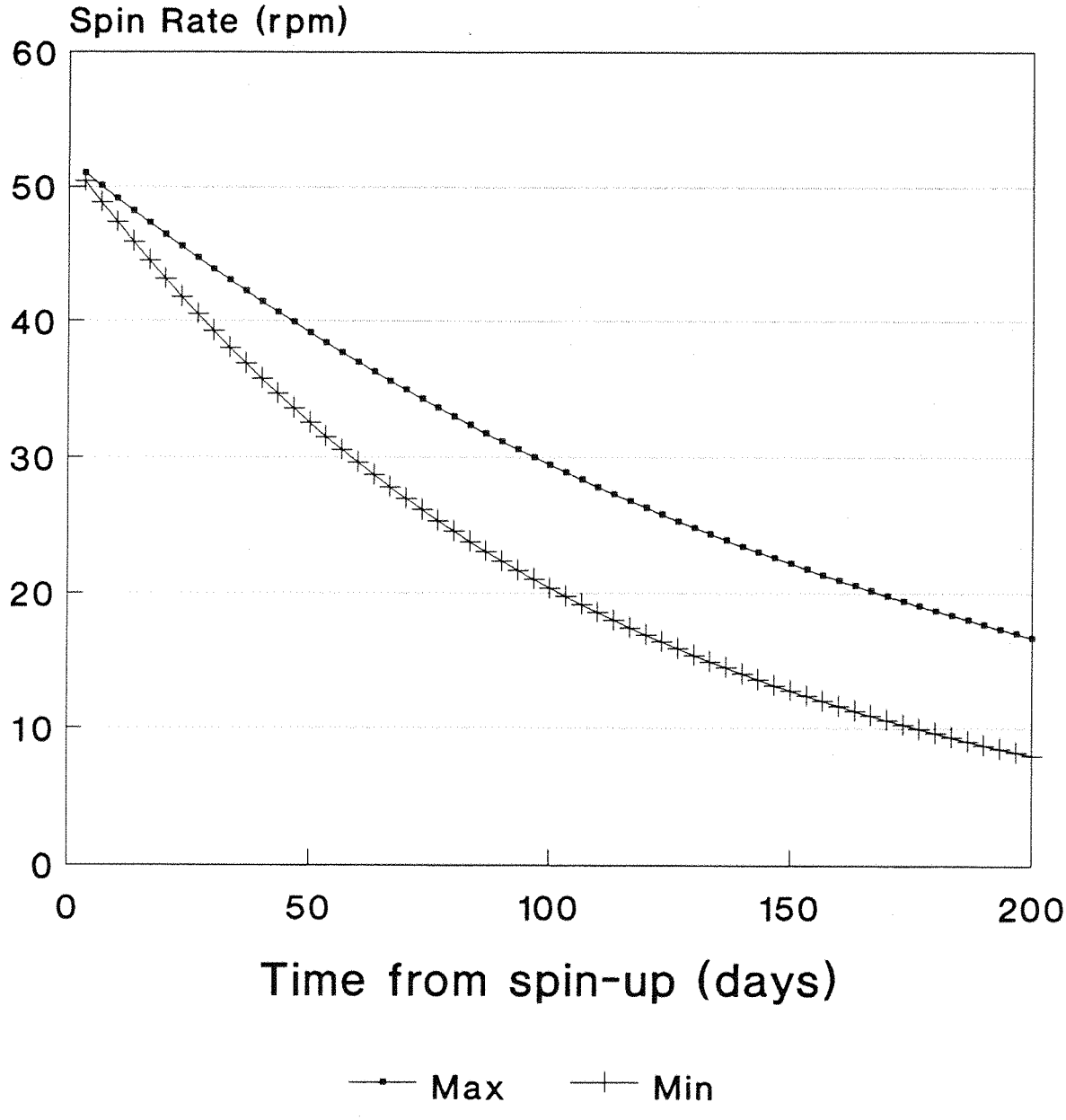

FIGURE 5.4

STRV-1 Eddy Current
Spin Decay

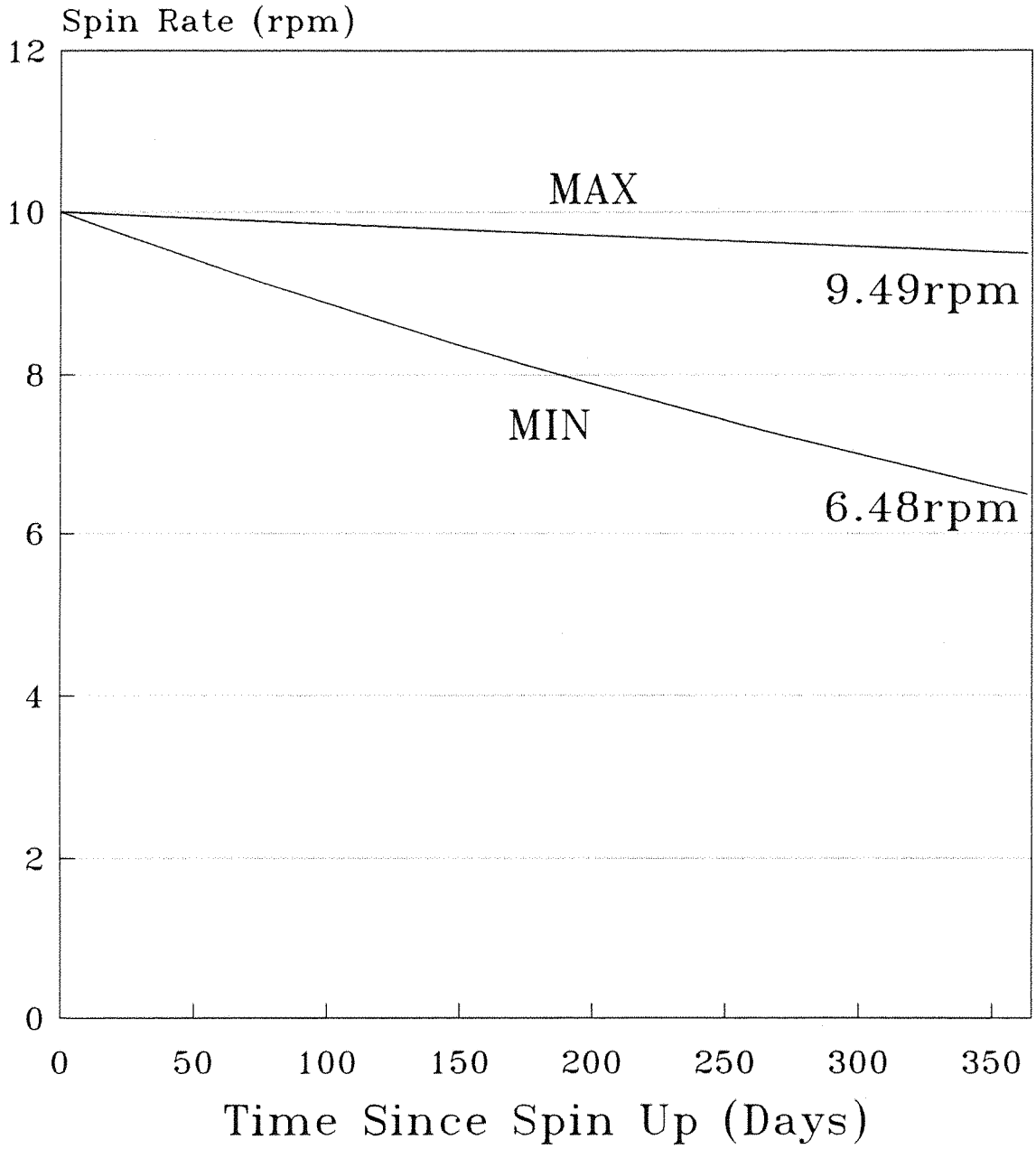

FIGURE 5.5

Final Spin Rate
v Conductivity

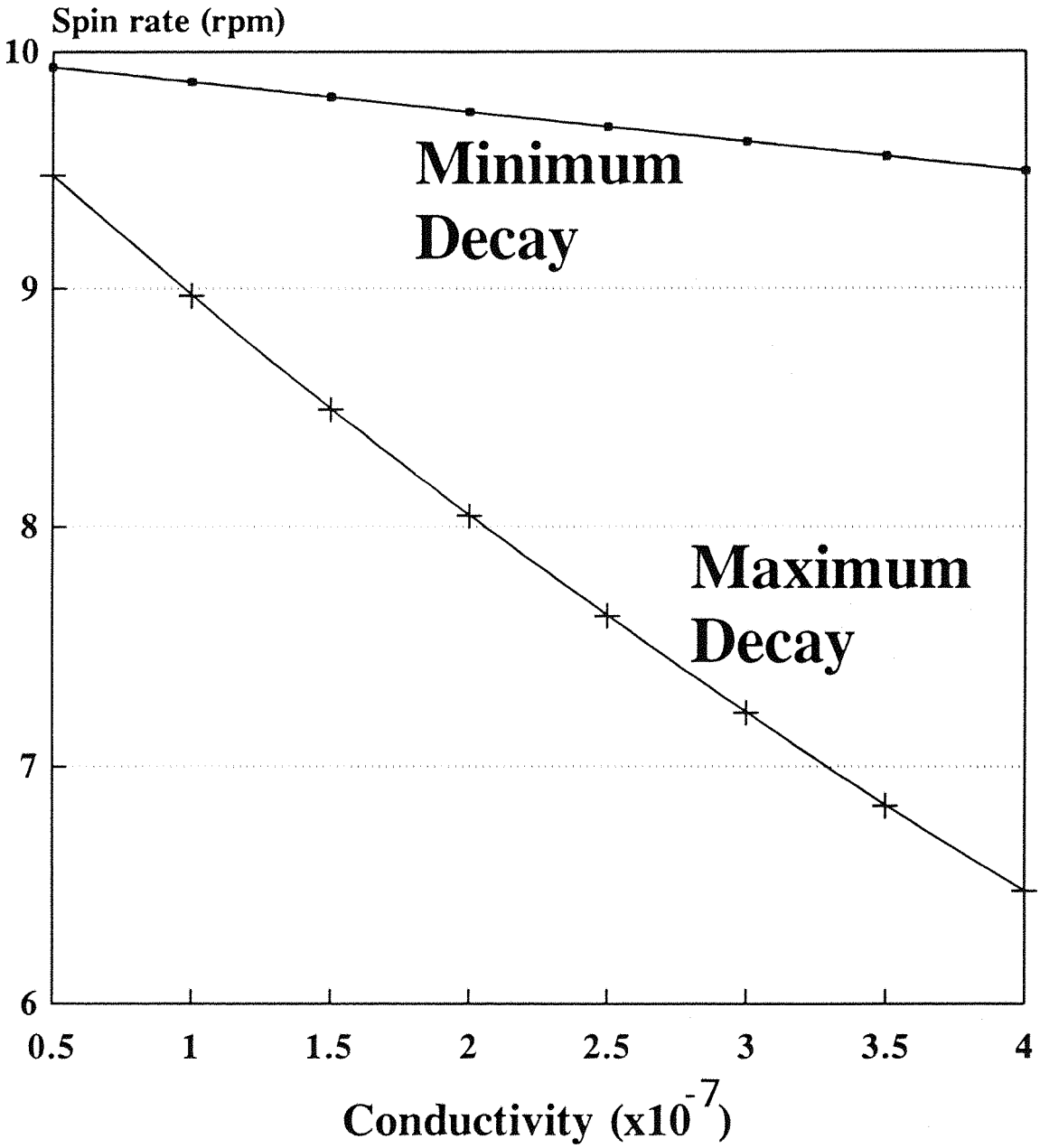

FIGURE 5.6

STRV Spin Decay
(Aerotorques in GTO)

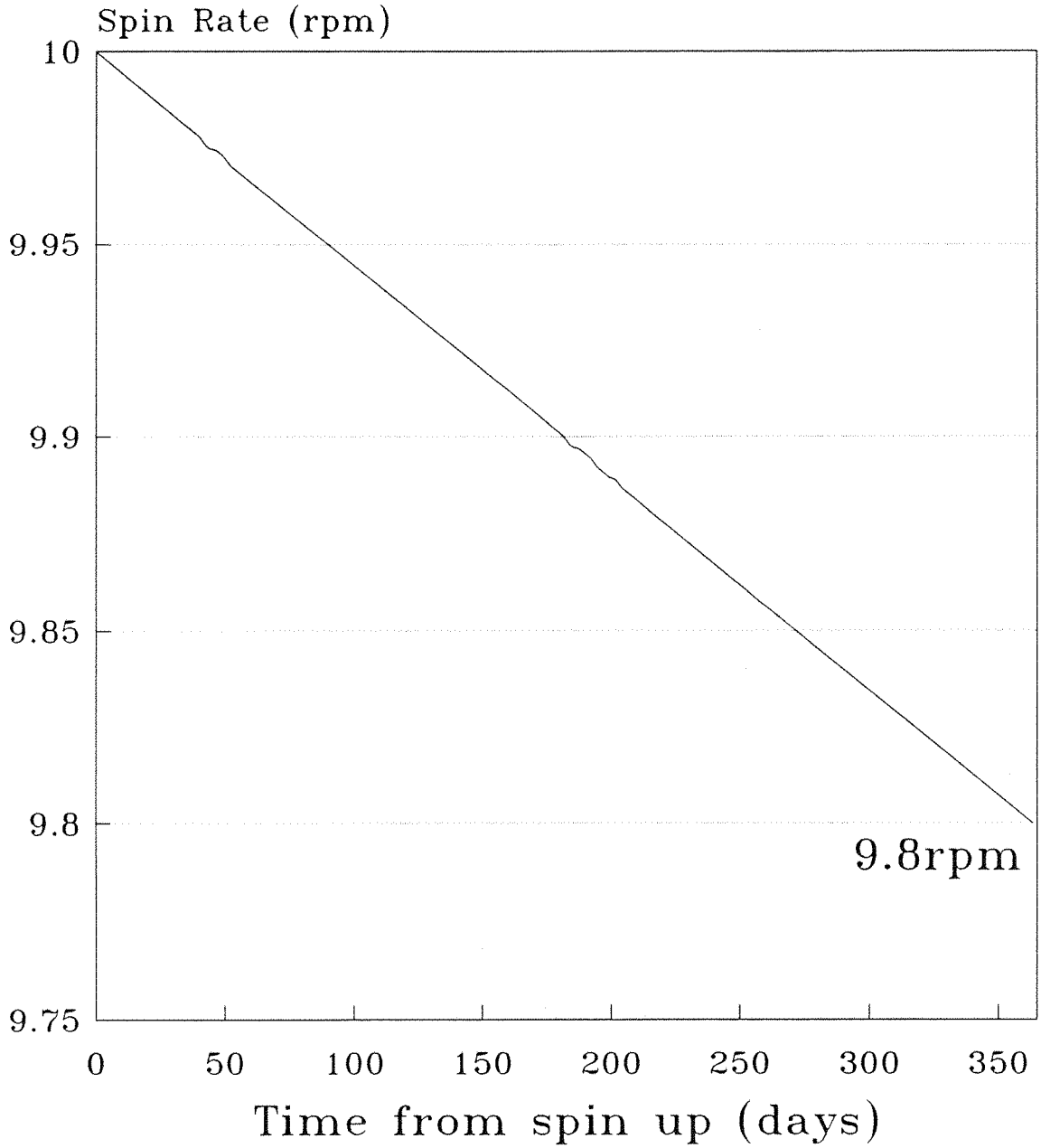

FIGURE 5.7

Data Storage Method

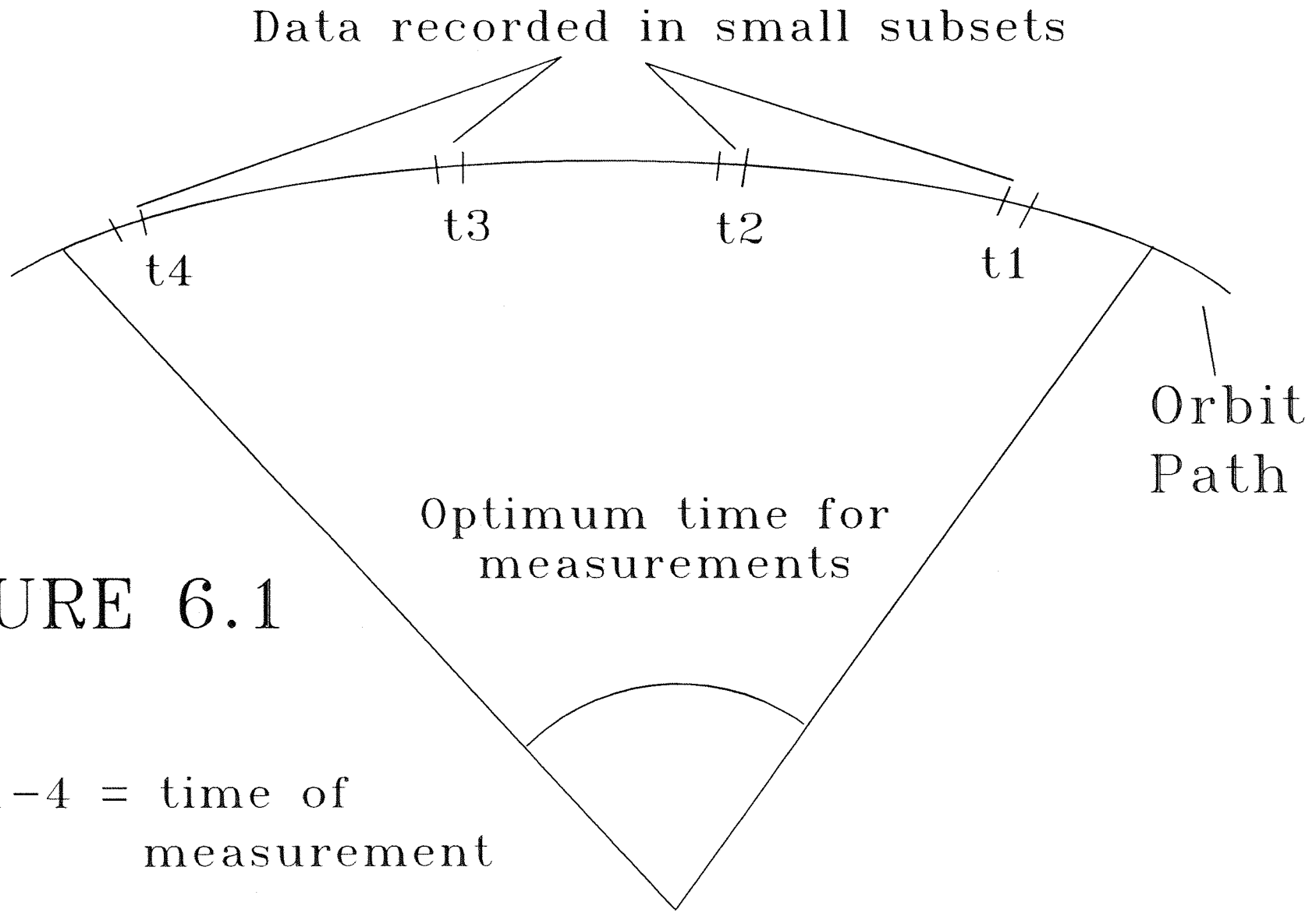

FIGURE 6.1

t1-4 = time of measurement

10 APPENDICES

Appendix A

To transform from inertial I, J, K components to the perigee reference frame the following matrix equation should be used...

$$\begin{bmatrix} \xi_p \\ \eta_p \\ \zeta_p \end{bmatrix} = \begin{bmatrix} \left(\begin{matrix}\cos\omega\cos\Omega - \\ \sin\omega\cos i\sin\Omega\end{matrix}\right) & \left(\begin{matrix}\cos\omega\sin\Omega + \\ \sin\omega\cos i\cos\Omega\end{matrix}\right) & (\sin\omega\sin i) \\ \left(\begin{matrix}-\sin\omega\cos\Omega - \\ \cos\omega\cos i\sin\Omega\end{matrix}\right) & \left(\begin{matrix}-\sin\omega\sin\Omega + \\ \cos\omega\cos i\cos\Omega\end{matrix}\right) & (\cos\omega\sin i) \\ (\sin\Omega\sin i) & (-\sin i\cos\Omega) & (\cos i) \end{bmatrix} \begin{bmatrix} I \\ J \\ K \end{bmatrix}$$

Appendix B

The b_i coefficients for the torque expressions are...

$$b_0 = \frac{R_z (A_1 + A_2)(2 - \sigma_n)}{\pi} \left[\frac{V_m}{V}\right]^2$$

$$b_1 = \frac{R_z (A_1 + A_2)\sigma_n\sqrt{\pi}}{4} \left[\frac{V_w}{V}\right]$$

$$b_2 = \frac{R_z (A_1 + A_2)(4(2 - \sigma_n) + 2\sigma_t)}{3\pi}$$

$$b_3 = \frac{(2A_0R_0 - A_1R_x - A_2R_y)\sigma_t}{2}$$

Appendix C

The following tables give the values used for the input files for the software analysis of the various spacecraft

SPACECRAFT DATA

Parameter	STRV-1	MARECS-A	SKYNET 4C
R_0 (m)	0.239	0.762	0.9187
R_x (m)	0.239	0.809	1.910
R_y (m)	0.239	0.809	1.4
R_z (m)	0.05	0.215	-0.1313
σ_n	0.9	0.9	0.9
σ_t	0.9	0.9	0.9
RA (degs)	-	2.53	253.523
DEC (degs)	-	-6.35	-14.942
ω_s (rpm)	10	65.3	63.244
I_{zz} (kgm^2)	2.5	352.7	481.557

ORBIT DATA

Parameter	STRV-1	MARECS-A	SKYNET 4C
h_p (km)	200	199.94	204.7
e	0.73	0.73	0.7301
i (degs)	0.7	10.565	7.009
Ω (degs)	178	273	178.8